University of Denver

Digital Commons @ DU

1-1-2010

Analysis and Design of a Feedback Controlled Adaptive Pneumatic Cast

Susan Renee Mueller
University of Denver

Follow this and additional works at: https://digitalcommons.du.edu/etd

Part of the Electrical and Computer Engineering Commons

Analysis and Design of a Feedback Controlled Adaptive Pneumatic Cast

_____

A Thesis
Presented to
the Faculty of Engineering and Computer Science
University of Denver

_____

In Partial Fulfillment
of the Requirements for the Degree
Master of Science

_____

by
Susan R. Mueller
June 2010
Advisor: Dr. Rahmat Shoureshi, Dean of SECS

Author: Susan R. Mueller
Title: Analysis and Design of a Feedback Controlled Adaptive Pneumatic Cast
Advisor: Dr. Rahmat Shoureshi, Dean of SECS
Degree Date: June 2010

Abstract

A pneumatic system with PID control for an actively controlled cast is designed. The cast is intended to aid healing of diabetic foot ulcers by relieving pressure from the sole of a patient's foot and distributing it to the calf. This is accomplished by a pneumatic system which maintains set pressure in multiple air bladders. The research began by defining an electrical circuit analogous to a single supply subsystem. Tests are performed to determine the coefficients for each component. These coefficients are used in a mathematical model to better understand the response of the system to pressure input. A controller is designed for a single subsystem using Ziegler-Nichols first method as a starting point. PID control is extended to each configuration option. Control theory is used to determine an optimal configuration of the bladder subsystems. Series, parallel, and a hybrid configuration are considered. The cost, complexity, and performance of each configuration is used in a weighted decision matrix to choose the best configuration. The parallel configuration is chosen as the optimal solution. Because the pump used in the design is capable of supplying all air bladders simultaneously, the parallel configuration can be simplified to a single subsystem. The model of the subsystem is validated against physical tests. The controller driving the single supply subsystem is used as a guideline for designing a modified duty cycle controller. This controller is implemented using simple pneumatic and electrical components.

Acknowledgments

I would like to thank a number of people who have made this research successful.

First of all, I would like to give my sincere thanks to my advisor, Dean Rahmat Shoureshi, for his patience, motivation, and knowledge in this research. I feel both honored and privileged to work with him. He has been a wonderful teacher from whom I have learned a great deal.

I would like to thank Dr. Yun-Bo Yi and Dr. Matt Rutherford for serving on my committee.

It has been my pleasure to work alongside Dr. Stephen Albert as we seek advancements in the treatment of diabetic ulcers. His immense knowledge of podiatry and enthusiasm for pursuing a new diabetic device has been inspiring. I look forward to our continued work together to address this important issue.

I am grateful to Scott Ferdinand for his expertise in electronics. His willingness to meet for testing on little notice and at all hours has made this research successful. Regardless of the emergency, Scott maintains a positive attitude and finds solutions to make even the most challenging of tasks possible.

I would also like to thank Benny Sarusi for writing the code for the microcontroller. Benny can do in a day what would take me months to accomplish. His continued support from his home in Israel through phone calls and emails has been a huge help.

To my dear husband, I am most grateful. Jake has encouraged me and supported me in my decision to leave my job and become a full-time student. He has made many sacrifices along the way, spending countless hours and enduring many late nights editing my thesis. His faithful love, encouragement, and prayers all along, I so appreciate. The past three years would have been much different without him. In the most stressful of times he is what kept me laughing.

Table of Contents

List of Figures

List of Tables

Chapter 1

Introduction

1.1 Motivation

In an effort to improve the quality of life for people suffering from diabetic foot ulcers (DFU), this research is focused on design and analysis of the pneumatic system for an adaptive and actively controlled semi-permanent/reusable cast. It is estimated that there are more than a million people in the United States who have been diagnosed with diabetic neuropathic foot ulcers[1]. That number is predicted to more than double within the next 25 years[2]. DFUs are treated by reducing pressure and shear on the ulcer. Doctors use modified shoe implants, walker braces, and Total Contact Casts (TCC) to heal ulcers. Although the TCC has a healing rate of about 90 percent it is used in less than 2% of cases[3]. This project focuses on improving the effectiveness of healing DFUs through an embedded pneumatic system. This Adaptive Cast can automatically form itself to a patient's leg, providing the capability of adjustment and re-use.

1.2 Diabetes Mellitus

Diabetes mellitus is an epidemic not only in the United States (US), but throughout the world. The Center for Disease Control's most recent statistic for the number of diabetics in the United States was reported in 2007 and estimates that nearly 8% of the population in the United States has diabetes mellitus[4]. That means approximately 24 million people were suffering from diabetes. It is estimated that by 2034 the number of people in the US with diabetes mellitus will increase to 44 million. That is nearly double the current population. It is predicted that this increase will triple the cost of treating diabetes[2]. According to Diabetes Care from May 2004, the number of diabetics in the world was estimated to be approximately 2.8 percent of the total population in the year 2000 and this is expected to nearly double to 4.4 percent in 2030. This would be an increase from 171 million to 2030 million people from the year span of 2000 to 2030[5].

Diabetes mellitus is defined by high levels of glucose in the blood as a result of defects in the production of insulin. Diabetes occurs when the body is unable to control insulin levels in the bloodstream. Glucose levels can be too high if the body does not produce enough insulin or if their body does not respond appropriately to the insulin being produced. Insulin is a hormone that is produced and released by the pancreas which allows the body to use glucose in the bloodstream as an energy source. Insulin facilitates the cells of the body to utilize glucose from the bloodstream that has resulted from digested carbohydrates absorbed in the intestines. With enough insulin the cells in the liver, muscle and fat tissue are able to convert glucose in the blood stream to glycogen, a long-term source of energy. Diabetes occurs when there is a breakdown in insulin production or effectiveness in the cells of the body.

There are two main ways that diabetes can occur, which are referred to as type 1 and type 2 diabetes. A person with type 1 diabetes has an immune system that destroys the pancreatic beta cells resulting in a lack of insulin production in the body. Without insulin, the body is unable to regulate blood glucose. This has been previously referred to as insulin-dependent diabetes mellitus (IDDM) or juvenile-onset diabetes. Only 5% to 10% of people diagnosed with diabetes are type 1 diabetic[4]. Type 1 diabetes is treated with insulin, either through injection or a pump, and patients must closely monitor their sugar intake and compensate with insulin appropriately.

About 90% to 95% of diagnosed cases of diabetes are type 2, also known as non-insulin-dependent diabetes mellitus (NIDDM), previously known as adult onset diabetes[4]. In type 2 diabetes, insulin is still being produced but at inadequate levels and there is a resistance of the cells to to the effects of insulin resulting in high blood sugar levels. Type 2 diabetes is correctable through diet and exercise[6]. When the body resists insulin, the cells in the liver, muscles, and fat tissue are unable to convert glucose into glycogen. This starves the cells of energy. High glucose levels over time can lead to complications with the eyes, kidneys, nerves or heart. Type 2 diabetes is treated through diet, exercise and medication.

1.3   Diabetes Complications

There are many complications with diabetes. Some of the more common complications are heart disease, stroke, high blood pressure, blindness, kidney disease, amputation, dental disease, and nervous system damage. People with diabetes are two to four times more likely to die from heart disease or have a stroke. They make up the majority of cases of blindness and kidney failure in the US. They are twice as likely to have dental disease. Roughly 60%-70% of all diabetics have some degree

of nervous system damage (diabetic neuropathy)[4]. When high glucose levels exist in the bloodstream for extended lengths of time, blood vessels can become damaged. These blood vessels bring oxygen to nerves and nerve coverings. Without adequate oxygen nerves are damaged. Nerve damage along with poor circulation and infection can lead to serious complications in the extremities. Nerve damage resulting from prolonged high glucose levels can cause a loss of sensation, often in the feet. Serious nerve damage can disfigure the foot resulting in excess pressure. Higher than normal pressure on the feet, trauma, or cuts can all result in diabetic ulcers. Since diabetics have poor blood circulation, foot injuries take much longer to heal than for a foot with normal blood circulation.

1.4   Diabetic Peripheral Neuropathy

In 2003, Diabetes Care published an article titled, "The Health Care Costs of Diabetic Peripheral Neuropathy in the U.S." The article revealed that nearly 6.8% of the total population of people suffering from diabetes has foot ulcers[1]. Assuming the rate has stayed the same, there are roughly 1,224,000 people in the US who have diabetic foot ulcers accounting for a $12 billion annual cost. Of the 1.2 million people, roughly 70,000 will suffer a lower limb amputation due to failed or lack of treatment. Within five years of the amputation, nearly half of these people will die. This is more than double the chance of death from prostate or breast cancer [7].

Specifically, diabetic peripheral neuropathy is a condition which is believed to be a result of diabetic microanioapthy (microvascular disease). Microangiopathy occurs when endothelial cells that line the blood vessels are exposed to elevated glucose levels for extended periods of time. The result is a thick, weak basement membrane which leaks, slowing the flow of blood. Without enough blood flow and oxygen,

nerves cannot maintain their proper function, resulting in neuropathy. Peripheral neuropathy is damage to the peripheral nerves, such as those in legs and feet.

1.5 Neuropathic Foot Ulcer Formation

Ulcers develop on the neuropathic foot due to several factors including overload, repetitive stress and shear; direct injury or cutting; continuous pressure; and heat or cold. Figure 1.1 is an example of a diabetic foot ulcer. With a healthy individual, these foot injuries will heal typically without complications or delay. However, the foot of a diabetic individual will have damaged nerves and poor circulation leading to the development of infection and serious wound formation. Of all of these factors, the most common factor causing ulcers in feet is overload. With sensory loss, the patient typically has balance dysfunction, is unaware of overload, and thus is unable to change to a protective gait. If the patient's foot is cut or experiences some other kind of trauma, the wound often goes unnoticed due to a lack of sensation. The delay of care along with other diabetic complications leads to lesions. The loss of sensation to touch implies a loss of sensation to temperature. If a patient is not careful they can burn their feet or let their feet get too cold. Too much heat or too much cold can also result in a diabetic ulcer[8].

Figure 1.1. A diabetic foot ulcer

Chapter 2

Historical Overview

2.1 Treatment Mechanisms

Once an ulcer has formed, peak plantar pressure (PPP) on the ulcer must be reduced for healing to occur [3] [9] [10] [11]. In addition to the contribution to ulcer formation caused by pressure, repetitive loading also causes inflammation which inhibits the healing mechanisms of the body[10]. Few comparisons have been made between treatment options in their effectiveness to reduce pressure, but one study shows the two leading options reduced pressure by 75%-85% [12]. Nonsurgical treatment of ulcers may include antibiotics, bandages, and debridement of tissue; but pressure relief is a requirement in the prevention of amputation [13] [14]. The presence of an ulcer exists in nearly 85% of all major amputations related to diabetes [15].

Although prescription of bed rest or use of a wheelchair may seem an obvious solution, these treatments reduce blood flow and ultimately increase mortality rate. In order to reduce wound pressure without limiting mobility, medical devices designed for this specific purpose are often prescribed. The most common treatments include

a modified shoe, walker, or Total Contact Cast (TCC) to reduce the plantar peak pressure while maintaining a mobile lifestyle.

2.2 TCC

The TCC (Figure 2.1) is considered the gold standard in DFU treatment. It is a fiberglass cast that is applied to the leg in a similar manner as a cast is applied to a broken leg. It creates total contact around the lower leg thus reducing the pressure on the sole of the foot. When compared to diabetic walkers and shoe modality the TCC healed a larger proportion of neuropathic, noninfected ulcers [11]. The study in which these comparisons were made showed the TCC had healing rates around 90%. Three other studies show the TCC has healing rates between 73%-100%[16].

Figure 2.1. Total Contact Cast

Although the TCC has a high healing rate, the device has many drawbacks which result in its use in less than 2% of cases [3]. These include formation of new ulcers, relatively high cost, time intensive application of TCC, and required specialized staff for application of the cast [11][15][16]. A survey of foot clinics in all 50 states and the District of Columbia in 2005 revealed that the two leading reasons the TCC is not chosen is patient tolerance (55.3% of respondents) and the time required to apply the cast (54.3%) [3].

2.3   Modified Shoes

Modified shoes range in design and functionality. Some diabetic shoes are deeper throughout to allow for insoles or orthotics. Inserts are used to reduce shock and more evenly distribute pressure. If a patient has an ulcer the insert is often cut so that pressure is relieved at the ulcer location. Modified shoes are used for both prevention and treatment of diabetic foot ulcers. They are used in more than 40% of DFU cases despite the suggestion of some studies which indicate they are an ineffective off-loading device [3][12]. It is often the cost that drives patients to choose a modified shoe over the TCC or walker. For clinicians the modified shoe is an attractive choice because of its high reimbursement amount, quick application, and ease of application[3]. Figure 2.2 shows a picture of a diabetic modified shoe.

Figure 2.2. A modified shoe for treatment of diabetic foot ulcers

2.4 Walkers

Diabetic walkers are another class of device used to treat DFUs. They are removable by the patient for observation and treatment of the ulcer. Some use air bladders designed to transfer the body load to the device while others are lined with foam to protect sensitive areas. No diabetic walker on the commercial market is self adjusting; all must be adjusted by the physician or patient. The Aircast, as its name indicates, has air bladders that are manually adjustable with a hand pump. Figure 2.3 is a picture of an Aircast XP Diabetic Walker^{TM}. The same study that reported the use of a shoe modality in more than 40% of DFU cases revealed that walkers were chosen in more than 15% of cases[3].

Figure 2.3. Aircast XP Diabetic Walker^{TM}

The effectiveness of walkers varies greatly. A study by Fleischli et. al. performed in 1997 shows that some walkers reduce pressure better than the TCC by as much as

10% while others lag behind the TCC in pressure off-loading [12]. However, pressure off-loading can only occur when the patient chooses to wear the product. The results of a study published in Diabetes Care in 2003 revealed that patients who were able to remove their walkers only wore them for 28% of their daily activity. This will obviously reduce the effectiveness of the device.

Chapter 3

System Parameters

The primary focus of this research is to develop a more effective device for healing foot injuries. The research was initiated by Dr. Stephen Albert, Chief of Podiatry at Denver Veterans' Affairs Medical Center. From more than 30 years of experience as a podiatrist, he recognized a need to improve upon the Total Contact Cast. As previously stated the TCC has a 90% healing rate but it is used in less than 2% of cases. The goal of this research is to design a control system which will measure pressure in an air cast and adjust the pressure to meet a desired set point. It is hypothesized that such a device will act as an effectively customized, continually adjusting support system in order to provide healing rates similar to the TCC with fewer drawbacks. In addition to the design of the control system, analysis and simulation of the control is performed on a lab prototype. Manufacture of a production prototype is not a goal.

This research uses a proven diabetic walker as a starting point. The walker is made by Aircast, a registered trademark of DJO, the largest non-surgical device company in the US. The focus of the research is on improved healing of foot injuries with the greatest emphasis on diabetic ulcers: the most common foot injury leading to lower leg amputation [17].

Prior to starting this research, one modification is made to the mechanical structure of the cast. Driven by the medical need to address the issue of immediate ulcer development following the removal of a cast or walker, an additional bladder is added to the sole of the cast. When a patient spends significant time in a cast with reduced pressure on the foot, the protective calluses are lost. The additional bladder is intended to help redevelop these protective calluses before the Active Cast is removed. After an ulcer has healed, over a period of a few weeks, a doctor will slowly increase the pressure until the patient is nearly walking on 100% of his/her body weight.

The primary means for treating diabetic wounds is to off-load body weight from the ulcer. As seen in Chapter 2, this is often accomplished via devices such as modified shoes, walkers/boots, and the Total Contact Cast. This research uses this same medically proven approach but automates the necessary adjustments to the device using electro-mechanical components and a feedback control design to monitor and alter the cast. The original means of transferring a portion of a patient's weight from the sole of the foot to the calf in the Aircast is the same, but the means of inflating the bladders to the correct pressure levels is different.

While the choice of components for this research is of obvious importance, the focus is not on the mechanical or electrical design. As the goals of the research could be completed with any number of available components, large effort is not devoted to the choice of parts. Instead, the choice of components is driven by size, cost, and availability. The solenoids, pump, and supply lines that meet some basic requirements are chosen. Requirements for the pump include input voltage no greater than 12VDC, low mass, small size allowing it to be mounted to the cast, flow rate high enough to fill the bladders from empty in about a minute, and pressure of at least 10 psi. The requirement for the solenoid is a 2-way or 3-way valve. It is not necessary for the valves to latch. They need to be small enough to fit on the cast. Although it may

have been possible to find a better suited pump or solenoid, that is not the focus of this phase of the research. The data sheets for the components chosen are located in Appendix A.

There are three possible configurations for the pump, solenoids, and bladders in the cast. One approach is to connect the bladders in series so that the pump supplies one bladder and the exhaust of that bladder supplies another bladder, and that exhaust supplies another bladder, and so on. A second option is to place the bladders in parallel. In this configuration the supply solenoids for each bladder are mounted to a manifold that is supplied by a single pump. If all five bladders need air at the same time, each bladder would see the same pressure and flow rate as a single bladder connected to the pump, assuming the pump can supply the necessary flow rate. The third option is a hybrid of series and parallel. The hybrid configuration consists of two bladders in series and that series in parallel with a set of three bladders in series. Multiple pumps are not considered in the current research.

Mathematical models are designed for each of the configurations. These mathematical models are compared and the best configuration is chosen. The engineering design decisions considered are cost, complexity, and performance. Each model is characterized by a transfer function.

3.1   System Modeling

The pneumatic system is made up of five smaller pneumatic subsystems. Regardless of the configuration, each subsystem contains one flexible semi-elastic bladder, two or three supply lines, two solenoid valves, and one pressure sensor. A simple subsystem can be seen in Figure 3.1.
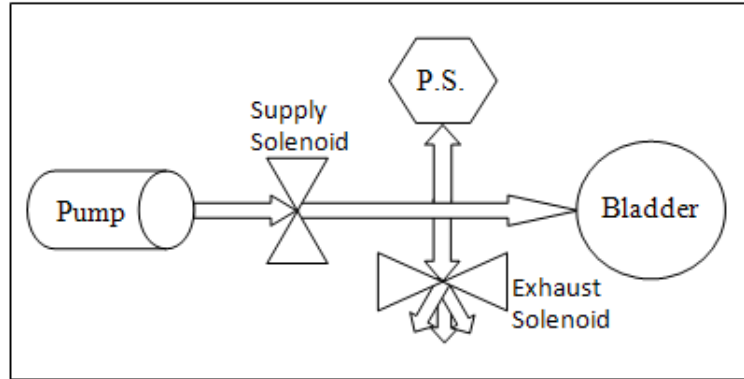
Figure 3.1. Subsystem

The controller for the subsystem is designed such that the exhaust and the supply valves are never open at the same time. For this reason the simple subsystem is considered as two smaller, independent subsystems: one subsystem which represents the supply and one which represents the exhaust. These can be seen in Figure 3.2 and Figure 3.3.
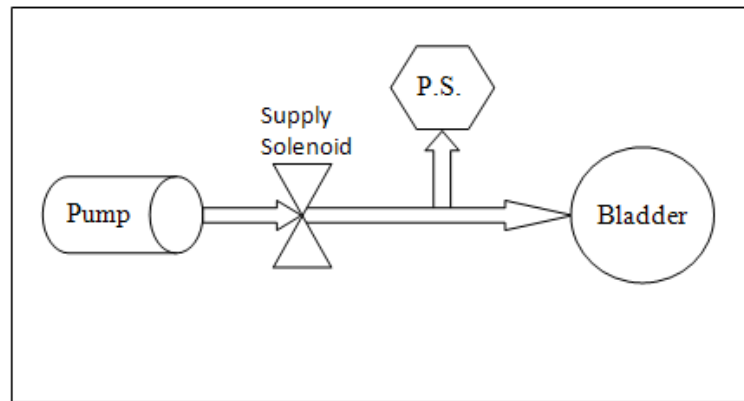
Figure 3.2. Supply subsystem
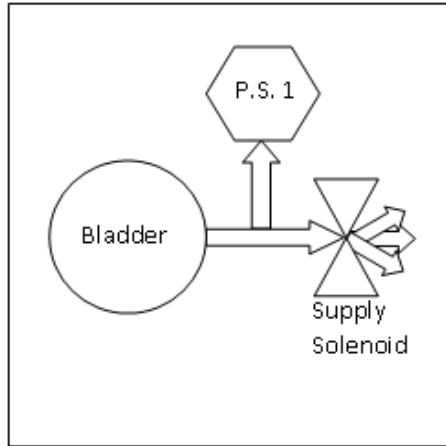
Figure 3.3. Exhaust subsystem

Analysis of air flow through a pneumatic system is complicated; however, dynamic control theory is commonly used in electrical systems to understand the flow of current. The pneumatic system and the relationships between components can be simplified by creating an equivalent electrical circuit. Pressure in the system is represented by electrical voltage, while air flow is analogous to current. Viscous effects of air flowing through a constriction, while difficult to account for explicitly, can be represented by resistance. Just as electrical resistance is the voltage drop across a resistor divided by the current flow, in a pneumatic system it is the pressure drop across the constriction divided by the air flow. A bladder, which stores air, is similar to an electrical capacitor which stores electrical charge. Inertial effects in a long tube must be accounted for with inductance when the length of a tube is much, much longer than the diameter. In this way all pneumatic components can be modeled using electrical components. Two electrical circuits are created to represent the supply and exhaust subsystems. Each of the three configurations (parallel, series, and hybrid) use the same supply and exhaust subsystems, so only two electrical circuits are needed to model the three different system configurations.

16

3.2 Supply

The supply subsystem, seen in Figure 3.2, is modeled using analogous electrical components. Just as the order of the components in the pneumatic system is important, so is the placement of the analogous electrical components in the circuit. The capacitance, C; resistance, R_2; and inductance, L_2 together characterize the behavior of the bladder. The bladder is constructed of semi-elastic material which stretches with increased pressure and compresses with a drop in pressure. This combination results in opposition to the flow of air, represented as L_2 in the supply circuit in Figure 3.4. The bladder fills with air much like an electrical capacitor stores current. The inertia to overcome the movement of the material of the bladder and the air in the bladder is represented as inductance. This transfer of energy in electrical circuits is represented by a capacitor and inductor in parallel. As in all real cases there are losses in the pneumatic system: the air molecules heat up, leak out, and pressure drops. These losses are represented by a resistor. Because the losses caused by the bladder inductance and capacitance occur simultaneously, the resistor is placed between the inductor and the capacitor. R_1 and L_1 characterize the behavior of air in the solenoid and supply lines. As air moves through the supply lines there are losses similar to those in the bladder. However, these are much smaller than the resistance due to the solenoid, so only the solenoid resistance is considered. R_1 represents the resistance of the solenoid. The tubes are much longer then their diameter, causing inertial effects to be large enough to be relevant. These effects are modeled with inductance, L_1 [18].

A transfer function is derived for the electrical circuit shown in Figure 3.4. The transfer function is equal to the ratio of the output pressure in the bladder to the input pressure of the pump. The components in Figure 3.4 can be represented by complex impedance in the Laplace domain. The circuit is simplified by grouping series
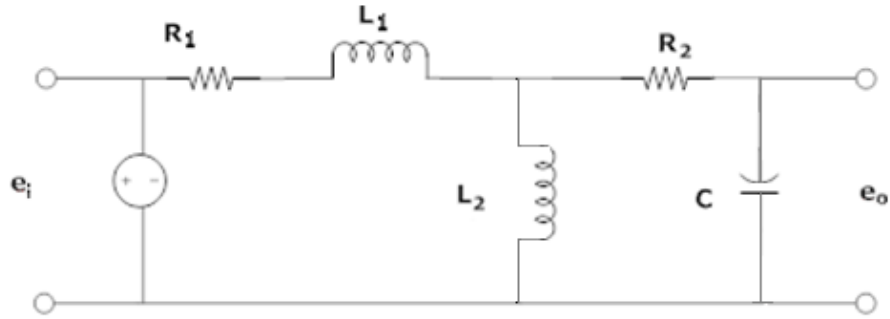
Figure 3.4. Electrical circuit representing supply subsystem

components into single complex impedances to create the circuit shown in Figure 3.5. This specific arrangement of impedances can be reduced to the transfer function seen in Equation 3.1 [19].
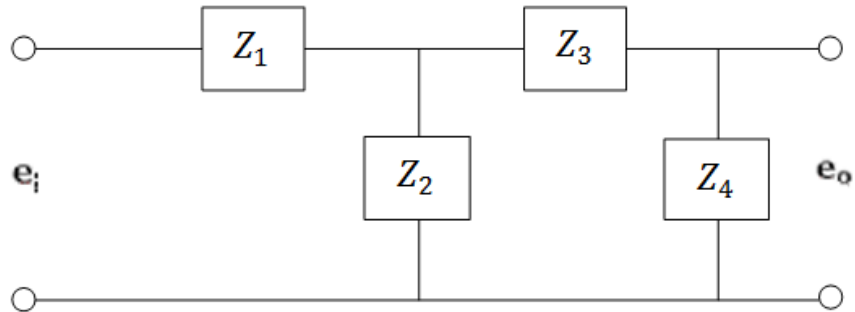
Figure 3.5. Complex impedance of supply circuit

$$\frac{E_o(s)}{E_i(s)} = \frac{Z_2 Z_4}{Z_1(Z_2 + Z_3 + Z_4) + Z_2(Z_3 + Z_4)} \tag{3.1}$$

$$Z_1 = R_1 + L_1 s \tag{3.2}$$

$$Z_2 = L_2 s \tag{3.3}$$

18

$$Z_3 = R_2 \tag{3.4}$$

$$Z_4 = \frac{1}{Cs} \tag{3.5}$$

The Laplace representation for each impedance, Equations 3.2-3.5, are substituted into Equation 3.1 to yield Equation 3.6.

$$\frac{P_o(s)}{P_i(s)} = \frac{L_2 s}{L_1 L_2 C s^3 + (L_1 R_2 + L_2 R_1 + L_2 R_2)C s^2 + (R_1 R_2 C + L_1 + L_2)s + R_1} \tag{3.6}$$

3.3   Exhaust

The resistance and inductance of air in the exhaust lines is the same as that in the supply lines. In the exhaust case there is no air moving into the bladder, only exiting. The bladder is modeled slightly differently in the exhaust circuit than in the supply circuit. For the exhaust scenario, the bladder is modeled with only a capacitor and resistor. There is no inductance in the bladder since it is only compressing the air out not stretching and compressing as in the supply case. There are losses as air exits like there are when air is being supplied to the bladder. The output of interest is the ratio of pressure in the bladder to atmospheric pressure explaining why e_o is a measure across both the capacitor and resistor (Figure 3.6).

A transfer function is derived from the electrical circuit seen in Equation 3.6. Since the components are in series, the denominator of the transfer function is the sum of the Laplace equivalents for each component, seen in Equation 3.7. The numerator

19
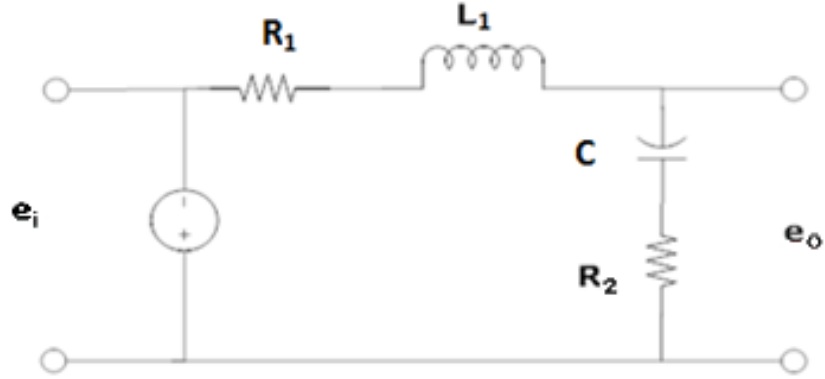
Figure 3.6. Electrical circuit representing exhaust subsystem

is the sum of the components making up the bladder pressure: C and R_2, seen in Equation 3.8. Figure 3.9 shows the exhaust transfer function.

$$P_i = R_1 + L_1 s + \frac{1}{Cs} + R_2 \tag{3.7}$$

$$P_o = \frac{1}{Cs} + R_2 \tag{3.8}$$

$$\frac{P_o(s)}{P_i(s)} = \frac{R_2 Cs + 1}{LCs^2 + (R_1 + R_2)Cs + 1} \tag{3.9}$$

3.4 Determination of Parameters

Modeling the dynamic response of the system requires measuring the coefficients for each component. The tests are performed using a single bladder (ankle bladder) from the active cast, the pump, pressure sensors, supply lines, and a flow rate sensor. When possible, a theoretical analysis for the components is performed to validate the test data.

20

3.4.1 Solenoid Resistance

The first component of the electrical circuit is the solenoid, R_1. To test the resistance of the solenoid the pressure and flow rate of the air before the solenoid and after the solenoid are determined. Equation 3.10 shows the relationship between pressure and flow which determines the resistance of the solenoid valve.

$$R_1 = \frac{\Delta P}{Q} \tag{3.10}$$

The change in pressure of the air across the solenoid divided by the flow rate through the solenoid is the resistance of the valve. A schematic of the pneumatic system for this test can be seen in Figure 3.7. The pump is connected to a solenoid and a pressure sensor. Air flowing out of the solenoid travels to the bladder, a second pressure sensor and an air flow sensor. The pressure and flow rate values found from this test can be seen in Table 3.1. The voltage to flow rate conversions are shown in Table 3.2.
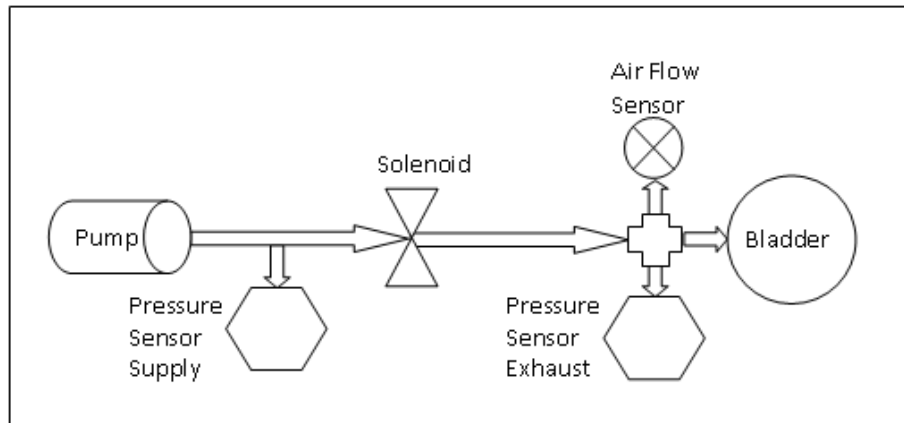
Figure 3.7. Solenoid resistance schematic

Table 3.1. Solenoid Resistance Test Results

Initial Pressure Sensor Voltage	0.940V
Final Pressure Sensor Voltage	0.360V
Initial Pressure	5.41 psi
Final Pressure	1.67 psi
ΔP	3.74 psi

Voltage of Flow Rate Sensor	3.8V
Flow Rate	$2.0 \ \frac{in^3}{s}$

Table 3.2. Datasheet Voltage to Flow Rate Conversion Table

Flow (SLM)	Nominal (VDC)
0	1.000
1	3.100
2	3.800
3	4.400
4	4.700
5	4.890
6	5.000

Initial flow rate calculation:

$$3.8V = 2\frac{L}{m} = 2\frac{in^3}{s} \tag{3.11}$$

The experimental value for solenoid resistance can be calculated according to Equation 3.10:

$$R_1 = \frac{\Delta P}{Q} = 1.87\frac{psi \cdot s}{in^3} \tag{3.12}$$

3.4.2 Supply Line Inductance

The supply lines used in this research vary in length, but the longest ones are 18 inches. Inductance is more of a factor for longer lines, so 18 inches is used as a worst

case example. The diameter is $\frac{1}{16}$ of an inch. The equation used to measure the inductance of the air in the supply lines can be seen in Equation 3.13

$$V_L = L\frac{di}{dt} \tag{3.13}$$

$$\Delta P = L_1\frac{dQ}{dt} \tag{3.14}$$

$$\Delta P = \frac{dp}{dt}\Delta t \tag{3.15}$$

$$L_1 = \frac{\frac{dp}{dt}\Delta t}{\frac{dQ}{dt}} \tag{3.16}$$

where V_L is the voltage across the inductor, $\frac{dp}{dt}$ is the change in pressure measured across the tube over time, Δt the time of measurement, and $\frac{dQ}{dt}$ is the change in flow rate over time.

The test setup for measuring inductance, L_1, includes a pump, airflow sensor, 18 inch supply line, and a pressure sensor. The pump is connected to an airflow sensor using a short $\frac{1}{16}$ inch supply line. The air flows through an airflow sensor into an 18 inch supply line to a pressure sensor. Figure 3.8 is a schematic of this test and Figure 3.9 is a picture of the test.
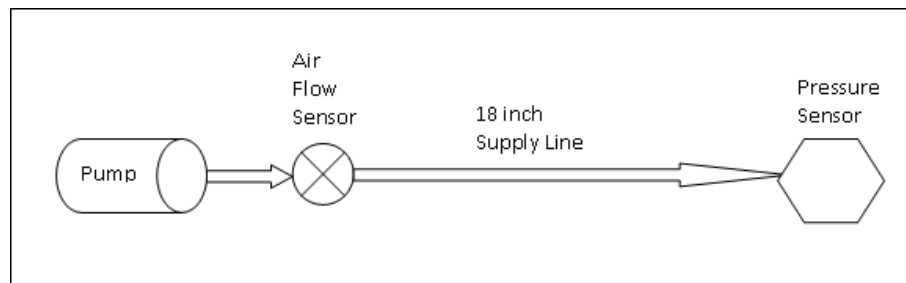
Figure 3.8. Schematic of supply line inductance test
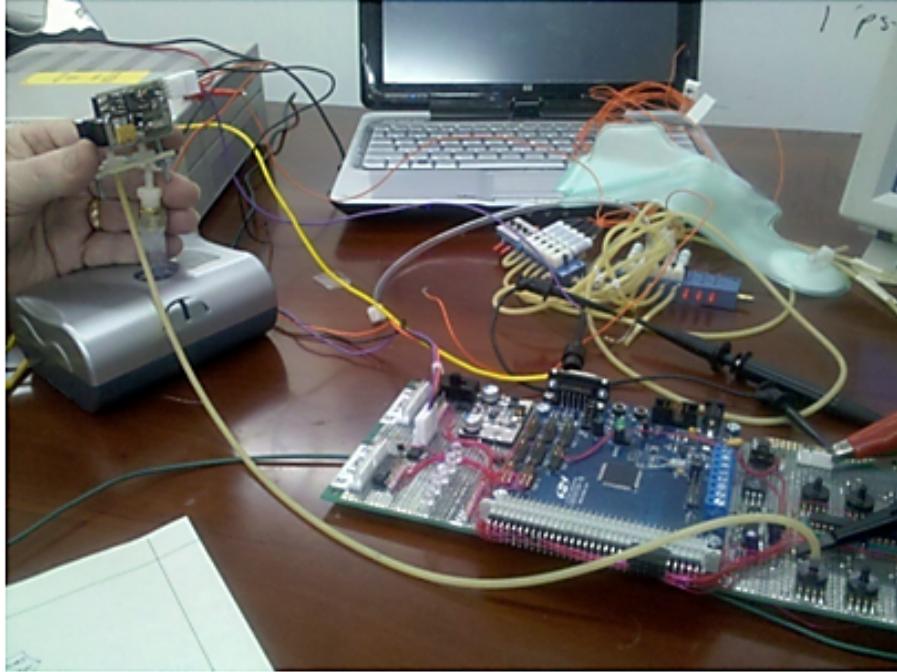
Figure 3.9. Picture of supply line inductance test

The two functions on the oscilloscope in Figure 3.10 represent the voltage readings of the flow rate sensor and pressure sensor from top to bottom, respectively. When the pump is powered on, the voltage reading of the flow rate sensor rises to 1.62V and then decays to 1.06V over 376 ms. The voltage in the pressure sensor starts at 0.720 V and rises to 2.28 V over 376 ms.

The voltage of the pressure sensor is converted to a psi value by the following equation:

$$\Delta P = (V_m \cdot 2 - 0.2) \tag{3.17}$$

where V_m is the measured voltage. Using this equation the initial and final pressures are calculated as 3.99 psi and 14.04 psi.

Using interpolation, the initial and final flow rate values are 0.3 $\frac{in^3}{s}$ and 0.029 $\frac{in^3}{s}$.
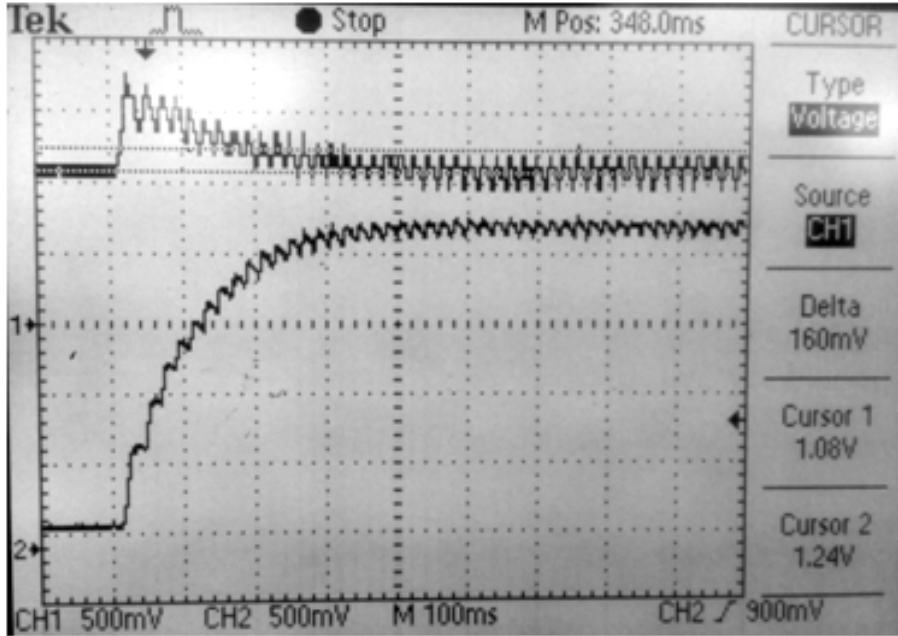
Figure 3.10. Supply line inductance test results on oscilloscope results

This test measures the inductance of the supply line. However, the resistance in the line affects the output as well. This resistance can be factored out of the test result using the time constant, τ, resulting in the true inductance. To do this the time constant is used to find the pressure drop across the added resistance. This pressure is subtracted out of the pressure drop across the system used to calculate inductance. The following equations show how the inductance in the supply line is determined.

$$\Delta P = \Delta P_L + \Delta P_R \tag{3.18}$$

$$\tau = \frac{L_1}{R} \tag{3.19}$$

$$\Delta P_R = \frac{L_1}{\tau} Q \tag{3.20}$$

25

$$\Delta P_L = \Delta P - \frac{L_1}{\tau}Q \tag{3.21}$$

$$L_1 = \frac{\Delta P - \frac{L_1}{\tau}Q}{\Delta Q} \tag{3.22}$$

After factoring out the pressure across the additional resistance, the final inductance in the supply line is calculated as $3.5 \ \frac{psi \cdot s^2}{in^3}$. All the data from this test is collected in Table 3.3.

Table 3.3. Supply Line Inductance Test Results

Initial Pressure Sensor Voltage	0.72 V	Initial Flow Rate Sensor Voltage	1.62 V
Final Pressure Sensor Voltage	2.28 V	Final Flow Rate Sensor Voltage	1.06 V
Initial Pressure	3.99 psi	Initial Flow Rate	$0.3 \ \frac{in^3}{s}$
Final Pressure	14.04 psi	Final Flow Rate	$0.029 \ \frac{in^3}{s}$
ΔP	10.05 psi	ΔQ	$0.271 \ \frac{in^3}{s}$

To validate the experimental result, a theoretical calculation is performed. Equation 3.23 is used to determine this value.

$$F = m\frac{dv}{dt} \tag{3.23}$$

$$\Delta PA = \rho l A \frac{d\frac{Q}{A}}{dt} \tag{3.24}$$

$$\Delta P = \frac{\rho l}{A}\frac{dQ}{dt} \tag{3.25}$$

$$V = L\frac{di}{dt} \tag{3.26}$$

Equation 3.25 is the pneumatic equivalent to Equation 3.26. Thus the formula for pneumatic inductance is:

$$L = \frac{\rho l}{A} \tag{3.27}$$

where ρ is the density of air, l is the supply line length, and A is the cross sectional area of the supply lines.

The theoretical value calculated for the supply line inductance is 6.6e-4 $\frac{psi \cdot s^2}{in^3}$. This value is clearly not within reasonable tolerance of the experimental value. The experimental value is used as the value for the supply line inductance because it is within the family of values calculated for each of the other components, and the theoretical value calculated for the supply inductance is not.

$$L_1 = \frac{\rho l}{A} = 6.6 \times 10^{-4} \tag{3.28}$$

3.4.3 Capacitance

Capacitance for the bladders is determined experimentally and theoretically using Equations 3.29 and 3.30.

$$C = \frac{1}{P}\int Q dt \tag{3.29}$$

$$C = \frac{Q}{\frac{\Delta P}{dt}} = \frac{\Delta V}{\Delta P} \tag{3.30}$$

There are four bladders in the Aircast, and a fifth is planned for the Active Cast. Two of the bladders in the Aircast (ankle bladders) have the same volume. It is anticipated that the volume of bladders in the Active Cast will be most similar to these. Therefore, the system will be optimized for bladders of this size. The volume of the air bladder is determined by filling it with water and emptying the water into a graduated cylinder. Figure 3.11 shows the equipment used for this measurement.

Figure 3.11. Equipment for measuring volume of bladder

A test is performed to measure $\frac{\Delta P}{\Delta t}$ of one of the ankle bladders from the Aircast. To determine the change in pressure over time, a single subsystem is connected. A schematic of this test is shown in Figure 3.12. The change in pressure calculated from this test is 4.84 psi over 8.6 seconds. The flow rate changes during this measurement by 1.23 $\frac{in^3}{s}$, averaging 1.99 $\frac{in^3}{s}$. Using an average flow rate and the $\frac{\Delta P}{\Delta t}$ measurement, the capacitance is calculated as 3.52 $\frac{in^3}{psi}$. Using the measured volume and the ΔP from the test, the capacitance is determined to be 3.72 $\frac{in^3}{psi}$.
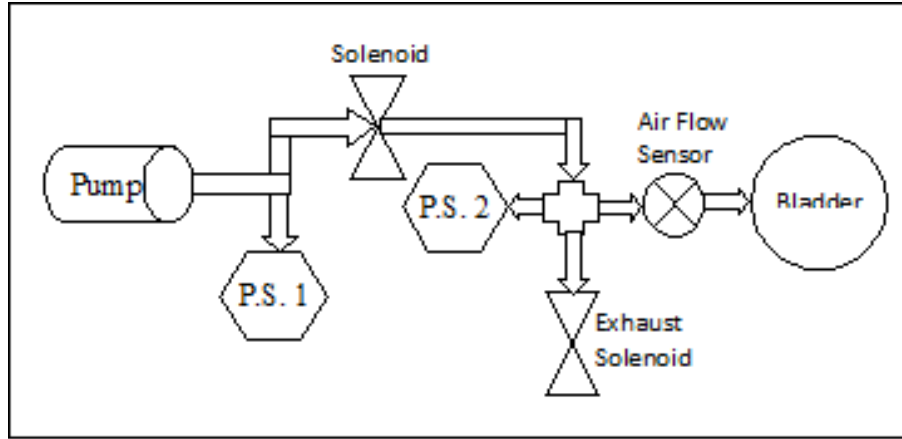
Figure 3.12. System test schematic

To validate the experimental result of the capacitance of the bladders, a theoretical value is calculated. Equation 3.31 is used to calculate the theoretical capacitance of the bladder. The same volume used in the experimental test is used here in the theoretical test. The density of air used is 1.28 $\frac{Kg}{m^3}$ which is the density at standard temperature and pressure. The gas constant of air is 287.75 $\frac{J}{kg \cdot K}$ assuming the air is dry. The temperature is 273.15 K.

$$C = \frac{\Delta V}{\rho R T} \tag{3.31}$$

In Equation 3.31 V is the volume of the air bladder, ρ is the density of air, R is the gas constant for air, and T is standard temperature.

The theoretical value calculated for capacitance is 1.25 $\frac{in^3}{psi}$, which is reasonably close to the experimental values. An experimental value is chosen due to likely errors arising from the assumptions made in the theoretical calculation: dry air, standard temperature, and standard pressure for a pressurized bladder.

3.4.4 Bladder Resistance

As air flows into the bladder, multiple phenomena occur to create resistance to the air flow. First, the inlet to the bladder includes a sharp change in direction that will resist the flow of air. Also, as the pressure increases in the bladder, the air molecules heat up, increasing resistance. To determine the resistance in the bladder, the pressure and flow rate of the air in the bladder is measured. A test is set up such that air from the pump travels through an airflow sensor and is measured by a pressure sensor as it flows into the bladder. A schematic for this test is shown in Figure 3.13, and the picture of the setup can be seen in Figure 3.14.
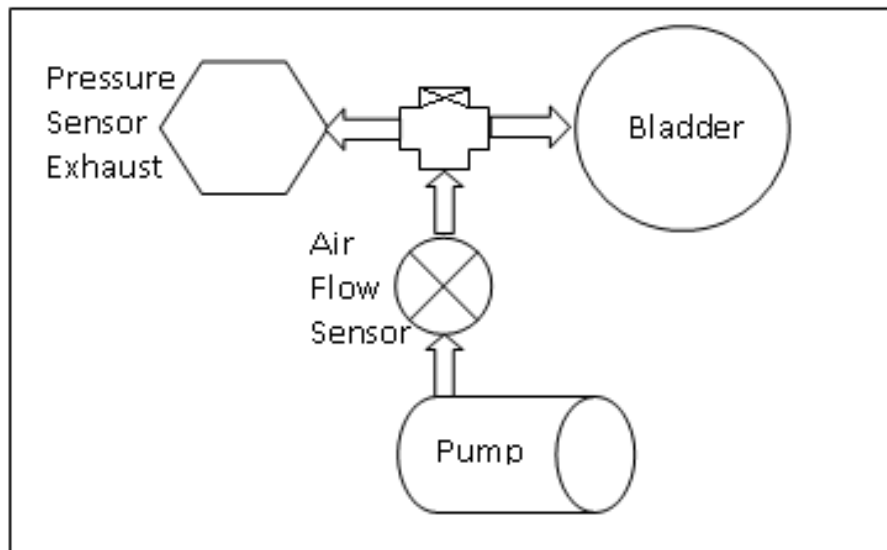
Figure 3.13. Bladder resistance test schematic

The two functions on the oscilloscope in Figure 3.15 represent the voltage readings of the flow rate sensor and pressure sensor from top to bottom, respectively. When the pump is powered on, the voltage in the flow rate sensor drops from 1.92 V to 1.46 V in 1.44 seconds while the pressure voltage reading ramps up from 0.156 V to 0.284 V.
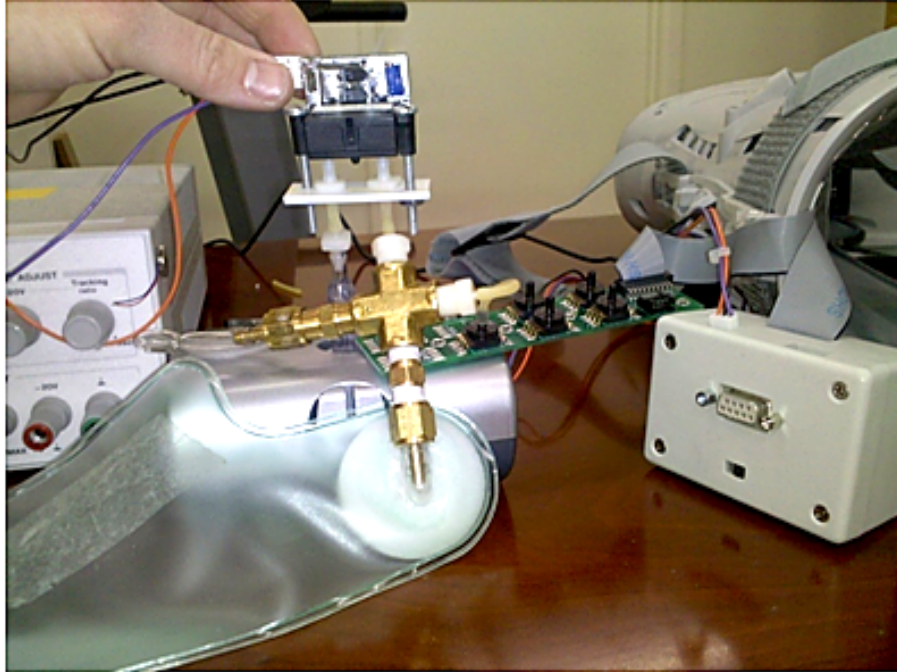
Figure 3.14. Bladder resistance test setup

The capacitance of the bladder affects the measurement of bladder resistance. This error can be factored out using the time constant, similar to the supply line inductance test. The time constant is used to find the pressure drop across the capacitor. This pressure is subtracted out of the pressure drop across the system. The following equations show how the resistance in the bladder is determined.
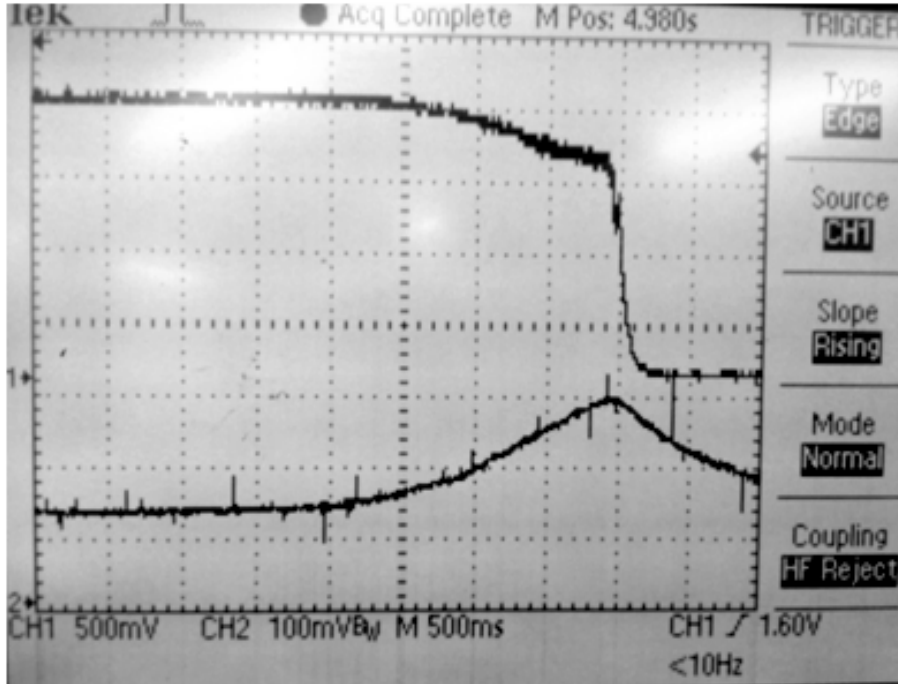
Figure 3.15. Bladder resistance test results shown in oscilloscope

$$R = \frac{\tau}{C} \tag{3.32}$$

$$\Delta P_R = \frac{\tau}{C}Q \tag{3.33}$$

$$\Delta P_C = \Delta P - \frac{\tau}{C}Q \tag{3.34}$$

$$R_2 = \frac{\Delta P - \frac{\tau}{C}Q}{Q} \tag{3.35}$$

Using these equations the resistance in the bladder is calculated as $0.34 \ \frac{psi \cdot s}{in^3}$. The data for this test is collected in Table 3.4.

Table 3.4. Bladder Resistance Test Results

Initial Pressure Sensor Voltage	0.156 V	Initial Flow Rate Sensor Voltage	1.92 V
Final Pressure Sensor Voltage	0.284 V	Final Flow Rate Sensor Voltage	1.46 V
Initial Pressure	0.361 psi	Initial Flow Rate	$2 \frac{in^3}{s}$
Final Pressure	1.185 psi	Final Flow Rate	$0.438 \frac{in^3}{s}$
ΔP	$0.824 \frac{psi}{V}$	Q_{av}	$1.219 \frac{in^3}{s}$

3.4.5 Bladder Inductance

Pneumatic inductance occurs when the flow of air changes the pressure distribution. Since the bladders are semi-elastic this phenomenon is present. It is expected that the inductance is small, but a test is conducted to measure the bladder inductance and confirm this expectation. The output of the air flow sensor is split between the bladder and the pressure sensor.
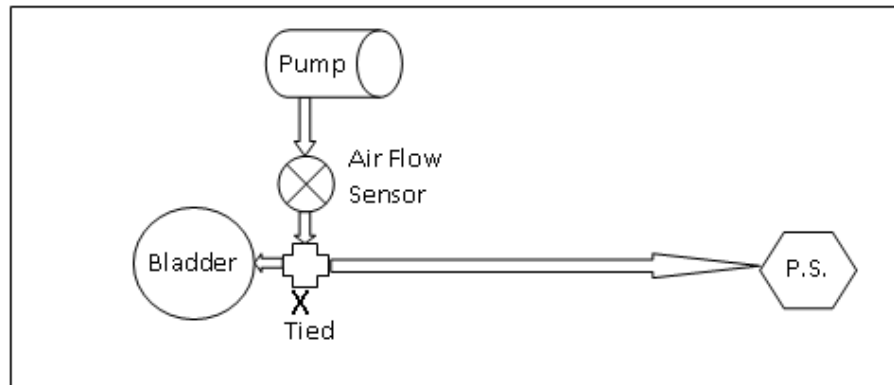
Figure 3.16. Bladder inductance test schematic
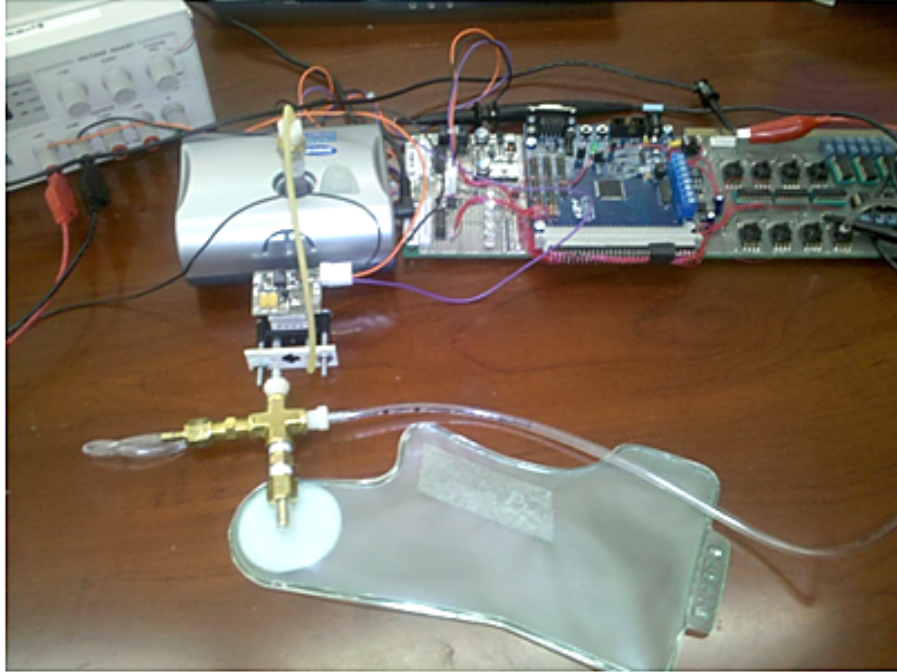
Figure 3.17. Bladder inductance test setup

From Figure 3.18, the initial voltage of the pressure sensor (top function) is 0.128 V and the final pressure reads 0.184 V. The bottom function is the voltage of the flow rate sensor over time. The initial voltage is 1.04 V and the final voltage is 4.96 V. The time span from when the voltage of the flow sensor began to rise and when it leveled out is 6.8 seconds.

The conversion from voltage to pressure is:

$$\Delta P = (V_m \cdot 2 - 0.2) \tag{3.36}$$

where V_m is the measured voltage.

$$3.22 \frac{psi}{V}(0.128 \cdot 2 - 0.2) = 0.180 \tag{3.37}$$
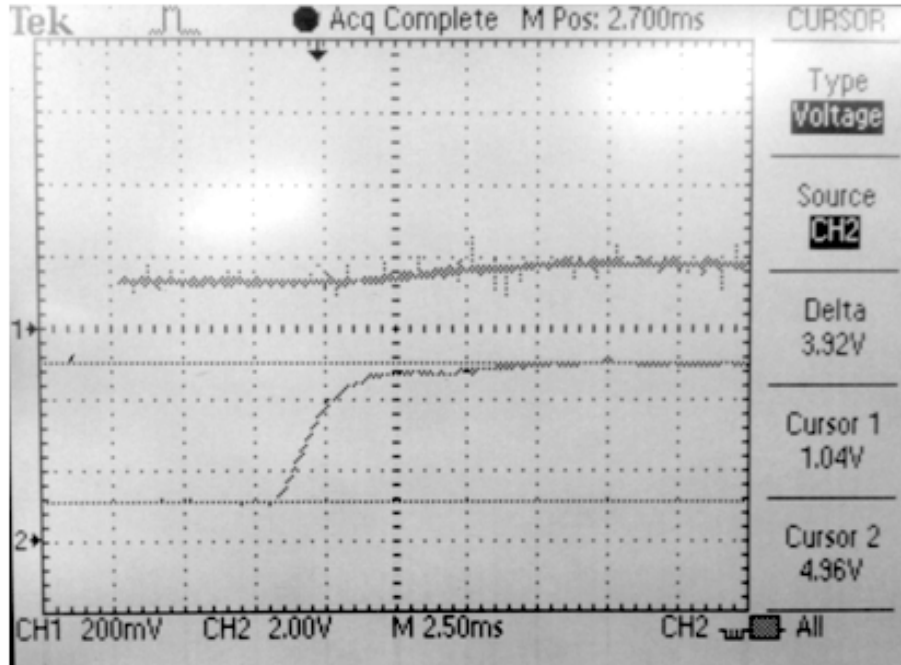
Figure 3.18. Bladder inductance test results shown in oscilloscope

$$3.22\frac{psi}{V}(0.148 \cdot 2 - 0.2) = 0.541 \tag{3.38}$$

Table 3.5. Bladder Inductance Test Results

Initial Pressure Sensor Voltage	0.128 V		Initial Flow Rate Sensor Voltage	1.04 V
Final Pressure Sensor Voltage	0.184 V		Final Flow Rate Sensor Voltage	4.96 V
Initial Pressure	0.180 psi		Initial Flow Rate	$0.02 \frac{in^3}{s}$
Final Pressure	0.541 psi		Final Flow Rate	$5.73 \frac{in^3}{s}$
ΔP	$0.361 \frac{psi}{V}$		ΔQ	$5.71 \frac{in^3}{s}$

35

Experimental value for inductance:

$$\Delta P = L_2 \frac{dQ}{dt} \tag{3.39}$$

$$\Delta P = \frac{dP}{dt} \Delta t \tag{3.40}$$

$$L_2 = \frac{\frac{dP}{dt} \Delta t}{\frac{dQ}{dt}} \tag{3.41}$$

$$L_2 = 4.3 \text{ x } 10^{-4} \frac{psi \cdot s^2}{in^3} \tag{3.42}$$

Table 3.6 shows the final values that were use for the mathematical model.

Table 3.6. Final Component Values

R_1	$1.87 \ \frac{psi \cdot s}{in^3}$
L_1	$3.5 \ \frac{psi \cdot s^2}{in^3}$
C	$3.72 \ \frac{in^3}{psi}$
R_2	$0.34 \ \frac{psi \cdot s}{in^3}$
L_2	$4.3 \ e^{-4} \frac{psi \cdot s^2}{in^3}$

Chapter 4

Control Theory

4.1 Transfer Function

A transfer function is a ratio of the Laplace transform of output to the Laplace transform of input, assuming zero initial conditions. Transfer functions in control theory can be characterized as either open-loop or closed-loop [20]. An open-loop transfer function is the output to input ratio of only the feed forward path of the system. There is no feedback loop in an open-loop transfer function. Figure 4.1 is the plant without control and Figure 4.2 is the feedforward open loop control system.
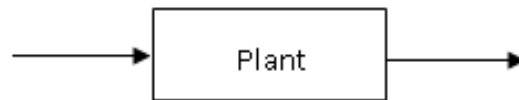
Figure 4.1. Open loop plant without control
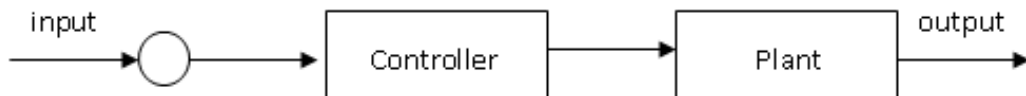
Figure 4.2. Open loop control

Closed loop transfer functions include a feedback path. The example of a closed loop system in Figure 4.3 shows a feedback path without a sensor. This is a system with unity feedback [21].
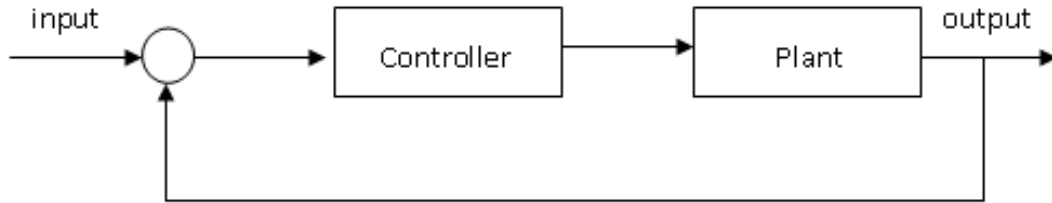
Figure 4.3. Diagram of open loop system

4.2 System Input

Although real world examples can have extremely varied system inputs, it is often useful in mathematical models to represent an input as an idealized step, ramp, pulse, or impulse. The system input used in this research is a pneumatic pump. When the pump is turned on the pressure increases very rapidly and then remains constant. This change in pressure can be closely represented by a step function. The input to the exhaust system, in contrast, is most closely like an impulse. Any foot movement that could result in pressures above the maximum set pressure can be treated as a pulse because of the duration.

4.3 Transient and Steady-State Response

The response of a system to a change in input over time is known as the transient response. For all systems with damping, this transient response has a finite length in time. As time goes to infinity, the system reaches steady state. Analysis of the transient system response is used to characterize important system parameters that indicate system performance. If the system does not perform as desired, control action

may be used to generate the desired system output. The system parameters calculated during transient analysis are used to determine the control action necessary and the characteristics of the controller. In this research the key system parameters used to evaluate system performance include overshoot, settling time, and steady-state error [22].

In order to design a controller, target values are necessary for the parameters of the transient system response. However, there is little direct medical research which can be used to determine the requirements for this response. Active control of the pneumatic system represents a step change in capability for devices intended to treat diabetic neuropathy. Additionally, it is not expected that the characteristics of the transient system response of a small pneumatic system will have a direct impact on healing rates. The response time of such a system is expected to be measured in seconds. Current treatment methods, such as the Total Contact Cast, are usually adjusted once every week. The response time for this research will be orders of magnitude shorter. Therefore, target values for the transient response parameters are based on Dr. Albert's experience treating diabetic wounds and physiological characteristics of the human body. Table 4.1 shows the desired parameters which drive the design of the controller [23].

Table 4.1. Desired System Response Parameters

Parameter	Value
Rise Time	< 2 seconds
Overshoot	< 10%
Settling Time	< 10 seconds
Steady-State Error	< 10%

4.4 Proportional Integral Derivative (PID) Control

Automatic controllers are used to alter the natural output of a system. Controllers evaluate the measured system output against the desired output and generate a control signal that can be used to minimize the divergence. The means by which a controller alters the system output is termed control action. There are five typical automatic control actions: two-position or on-off, proportional, proportional-integral, proportional-derivative, and proportional-integral-derivative. A two-position controller and a proportional-integral-derivative (PID) are both examined in this research.

Two pressure set points are determined for the bladders: a minimum and maximum value. If the pressure in a bladder exceeds the maximum value, a negative error signal is created which opens an exhaust valve. The exhaust condition is controlled by a two-position controller: the exhaust valve remains open until the pressure in the bladder drops below the maximum set value. If the pressure in a bladder drops below the minimum value, a positive error signal is created, opening an inlet valve. This supply condition is controlled by a PID controller. The exhaust system is controlled by only an on or off position controller. No analysis is needed for the exhaust.

Each portion of the PID controller has a specific function. The proportional control is based on the amount of error in the output. When the error is large, the proportional control output will be large. A proportional controller will decrease the rise time and stead-state error, but it will increase the overshoot. A proportional controller has a small effect on the settling time.

Derivative control output is proportional to the rate of change of the error signal. Since it is based on the error signal rate of change, it predicts future error levels and attempts to correct for them. When the error is increasing rapidly, the derivative

control output also increases rapidly to correct the response. This increases system stability, reduces overshoot and settling time, and has only a small effect on system rise time and steady-state error. Derivative control is not used by itself because if the error signal is constant, the rate of change is zero so the derivative control correction is also zero.

An integral controller integrates the past error signal. Because this is an accumulation of all past instantaneous errors, the integral control output may not decrease as the error approaches zero, but may in fact increase. Therefore, integral control can increase both overshoot and settling time. However, it will decrease rise time and eliminate steady state error once steady state has been achieved. Note that neither a proportional controller nor derivative controller eliminates steady-state error [24] [25] [26].

4.5 Root Locus

Root locus graphs are design techniques used to find the best parameters for control systems. A root locus graph is a plot of the locus of the roots of the characteristic equation with the real axis as the abscissa and the imaginary axis as the ordinate. Poles of the open loop denominator and zeros of the open loop numerator are plotted on a root locus plot. Lines, known as branches, are drawn starting at poles and ending at zeros or infinity. The root locus is useful for investigating the effect of varying a system or controller parameter on the overall closed loop system response. It is helpful in understanding system stability, natural frequency and damping characteristics. The location of the branches are determined by the magnitude of and angle between each pole-zero pair. A branch represents the closed loop path of the poles as the system gain increases from zero to infinity. If the branches of the root locus plot lie

entirely in the left half of the s-plane, the system is stable. If a branch crosses the imaginary axis into the right half plane, the system could become unstable if the gain is large enough. A system is said to be marginally stable when the pole starts at the origin and the path of the branch will take it into the right half plane with any increase in gain [27] [28] [29].

4.6   Ziegler-Nichols

The Ziegler-Nichols (ZN) method is a guideline used for tuning PID controllers. ZN rules help determine proportional gain, derivative time and integral time to find the optimum PID values. There are two ZN methods. The first method is applied to systems which are stable and have no tendency to become unstable and the second method is for systems which are unstable or by some control parameters could go unstable. Ziegler-Nichols first method is applied to the single supply subsystem because it is stable with no tendency to become unstable. The first method of ZN only applies to systems whose transient response to a step input has an initial slope of zero but increases and levels off with a slope of zero, creating an 's-shaped' curve as seen in Figure 4.4. The blue curve in the plot is the transient response of the open-loop plant. The delay time, L, of the transient response is calculated as the amount of time between the start time to the intersection of the tangent line with the abscissa. The time constant is the time between the intersection of the tangent line with the abscissa and the intersection of the tangent line with the settling value.

Equation 4.1 is the ZN approach to tuning a PID controller [30] [31] [32].

$$G_c = K_p(1 + \frac{1}{T_i s} + T_d s) \tag{4.1}$$
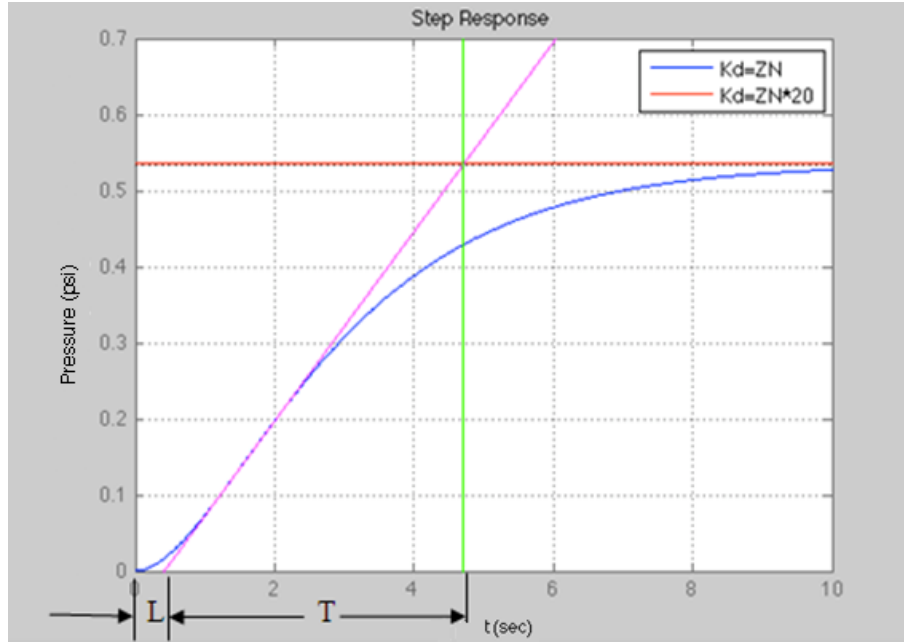
Figure 4.4. Ziegler-Nichols curve of plant

Table 4.2. Ziegler-Nichols First Method

Type of Controller	K_p	T_i	T_d
P	$\frac{T}{L}$	∞	0
PI	$0.9\frac{T}{L}$	$\frac{L}{0.3}$	0
PID	$1.2\frac{T}{L}$	2L	0.5L

From Equation 4.1 and Table 4.2 the following formulas were derived to determine K_p, K_i, and K_d [33]

$$K_p = 1.2\frac{T}{L} \tag{4.2}$$

$$K_i = 0.6\frac{T}{L^2} \tag{4.3}$$

$$K_d = 0.6T \tag{4.4}$$

where K_p is proportional control gain, T_i is integral time, and T_d is derivative time.

Chapter 5

Mathematical Model

In order to design a controller for the Active Cast it is necessary first to examine the response of the system without control. The behavior of the pneumatic system alone will determine what type of control is necessary and the controller values appropriate for creating the desired output. The main factors used to determine control action are rise time, overshoot, settling time, and steady-state error of the transient response of the system.

5.1   Characterization of Supply Subsystem

The transient response of the supply subsystem is shown in Figure 5.1. This plot shows the response of the bladder pressure to a step input. The rise time of the transient response is about 2 seconds. The peak pressure never reaches the desired input pressure, so there is no overshoot. It takes about 14 seconds for the system to reach steady-state, and the steady-state error is about 100%. It is obvious from this graph that without a controller, the pressure in the bladders can never reach the desired set point.
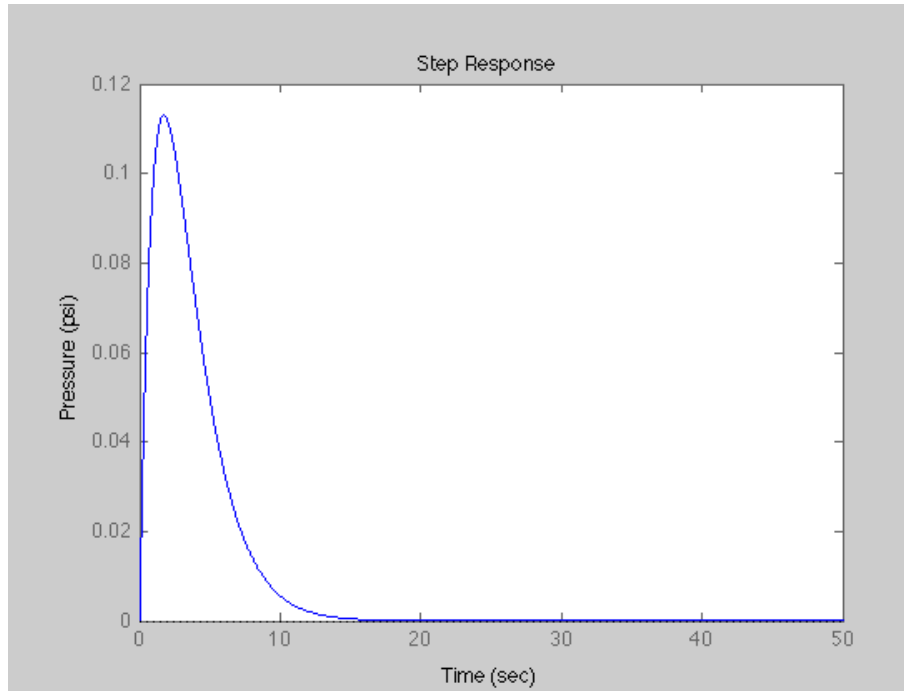
Figure 5.1. Transient response of plant

Stability is the first characteristic of the system determined. If the system is unstable or marginally stable then that characteristic would be of highest importance. Figure 5.2 shows the root locus plot of the open loop plant. All of the branches lie in the left half of the s-plane, so the system is always stable.

Root locus is also useful for determining the desired gain of the proportional controller, K_p. Proportional control is the simplest controller and is typically implemented first to determine if the desired system parameters can be met. Figure 5.2 shows the root locus of the plant with a unity proportional controller. The pink squares represent the closed loop poles. These squares move along the blue branches from the the poles, 'x' to the zeros, 'o' as the proportional control is increased from zero to infinity [21]. The desired location of the closed loop system poles is determined by the desired system parameters. The black, vertical line in the figure represents the desired settling time of 10 seconds. To reach a settling time of 10 seconds or
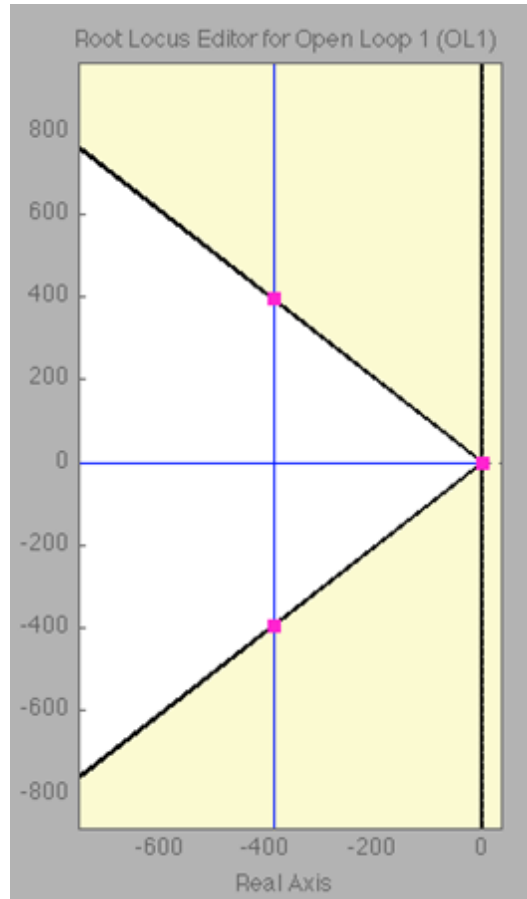
Figure 5.2. Root locus of the plant

faster, all of the pink squares must lie to the left of the vertical line. The diagonal lines represent a damping value of .707. If a closed loop pole lies on this line the desired damping is achieved. If the closed loop pole lies between the diagonal lines the damping is greater than .707, and if it lies outside the lines the damping is less than .707. If poles lie on the real axis, the system damping ratio is 1.

Figure 5.2 shows the closed loop poles that have been moved to the critically damped location. This demonstrates the ability for the system to be critically damped, but Figure 5.3, which is an enlarged view of Figure 5.2, indicates how critical damping affects the settling time. The pink square in Figure 5.3 is on the

right side of the vertical line. This illustrates that increasing K_p alone is not enough to achieve a critically damped system that settles at 10 seconds or faster.
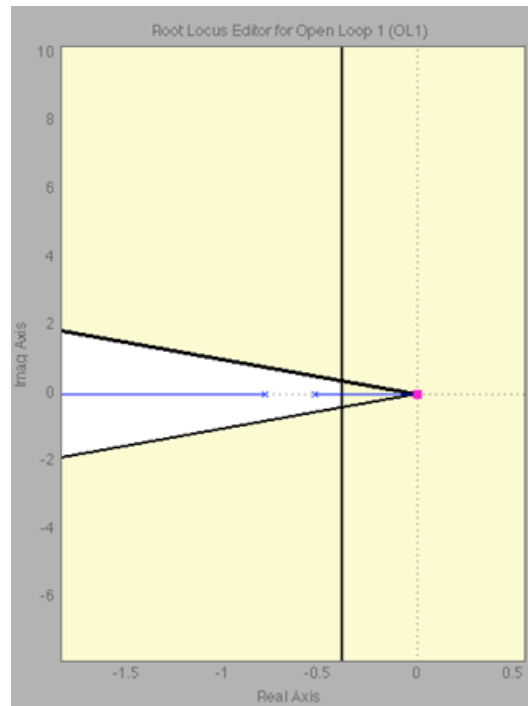
Figure 5.3. Root locus of the plant enlarged

Additionally, proportional control alone will not eliminate steady state error. The original transfer function (Equation 3.6) has an 's' term in the numerator which results in a zero at the origin of the root locus plot. This 'zeroes out' the system response, bringing the transient response down to zero as seen in Figure 5.1. This indicates that zero steady state error cannot be achieved. The zero at the origin must be cancelled for the system to respond correctly to the step input. An integral controller can be added to the system to cancel this zero. The combined effect of proportional-integral (PI) control on the transient response is shown in Figure 5.4. Here, the steady state value is much less than the step input value of one and the settling time is greater than ten seconds. Figure 5.5 shows the root locus plot of the plant with PI control. The zero at the origin is cancelled.
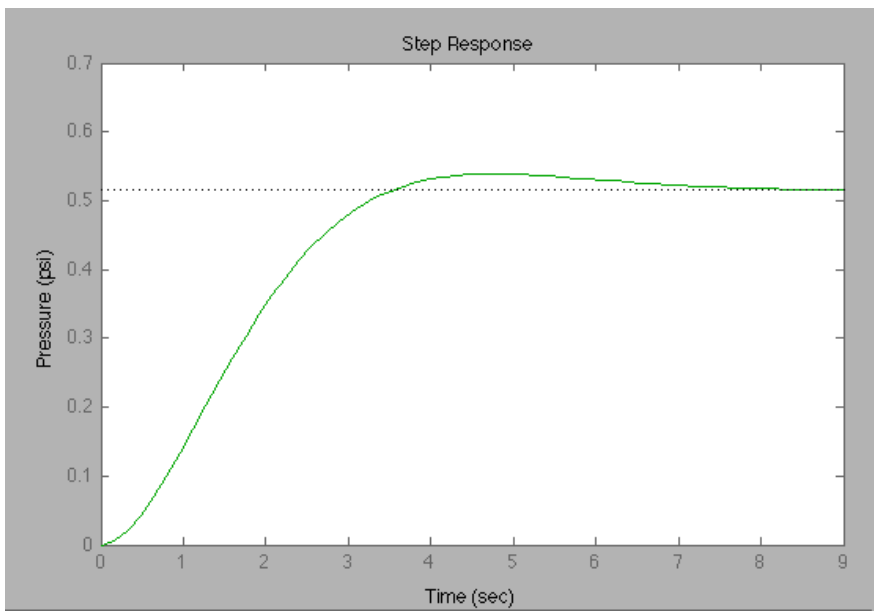
Figure 5.4. Transient response of plant with PI control
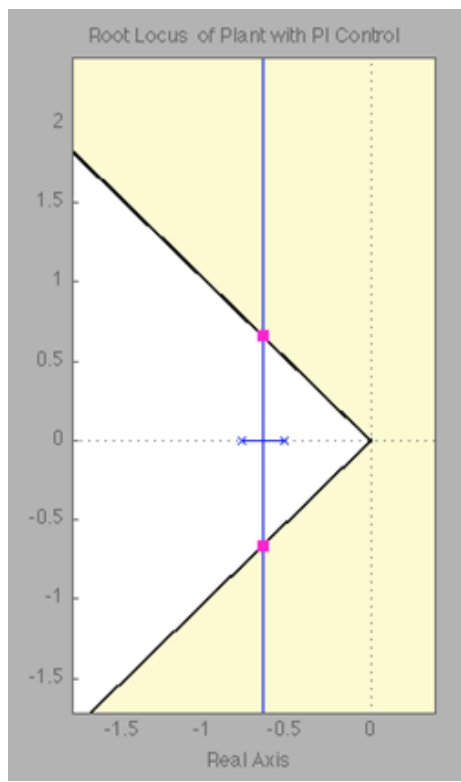
Figure 5.5. Root locus of plant with PI control enlarged

Equation 5.1 shows the transfer function of the plant with the measured coefficients inserted and with PI control. It can be seen that the 's' term in the numerator is no longer present. However, there is no integral in the transfer function. Because an 's' is present in the plant transfer function numerator two integrals are necessary, one to cancel the 's' and one to allow for integral control. Logically the next controller implemented is a proportional-integral-integral (PII). The root locus of the plant with PII control is displayed in Figure 5.6. Critical damping can be achieved, but settling times faster than 10 seconds cannot. The transient response in Figure 5.7 confirms this. It appears that the settling time is about 25 seconds.

$$\frac{P_o}{P_i} = \frac{357.5}{s^3 + 789s^2 + 1047s + 334.1} \tag{5.1}$$
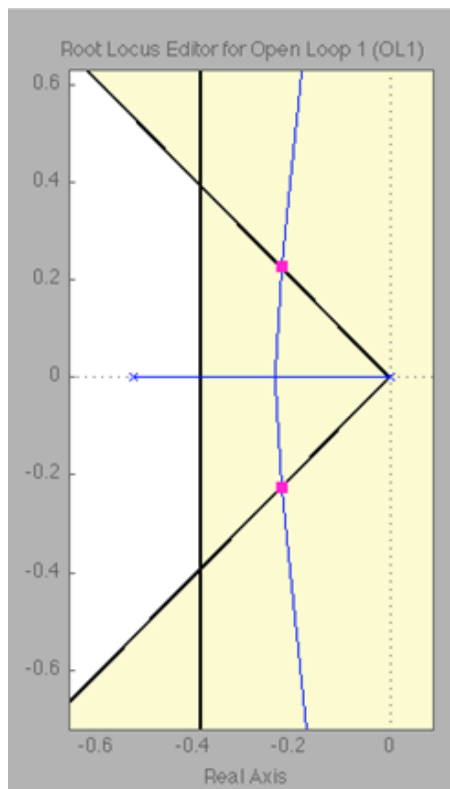
Figure 5.6. Root locus of the plant with PII control

49
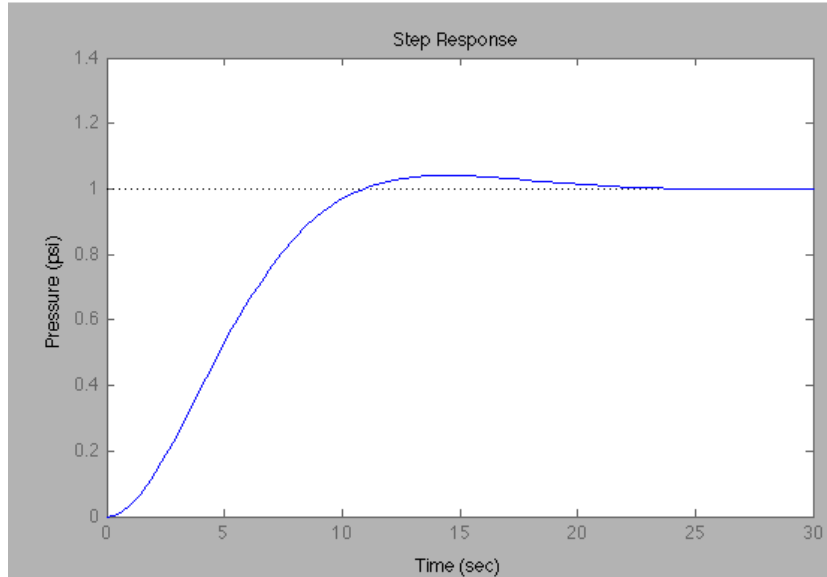
Figure 5.7. Transient response of the plant with PII control

The control can be further improved by adding a derivative controller. Figure 5.8 is the root locus of the closed loop plant with proportional-integral-derivative-integral (PIDI) control. Here the system is critically damped and the settling time is less than 10 seconds. The transient response of the plant with PIDI controller is included in Figure 5.9.
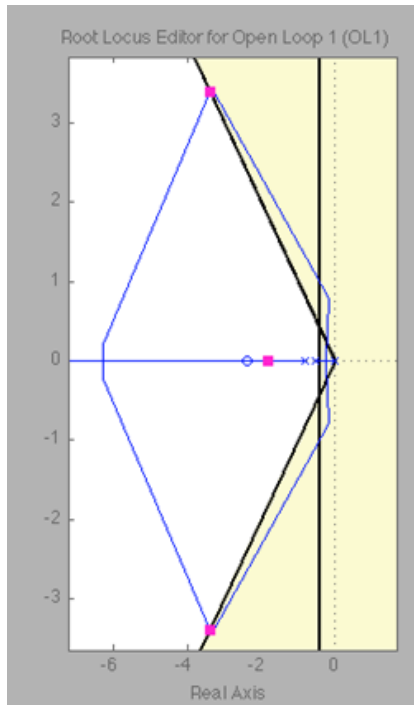
Figure 5.8. Root locus of plant with PIDI control
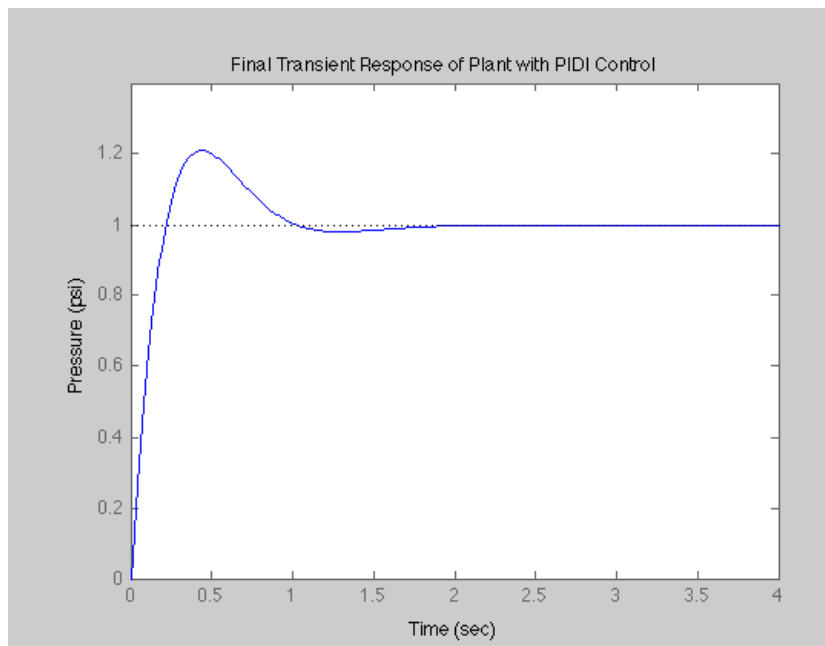
Figure 5.9. Transient response with PIDI control

51

PIDI control allows the system to settle faster than 10 seconds and reach zero steady-state error. However, the overshoot is greater than the target value of 10%. An enlarged view of the transient response with PIDI control (Figure 5.10) indicates an overshoot of about 20%. This can be reduced by adjusting the T_d value in the controller. Figure 5.11 reveals the impact T_d has the on system response. Each function in the graph is a closed loop plant with PIDI control but T_d has been varied by a multiple of the Ziegler-Nichols T_d value. As T_d increases in value, the overshoot is reduced. Doubling the Z-N value brings overshoot within the target value. The response of the plant with the final PIDI value is shown in Figure 5.12. This controller meets all design requirements.
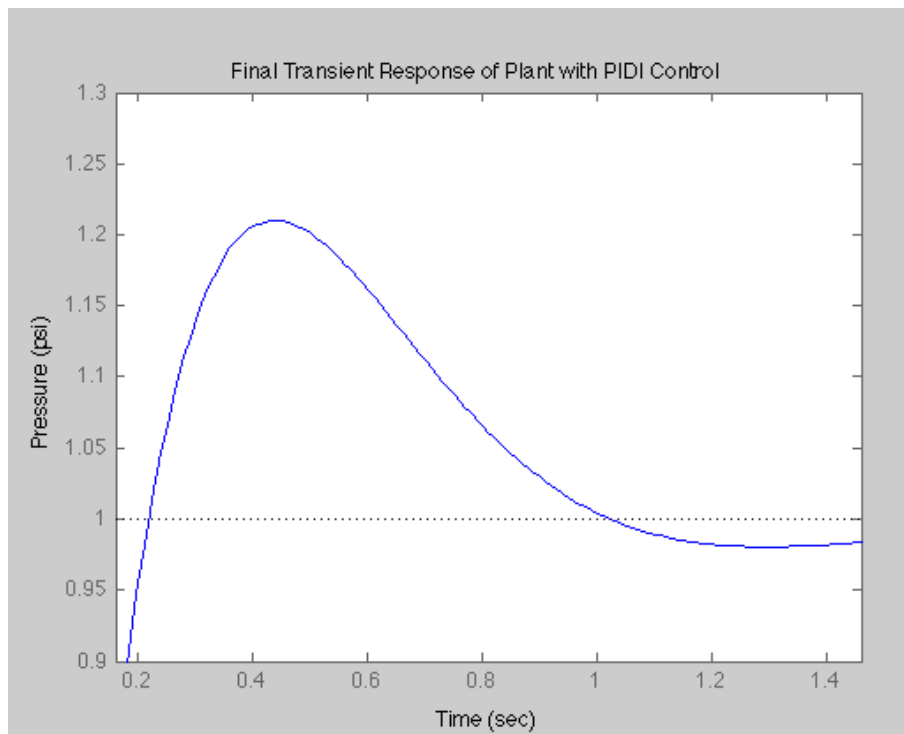
Figure 5.10. Transient response of the plant with PIDI control enlarged
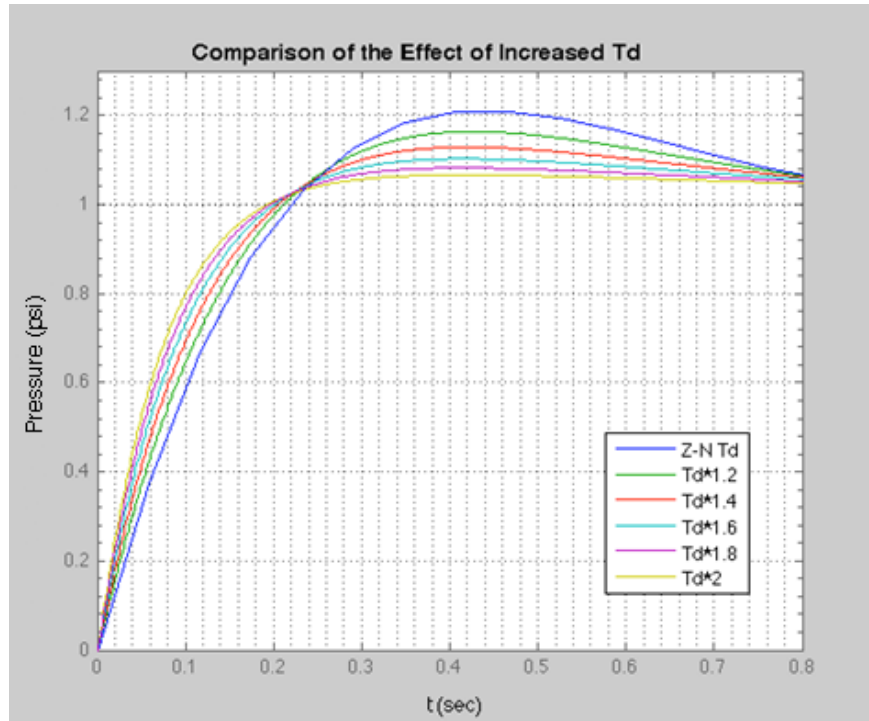
Figure 5.11. Transient response of the plant with PIDI control varying T_d
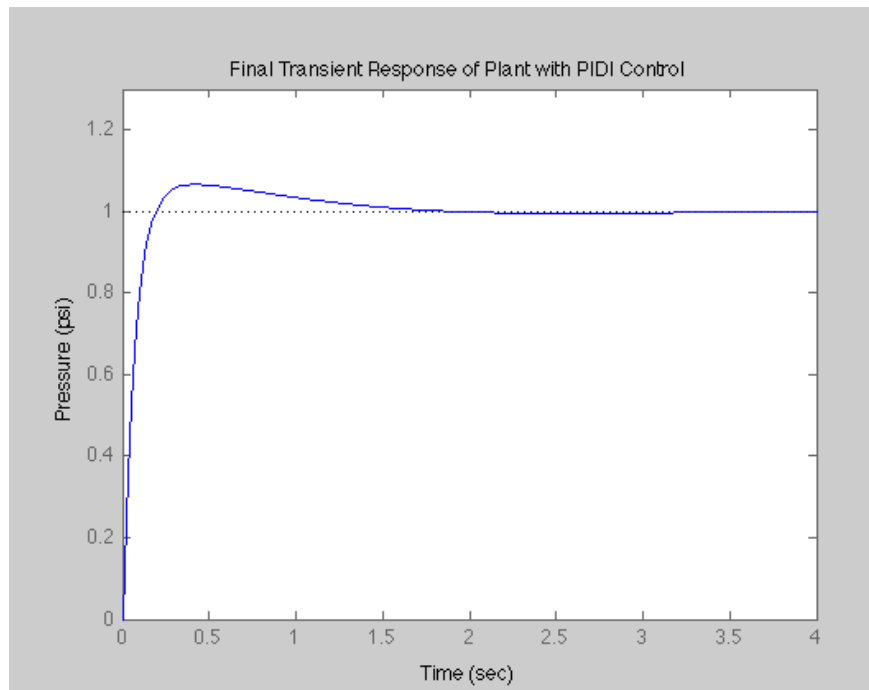
Figure 5.12. Final transient response with PIDI control

5.2 Sensitivity Analysis

A sensitivity analysis is performed for the three largest coefficients: supply line resistance, R_1; supply line inductance, L_1; and capacitance of the bladder, C. This analysis is intended to show how potential errors in the component measurements could affect the behavior of the system. It is assumed that in a controlled laboratory environment the values could be measured within 50% of the true values. Therefore, the measured values are perturbed by up to 50%, both alone and in combination, in order to determine if the controller can maintain the desired system parameters if the measured coefficients are innacurate but within tolerance. The remaining two parameters, R_2 and L_2, are comparatively very small and variation in these values will have little effect on the system. The measured values of R_1, L_1, and C are increased and decreased by 25% and 50%.

First, the sensitivity of the response to errors in the measurement of individual component coefficients is examined. Figures 5.13, 5.14, and 5.15 show the effect of changes to C, L_1, and R_1 by 25% and 50% in both directions. The changes have a small effect on the system response.
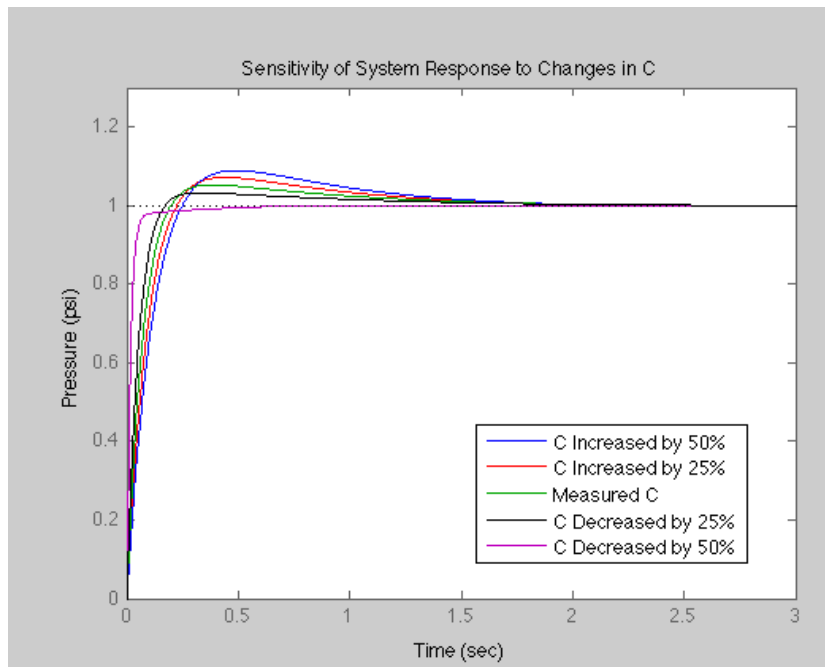
Figure 5.13. Sensitivity of transient response to changes in capacitance
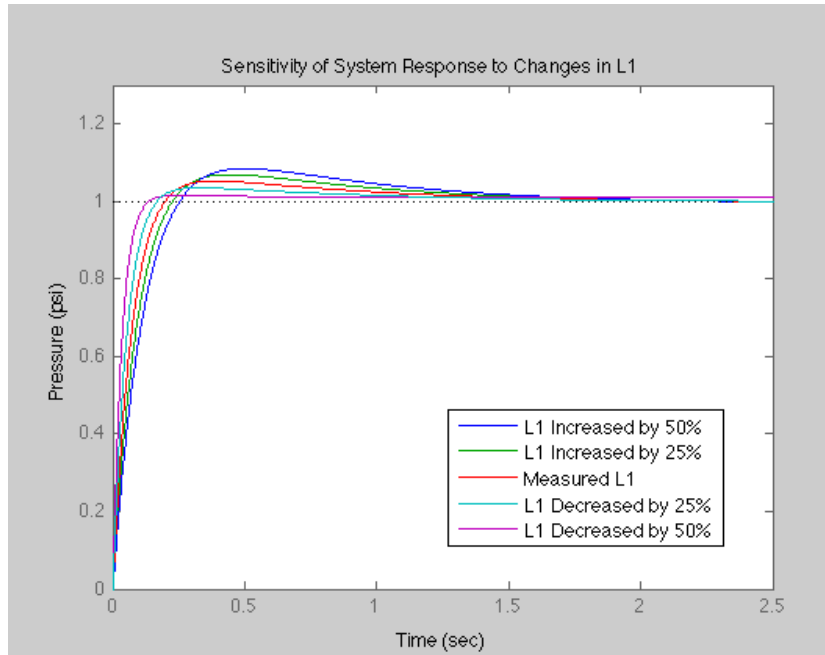
Figure 5.14. Sensitivity of transient response to changes in supply line inductance
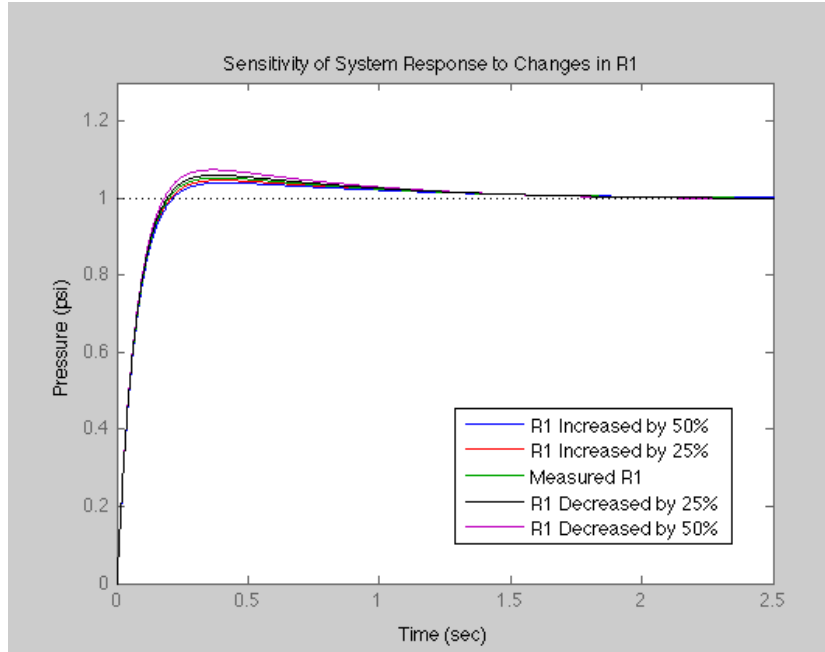
Figure 5.15. Sensitivity of transient response to changes in supply line resistance

An enlarged view of the overshoot and steady-state error for each of the figures is shown below. All system requirements are met in all cases. The worst case deviation in steady-state error occurs for the 50% decrease in the value of L_1. The steady-state error is less than 1%. For the purpose of this research, errors less than 1% can be considered negligible.
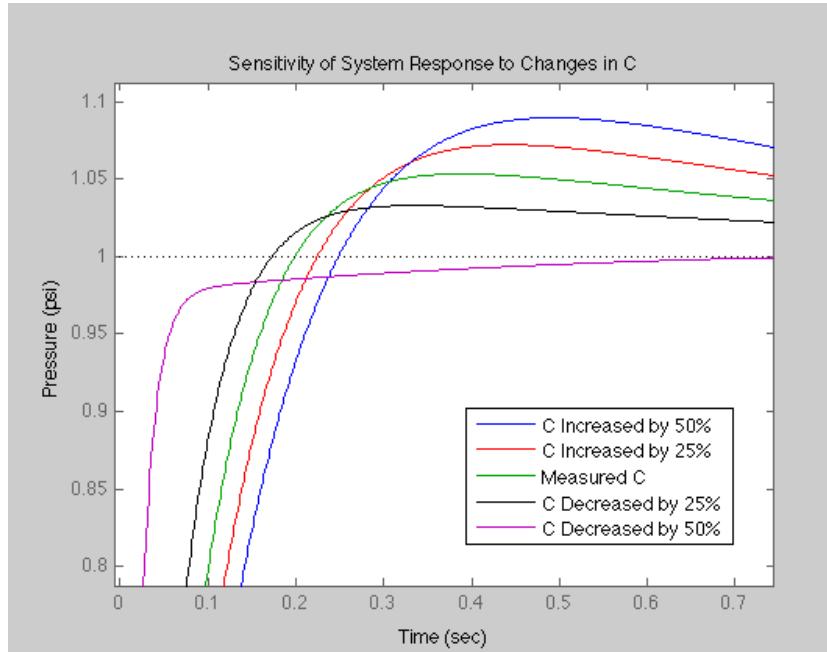
Figure 5.16. Enlarged view of sensitivity of overshoot to changes in capacitance
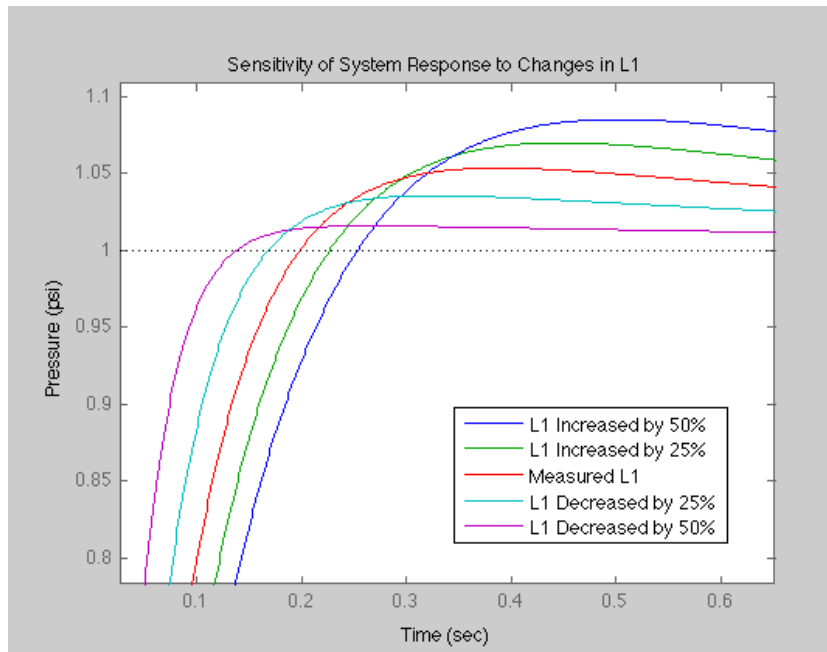
Figure 5.17. Enlarged view of sensitivity of overshoot to changes in supply line inductance

57
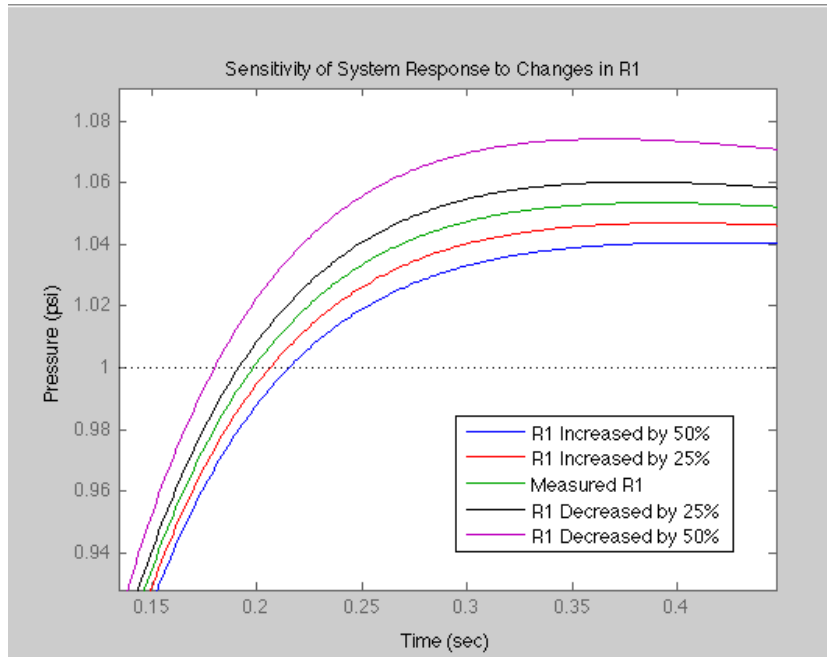
Figure 5.18. Enlarged view of sensitivity of overshoot to changes in supply line resistance
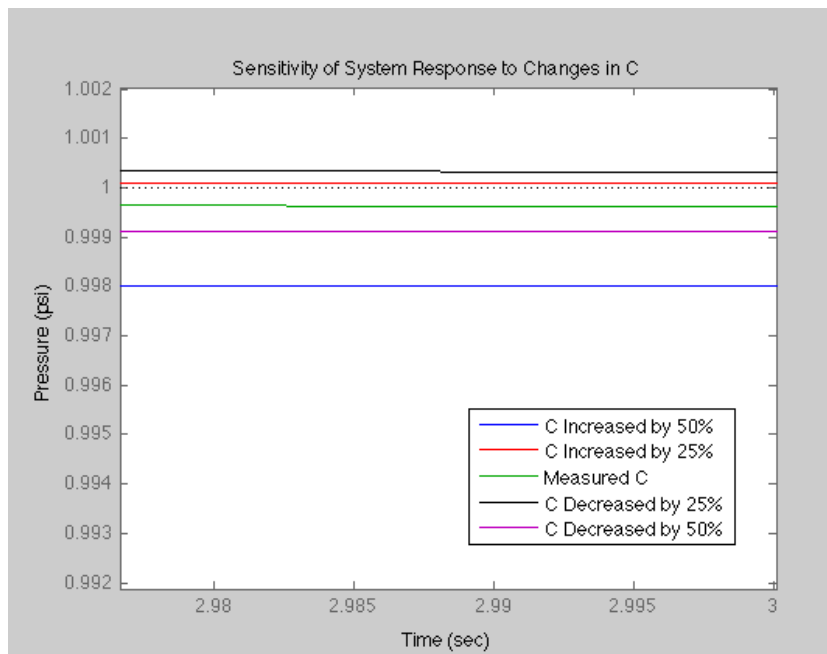
Figure 5.19. Enlarged view of sensitivity of steady-state error to changes in capacitance
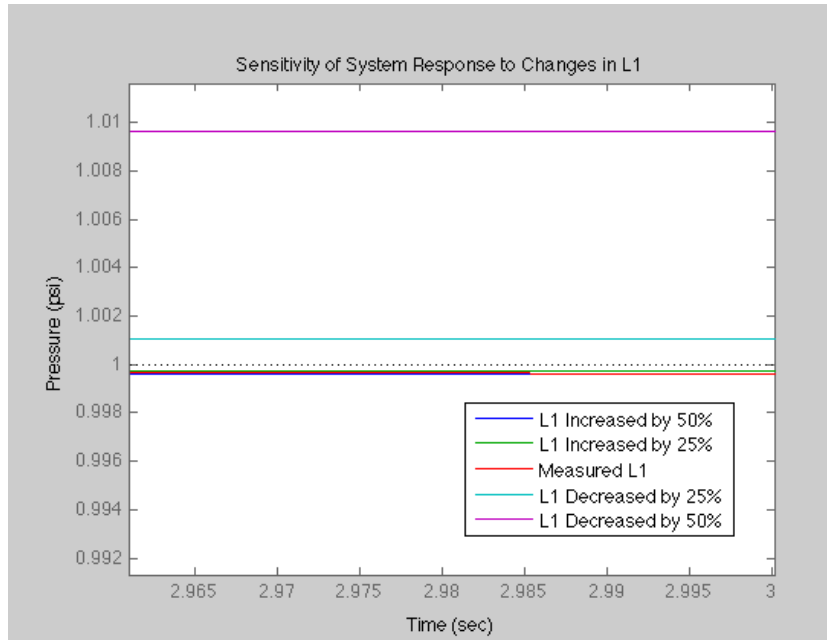
Figure 5.20. Enlarged view of sensitivity of steady-state error to changes in supply line inductance
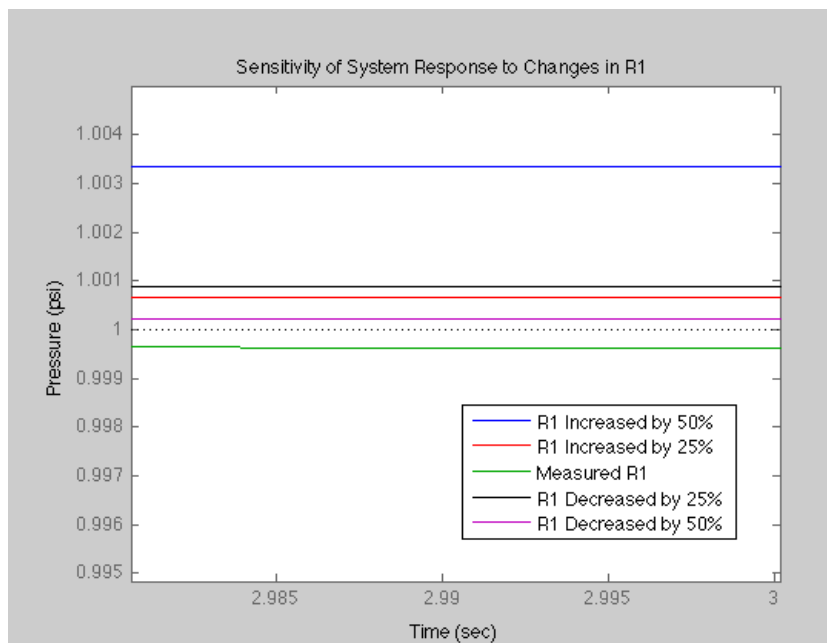
Figure 5.21. Enlarged view of sensitivity of steady-state error to changes in supply line resistance

The effect of variation of all parameters at once results in the plot in Figure 5.22. Even the worst case variation results in a settling time that is still well within the requirement. The overshoot reaches a maximum of 12%, slightly over the goal value of 10%.
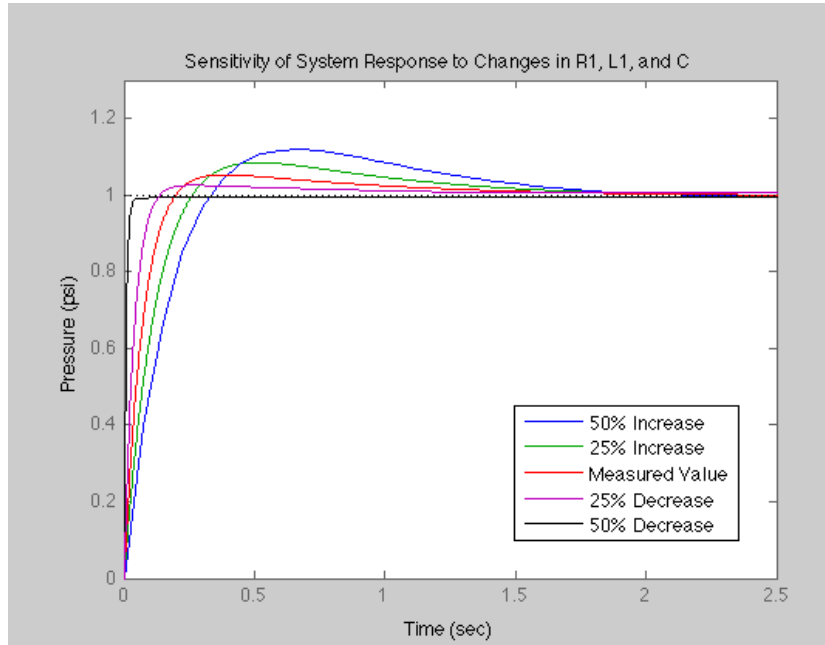
Figure 5.22. Combined effect of variation of C, L$_1$, and R$_1$

5.3 Configuration Options

The supply subsystem analyzed above contains all components necessary for the three configuration options: series, parallel, and hybrid. The layout and number of components are slightly different for each configuration, but all configurations contain one pump, five bladders, and five pressure sensors. The major difference between the three configurations is the airflow path used to supply the bladders. The parallel configuration supplies each bladder directly from the pump while the other two configurations use the exhaust of some bladders to supply others.

5.3.1 Series

In the series configuration the exhaust for each bladder is the input to the next bladder. The final bladder exhausts into the atmosphere. The are six solenoids, one valve before each bladder and one valve after the fifth bladder. Figure 5.23 is a schematic showing five bladders in series.
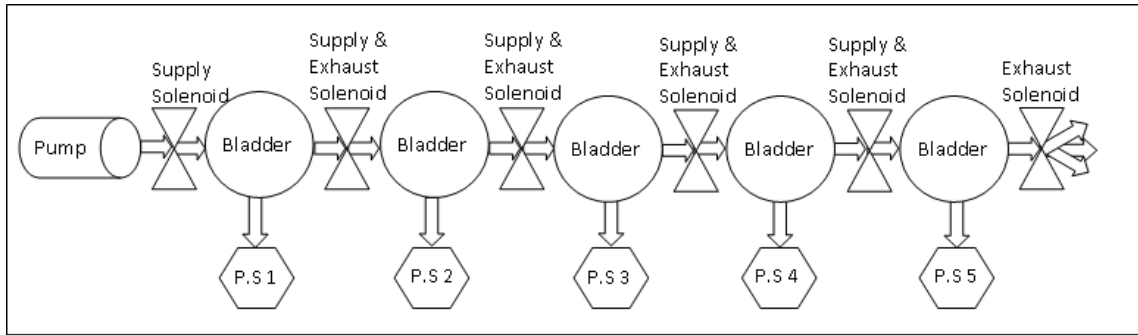
Figure 5.23. Five bladders in series

Transfer functions combined in series are multiplied together. The combined transfer function becomes increasingly complex with each subsystem added in series. To demonstrate the complexity, a comparison is made between the transfer functions of two subsystems and three subsystems in series. These transfer functions are presented in Equations 5.2 and 5.3.

$$\frac{P_o}{P_i} = \frac{s^2}{\alpha_1 s^6 + \alpha_2 s^5 + \alpha_3 s^4 + \alpha_4 s^3 + \alpha_5 s^2 + \alpha_6 s + \alpha_7} \tag{5.2}$$

$$\frac{P_o}{P_i} = \frac{s^3}{\beta_1 s^9 + \beta_2 s^8 + \beta_3 s^7 + \beta_4 s^6 + \beta_5 s^5 + \beta_6 s^4 + \beta_7 s^3 + \beta_8 s^2 + \beta_9 s + \beta_{10}} \qquad (5.3)$$

Controllers for two subsystems in series, three subsystems in series, and five subsystems in series are designed. For each controller there is one more integral controller than the number of 's-terms' in the numerator. This is to cancel all the zeros at the origin plus add a system integrator to achieve zero steady-state error. This is the reason for more integrals for a higher number of systems in series. Also, each controller has gain and derivative control. The hybrid configuration discussed later in the chapter is made up of two and three subsystems in series. The series configuration under consideration is made up of five supply subsystems in series.

The Ziegler-Nichols method is a good approximation to determine values for K_p, T_i, and T_d for systems which are always stable, such as the single supply subsystem. When two or more of these subsystems are connected in series, they have a tendancy to become unstable, as can be seen in Figures 5.24 , 5.25, and 5.26. Therefore, the Z-N first method is not expected to yield accurate results. However, this method can still be useful in understanding the controller characteristics that are needed. For example Figure 5.27 shows how the Z-N first method curve changes with more subsystems in series. The 'L' value increases as subsystems are added. This trend, along with the K_p, T_i, and T_d values used in the single supply subsystem, is used to aid the trial and error approach for determination of the K_p, T_i, and T_d values for two, three and five systems in series.
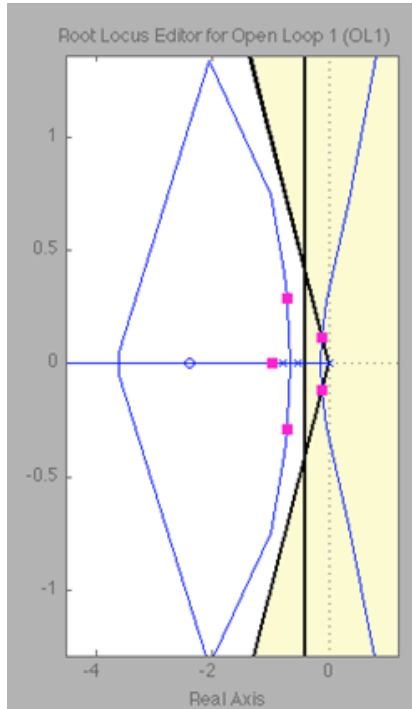
Figure 5.24. Root locus of two subsystems in series with PIDII control
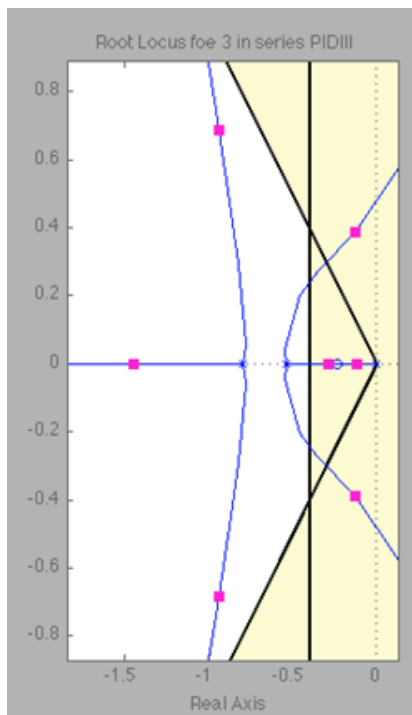
Figure 5.25. Root locus of three subsystems in series with PIDIII control
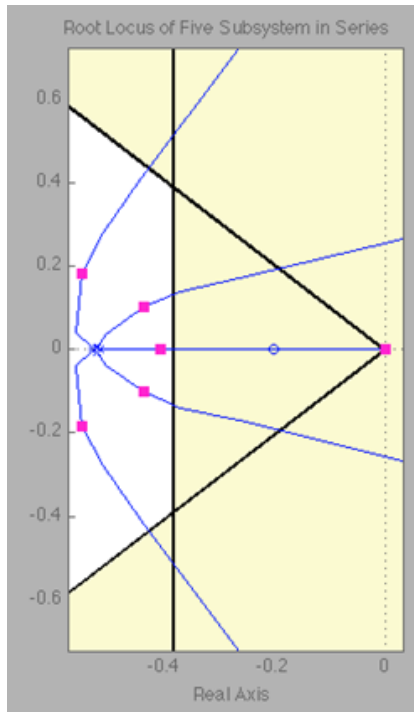
Figure 5.26. Root locus of five subsystems in series with PIDIIIII control
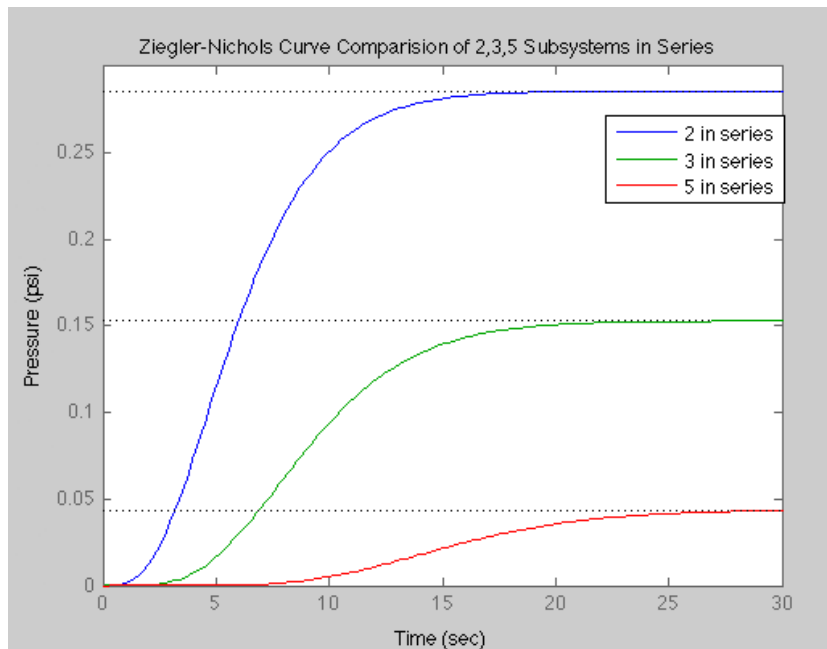
Figure 5.27. Root locus of two subsystems in series with PIDII control

From the root locus plots in Figures 5.24 , 5.25, and 5.26 it is clear that settling times less than 10 seconds are unachievable for two, three, and five subsystems in series. However, an overshoot of less than 10% is possible. Figure 5.28 is a comparison of the the transient responses for two, three and five subsystems in series. In each plot the overshoot is within the design parameters, but a higher number of systems in series results in longer settling times.
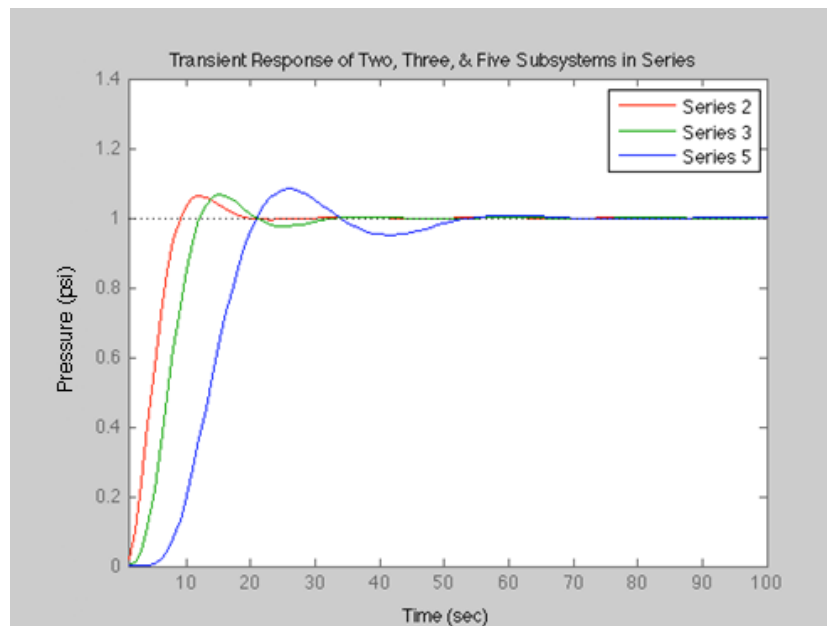
Figure 5.28. Comparison of 2, 3, and 5 supply subsystems in series

Increasing the number of subsystems in series increases the complexity and effect a single controller has on the overall system. Five supply subsystems in series have a much longer settling time and more integrators than only two subsystems in series. However, for just two subsystems in series, the design parameters are not met. The addition of subsystems in series causes the output to become more difficult to control. Because the input to each downstream bladder is the output from the previous bladder, any oscillation or overshoot is amplified, thus making it increasingly complex to control. Controllers placed between the bladders could be used to smooth the

flow and mitigate this amplification effect. However, this would result in a significant increase in controller complexity.

5.3.2 Parallel

The parallel configuration (Figure 5.29) is very similar to the single supply subsystem. The path of air from the pump to an individual bladder is the same. Because the bladders are supplied from a single source in parallel configuration, the transfer functions for each subsystem are added. This results in a transfer function of the same form as the supply subsystem but with different coefficients. The controller can be designed in the same way and the resulting root locus and transient response are shown below in Figures 5.30 and 5.31.
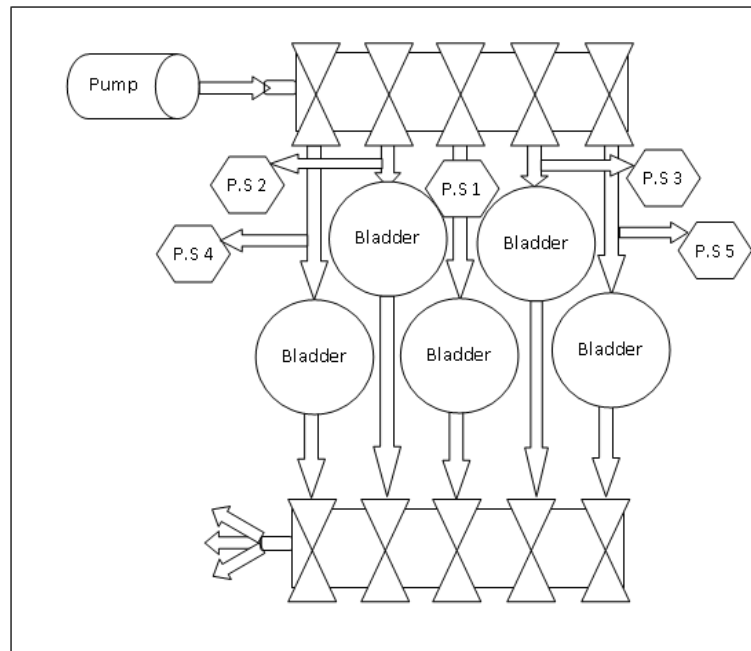
Figure 5.29. Schematic of the five subsystems in parallel
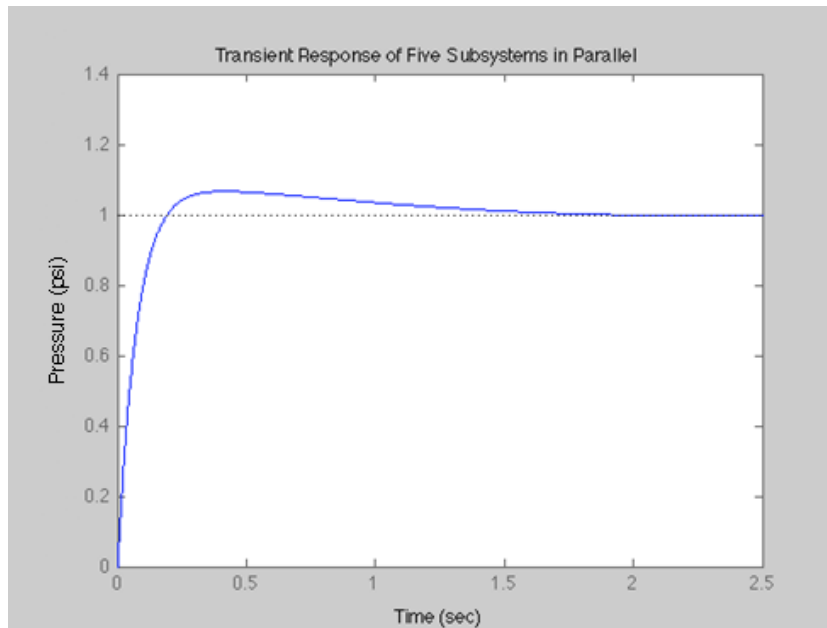
Figure 5.30. Transient response of five subsystems in parallel
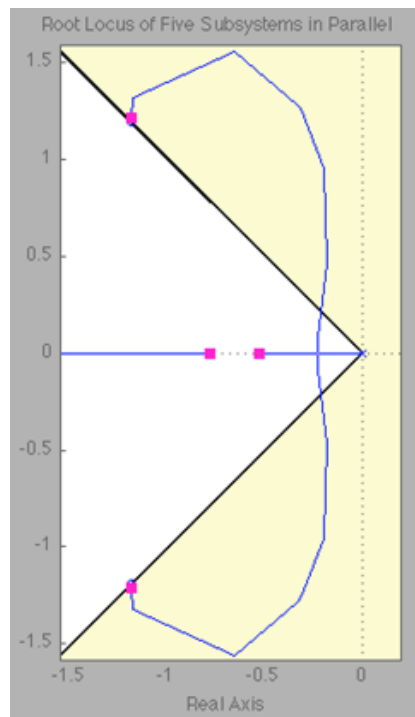
Figure 5.31. Root locus of five subsystems in parallel

67

One important issue with the parallel configuration is the mass flow rate of the pump. Although the pump will supply a constant pressure no matter which of the valves to the bladders are open, it can only supply air up to a maximum mass flow rate, listed as 3.5 $\frac{in^3}{s}$. If multiple bladders require airflow at the same time, the supply from the pump is split between the bladders and the pump must be able to supply air at the necessary flow rate. In the supply line inductance test described in Section 3.4.2, a worst case condition was tested. Here, the flow rate from the pump into a supply line at atmospheric pressure was measured. The maximum tested flow rate was 0.3 $\frac{in^3}{s}$. If all five bladders require air supply at the same moment, a total of 1.5 $\frac{in^3}{s}$ would be required. The pump is able to supply more than double this amount, so it is deemed sufficient.

5.3.3 Hybrid

The hybrid configuration is a combination of the parallel and series configurations. Three subsystems are connected in series, and these are placed in parallel with a group of two subsystems in series (Figure 5.32). The transfer functions of the three subsystems in series are multiplied together. The result is added to the product of two subsystems. The controller for the hybrid configuration is determined in a similar manner as the controller for two and three subsystems in series. Figures 5.33 and 5.34 represent the root locus and transient response for the hybrid configurations.
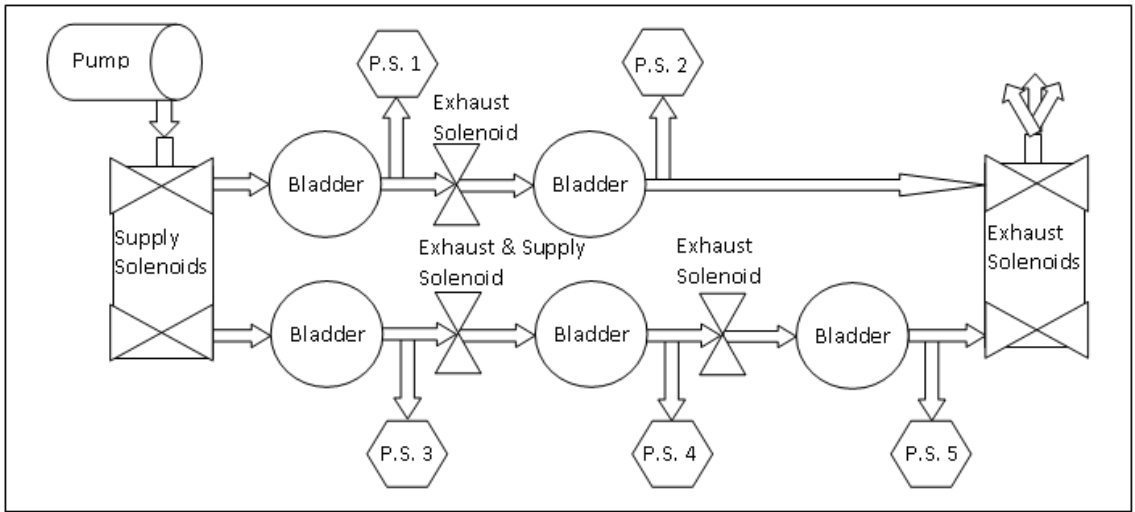
Figure 5.32. Schematic of the hybrid configuration
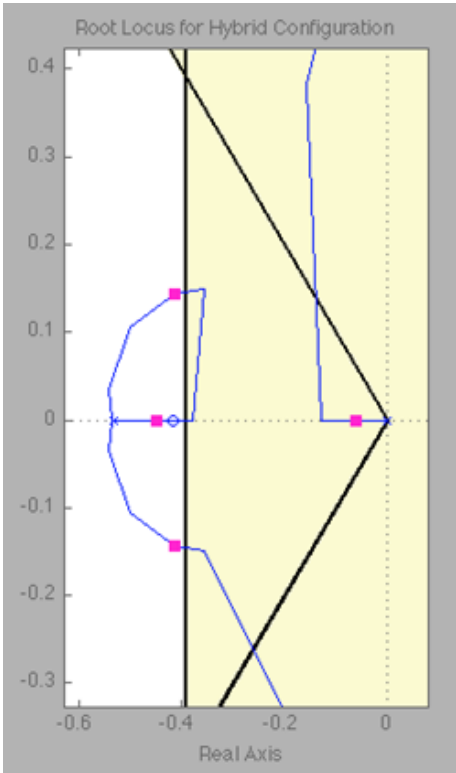
Figure 5.33. Root locus of the hybrid configuration

69
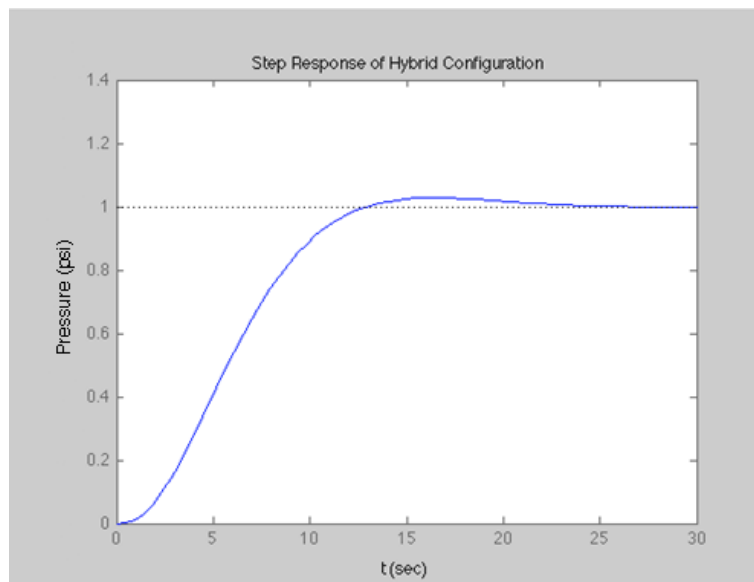
Figure 5.34. Transient response of the hybrid configuration

Chapter 6

Performance Analysis and Implementation

The parameters used to measure performance in this research are settling time, overshoot, and steady-state error. The target values for each are discussed in Section 4.3 and shown in Table 4.1. The results of Chapter 5 show that all three system configurations can be controlled to reach the desired pressure set point without exceeding the maximum allowable overshoot of 10%. However, the systems do not all settle within 10 seconds. The parallel configuration settles in less than 10 seconds. The series configuration settles at 90 seconds and the hybrid configuration settles at 40 seconds. Figure 6.1 compares the transient response of the three configurations and Figure 6.2 is a close up of the overshoot for the three configurations. The three performance parameters calculated for each of the configurations are displayed in Table 6.1.
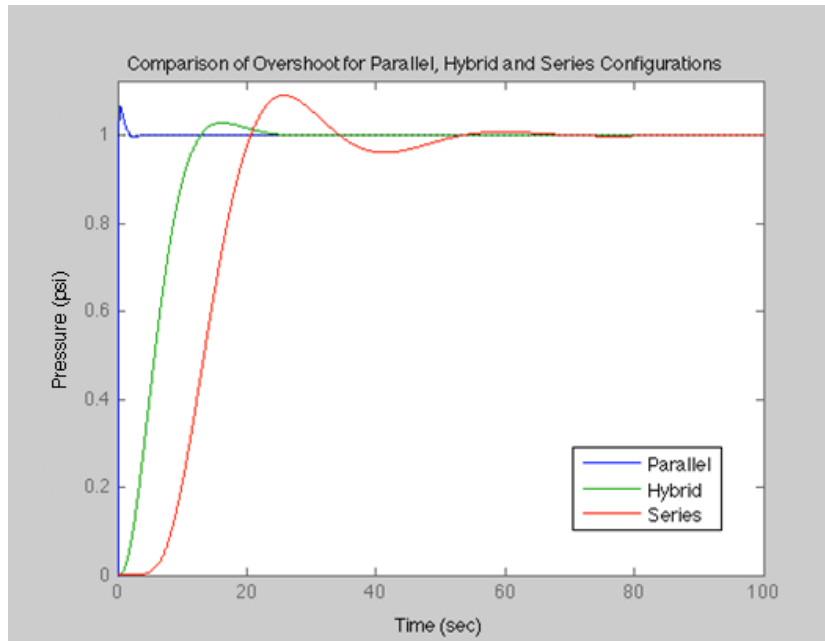
Figure 6.1. Comparison of hybrid, series and parallel configurations
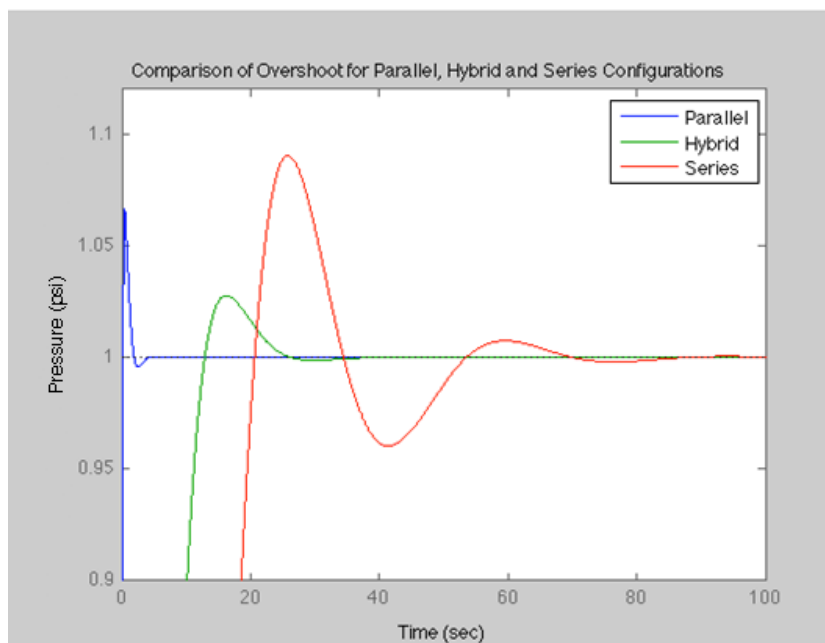
Figure 6.2. Enlarged view comparing differences in overshoot between hybrid, series and parallel configurations

72

Table 6.1. Comparison of Performance Between Three Configurations

	Settling Time (seconds)	Overshoot (%)	Steady-State Error (%)
Parallel	7	7	0
Hybrid	40	3	0
Series	90	9	0

Performance is the most important of the three design attributes. If the system requirements cannot be met, then the complexity and cost of the design are of only small concern. But complexity and cost should not be ignored once potential solutions are identified. Variations in controller complexity are related to the complexity of implementation of the controller rather than controller design. Since the Active Cast is intended to allow a person to maintain mobility while using the device, the footprint for each configuration can represent the cost of the potential solution.

The controller designed in this research is insufficient for the series configuration to meet the design specifications. For the performance listed in Table 6.1 the controller requires six integrators, more than the parallel or hybrid configurations. The most complex portion of the controller is the implementation of the control. Since the air supplied to each bladder after the first is the exhaust from the previous bladder(s), a great deal of logic is required. For instance, in order to supply air to the fourth bladder solenoids one through four must be open while solenoids five and six remain closed. If the first bladder becomes over pressurized in the process, solenoids two through six must open to exhaust it while solenoid one must be closed. The total number of logic sequences required to completely define every possible combination of on/off is the number of positions for each solenoid, two, raised to the power of the total number of solenoids. In the series configuration there are six solenoids, resulting in 64 (2^6) possibilities. The controller must be programed for each potential

73

sequence. If multiple variances occur at the same time, such as increased pressure in bladder two but under-inflation of bladder four, the conflicting solutions to these simultaneous problems result in further complication to the programming.

Each bladder is always in one of three states: filling, exhausting, or no change. There are five bladders, so at any giving time there are 243 possible situations (3^5). There are 64 different possible solenoid states. There are 179 more situations than solenoid states so there is some overlap, where one state will apply in more than one situation. A simple example of this would be when the last two bladders are both over-pressurized. Solenoids one through four should be closed and solenoids five and six are both open. This logic sequence for is also the solution for bladder four over-pressurized and bladder five on target. In order to completely define the controller, he 64 states must be mapped across the 243 situations.

The benefit of the series configuration is the small footprint of the components. There are only six solenoids in the series configuration, which is less than the parallel or hybrid. Thus, the spatial cost of choosing the series configuration is better than either of the other two configurations. Another benefit to the series configuration is that all the air from the pump flows into one bladder, so flow rate of the pump is less of a concern with bladders in series than parallel or hybrid.

The response of the hybrid configuration under PIDIII control is discussed in Section 5.3.3. The desired pressure set point can be met without exceeding the maximum overshoot, but the time required to reach the desired pressure is four times longer than desired: 40 seconds rather than 10. The hybrid configuration shares the series configuration strength of a low number of components. Because the solenoid controlling the exhaust of a bladder may also control the supply of another bladder, fewer solenoids are needed, in this case seven. The hybrid configuration represents an engineering tradeoff between spatial cost and control complexity. Although the spatial

cost is relatively low, this configuration shares some of the control complexity of the series configuration. While the addition of bladders in series increases the spatial cost linearly, the control complexity is affected exponentially. As with the series configuration logic sequences are required for every possible combination of opened or closed solenoids. The hybrid configuration requires 24 logic sequences to completely define every possible on/off scenario. Although there are more solenoids than the series configuration, there are fewer logic sequences required because three of the solenoids are independent from the other four.

The parallel configuration has the best performance of all. This configuration is the only one to meet all three design requirements. Additionally, parallel control is the least complicated to implement. Each bladder is independent of the others, so detailed logic sequences are not required. Although there could be some controller implementation complexities for large disturbances, this would be true for all configurations. The parallel system is the least complex to implement.

The best configuration is chosen based on a weighted decision matrix. In each category, the best configuration is given a score of 100. The other configurations are scored relative to the leading configuration. Performance is the highest in importance and given weight of 0.75. Additionally, components must be portable and compact enough to fit on the cast or the solution is of little value. These spatial factors are shown here as spatial cost. Because all configurations can fit on the cast, the weight for the cost is relatively low. The complexity of each configuration is based on the complexity of implementation. Table 6.2 shows the results of the decision matrix with the parallel configuration as the chosen solution.

Table 6.2. Weighted Decision Matrix

Options	Performance	Cost	Complexity	Rank
Weight Factor	.75	.15	.1	1.0
Parallel	100	70	100	95.5
Hybrid	80	90	60	79.5
Series	60	100	40	64

6.1   Model Adjustments

The controller designed for the parallel configuration in Section 5.3.2 is not constrained by use of any realistic pressure source. It uses a very high gain, 153 psi, in order to reach the desired setting value in a very short time. However, in order to use the controller in a physical system, the gain required by the controller must be supplied by an actual pressure source. While 153 psi is certainly achievable using large equipment in a laboratory environment, it is not feasible for a mobile device that is worn by a patient. Therefore, the controller must be adjusted in order to find a gain that will meet the design requirements and can be produced by an available pump. Figure 6.3 displays the response of the system under PIDI control with K_p varied from the ideal value of 153 down to 7. Note that for clarity the effect of K_p on K_d is cancelled so that only K_p and K_i are changed. The smallest K_p value with a settling time within 10 seconds is 14 psi (within 1.5%). This is roughly equivalent to the output of the pump used in characterization of the pneumatic system components (14.5 psi). Therefore the pressure output of this pump is sufficient to control the system response within the desired system parameters. A modification of the Ziegler-Nichols T_d value from 2 to 6 further improves system response with the reduced gain. The transient response of the system with 14 psi (Figure 6.4) has a 10% overshoot and settles within 1.5% of the desired zero steady-state error in 10 seconds. This transient response acceptably meets the desired parameters.

76
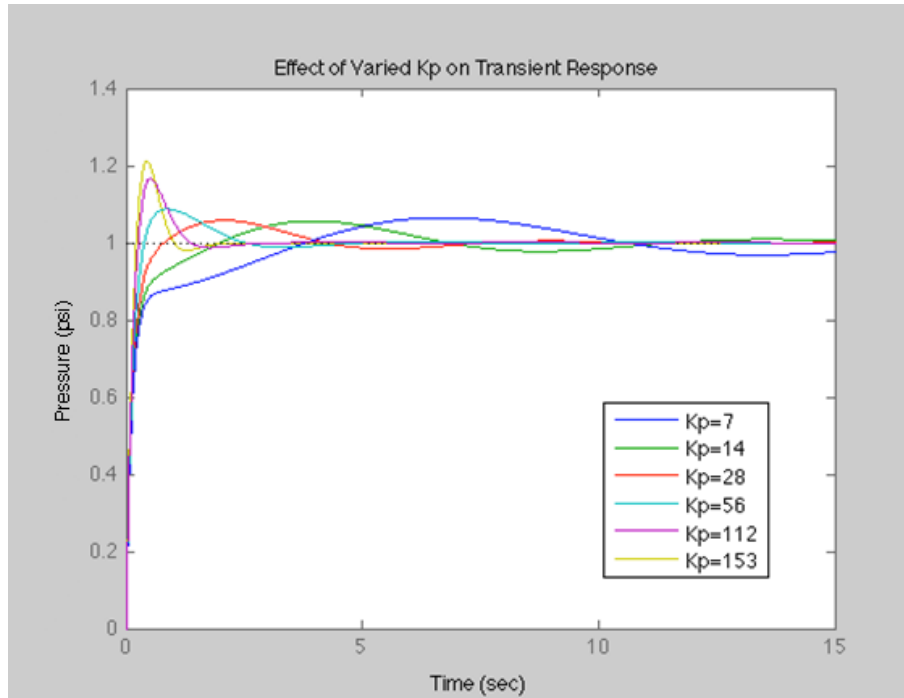
Figure 6.3. Transient response with varied K$_p$
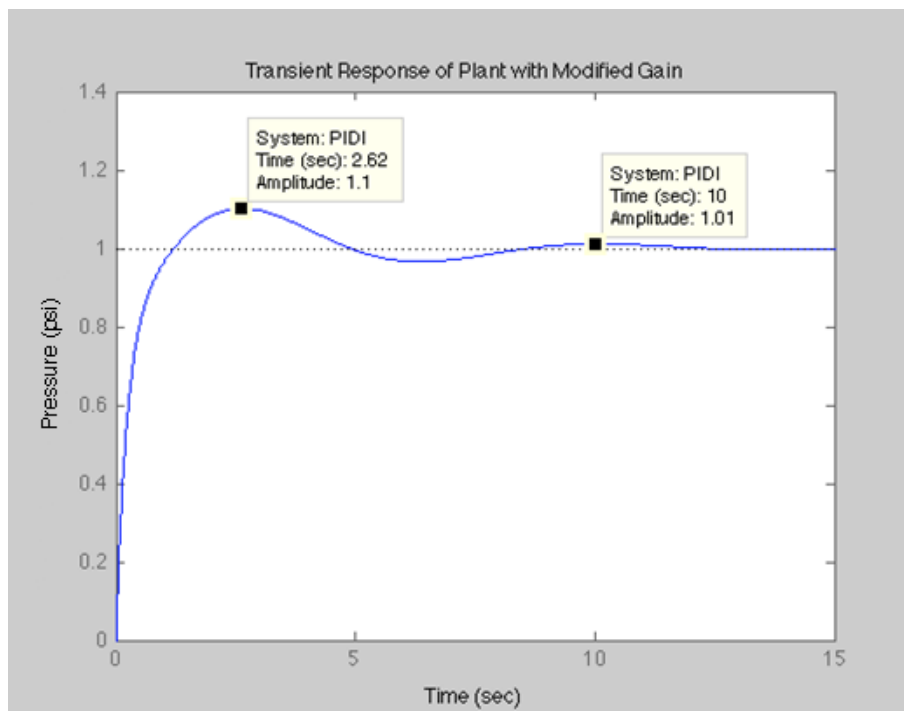
Figure 6.4. Transient response of plant with PIDI control and 14 psi input

77

6.2 Validation

Before implementing the PIDI controller, the model of the supply subsystem is evaluated against the equivalent physical system to determine model confidence. The physical system has a gain of 14.5 since the desired output is set to 1 psi and the pump pressure is 14.5 psi. For this validation exercise, feedback control is not included in either the mathematical model or the physical system. The model gain is adjusted to match the physical system gain of 14.5.

Some assumptions must be made in order to match the mathematical model to the physical system. The presence of an 's' term in the numerator of the transfer function in the mathematical model has a gross effect on the system behavior. The predicted response of the mathematical model with the 's' term is not similar to the physical system. This term represents the inductance of the bladder and has a much smaller coefficient than the other terms in the transfer function (much smaller than 1). Because the coefficient is so small this term can be assumed to be zero [34]. Additionally, when testing the physical system, there is some delay in the response as the air bladders are expanded to reach their full volume. The bladder begins the experiment fully collapsed (for repeatability). As air initially flows into the bladder, the volume increases until it reaches the nominal value. During this time the pressure in the bladder remains essentially at atmospheric. The bladder has no mechanism to hold elevated pressure until it reaches full volume allowing surface tension to resist the internal pressure. By the time the bladder has reached nominal volume the inductance of the bladder has been overcome. Figure 6.5 shows pictures of three separate test runs which demonstrate this behavior. In each of these, it takes roughly 8.2 seconds for the pressure in the bladder to begin to rise, by which point the inductance is fully overcome. This gives further justification for removing the 's' term .
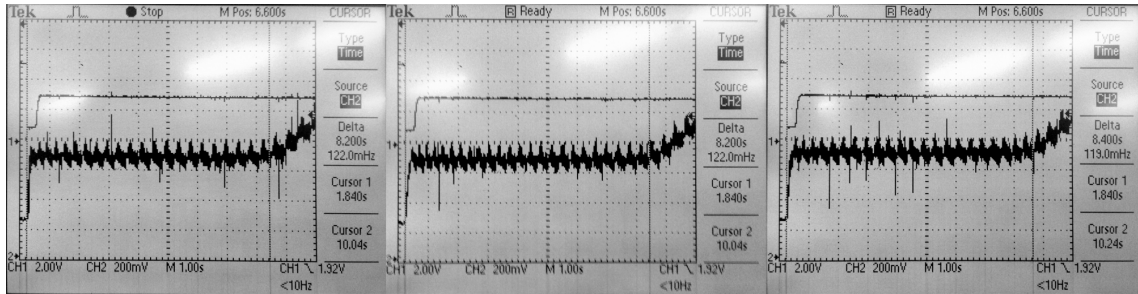
Figure 6.5. Three measurements of physical system transient response with 14.5 psi input

Figure 6.6 is the open loop response of the modified transfer function with a gain of 14.5 psi. The model rises to 1 psi in 0.96 seconds where in the physical system the pressure rises to 1 psi between 1.5 and 2 seconds. Three different tests of the physical system confirm this result. Figure 6.7 is the result from the schematic seen in Section 3.4.3 used to determine pressure for the capacitance coefficient. In this test the bladder rises to 1 psi in 2 seconds. The second test verifying this result is from the R_2 coefficient test (Figure 6.8). In this test the physical system reaches 1 psi in 1.75 seconds. The final test is the setup of a single subsystem with supply and exhaust solenoids and one pressure sensor, seen in Figure 6.9. The result of this test (Figure 6.10) shows the bladder reaching 1 psi in 1.63 seconds. These three tests show similar results despite the slightly different configurations. The physical system with 14.5 psi input reaches 1 psi in an average of 1.79 seconds. This is very close to the model prediction of 0.96 seconds. The model represents the physical system well for a pressure range of 0 to 1 psi.
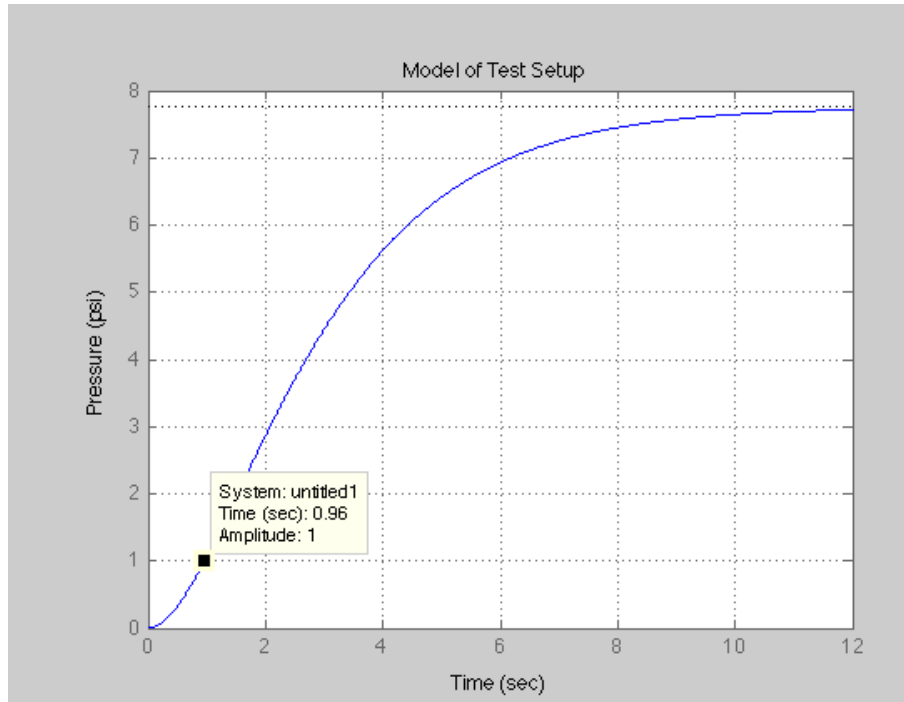
Figure 6.6. Transient response of open loop modified plant and 14.5 psi input
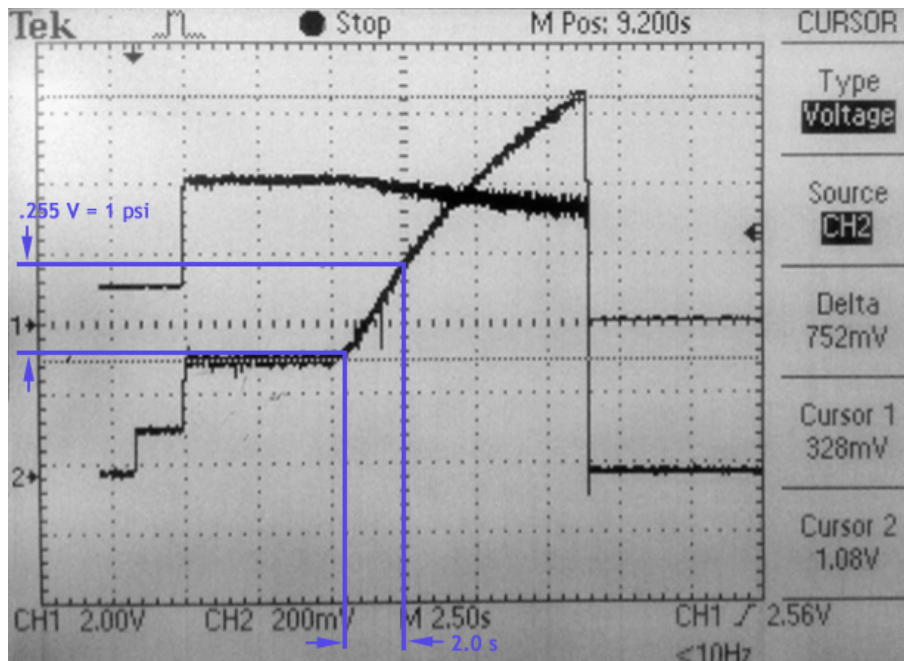
Figure 6.7. Result from capacitance coefficient test
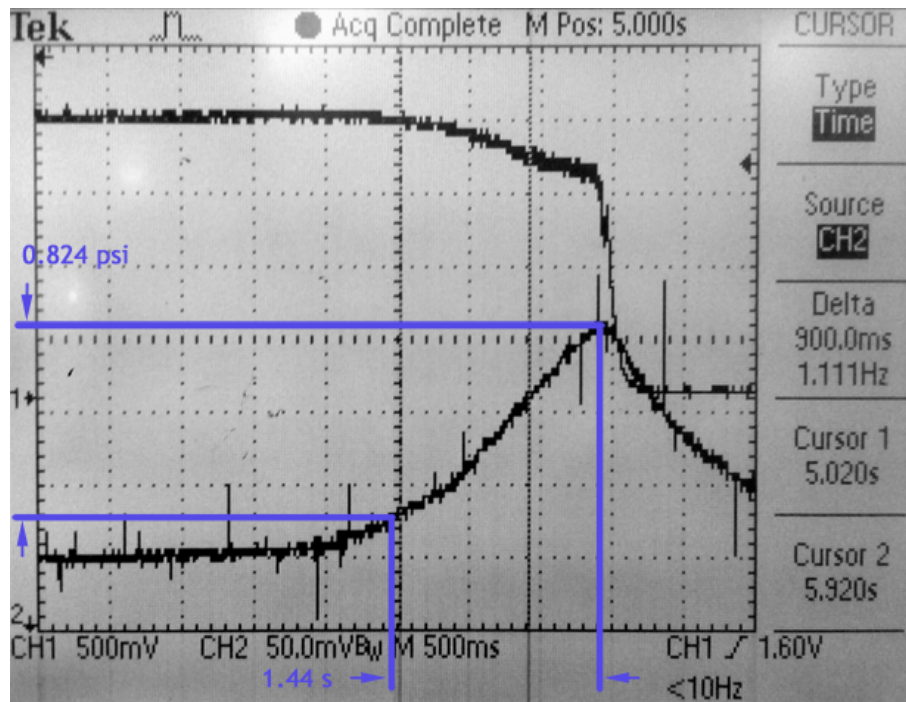
Figure 6.8. Result from R$_2$ coefficient test
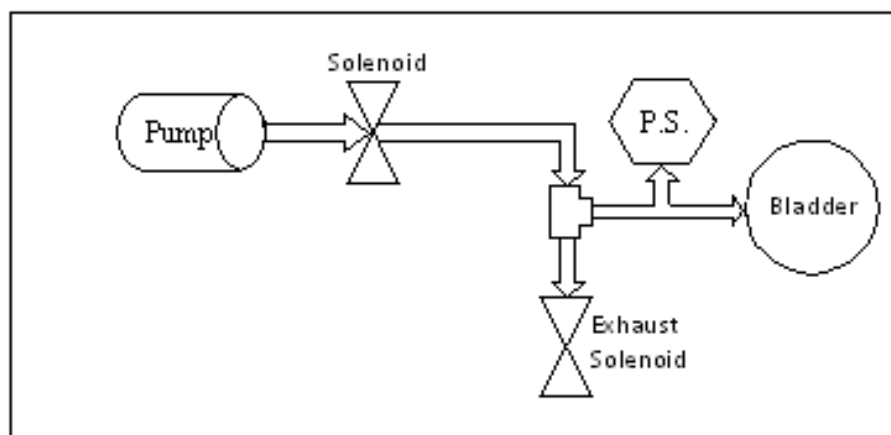
Figure 6.9. Schematic of test setup of single supply and exhaust subsystem combined
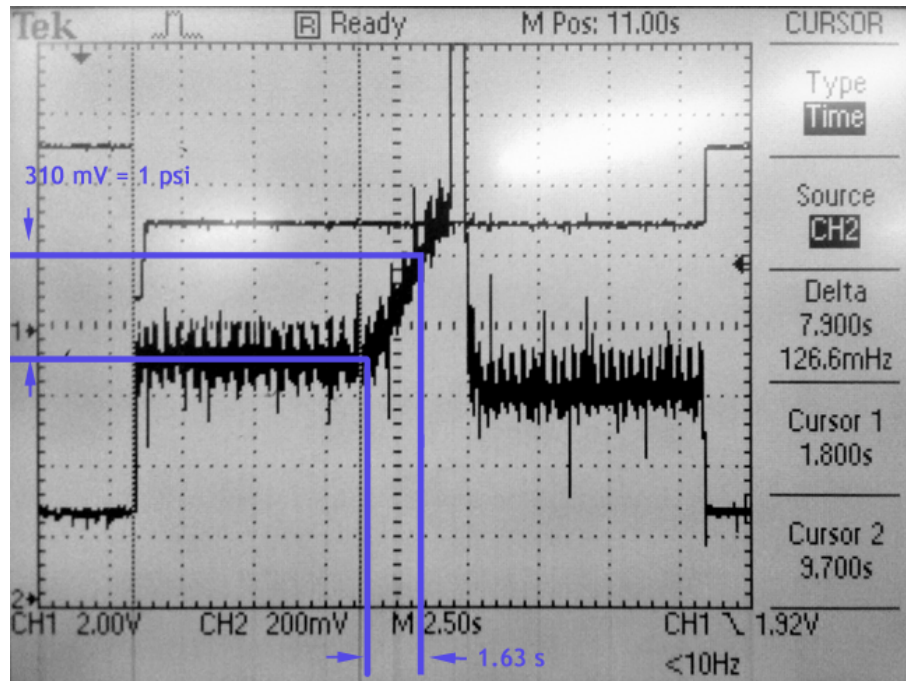
Figure 6.10. Physical system with supply and exhaust solenoids

6.3. Implementation

The controller driving function modifies the input signal to the plant in order to generate a desired response from the plant. The signal which the controller feeds to the plant is the ratio of controller output to system input with the plant included in the feedback path (Figure 4.3). This function is referred to as the driving function, Equation 6.1. Calculation of the controller function requires modification of the closed loop block diagram in Figure 4.3 to look like the block diagram in Figure 6.11.

$$\frac{P_o(s)}{P_i(s)} = \frac{Controller}{1 + Controller \cdot Plant} \tag{6.1}$$
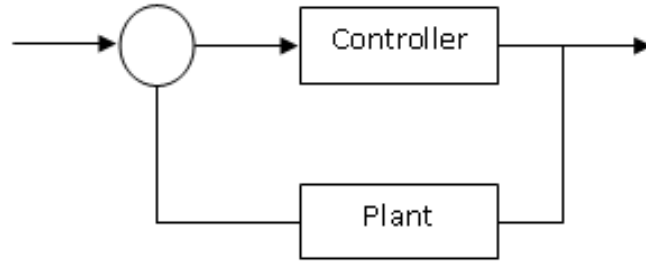
Figure 6.11. Controller Function Block Diagram

Combining the transfer functions of the controller and the plant into Equation 6.1 yields the result seen in Equation 6.2. This can be simplified to Equation 6.3. The driving function is plotted in Figure 6.12.

$$\frac{P_o(s)}{P_i(s)} = \frac{0.07s^7 + 52.12s^6 + 110.7s^5 + 127s^4 + 83.64s^3 + 21.08s^2}{0.004s^7 + 3.08s^6 + 15.87s^5 + 10.72s^4 + 11.27s^3} \qquad (6.2)$$

$$\frac{P_o(s)}{P_i(s)} = \frac{0.048s^6 - 157.69s^5 - 54.29s^4 - 106.96s^3 + 21.08s^2}{0.004s^7 + 3.08s^6 + 15.87s^5 + 10.72s^4 + 11.27s^3} \qquad (6.3)$$
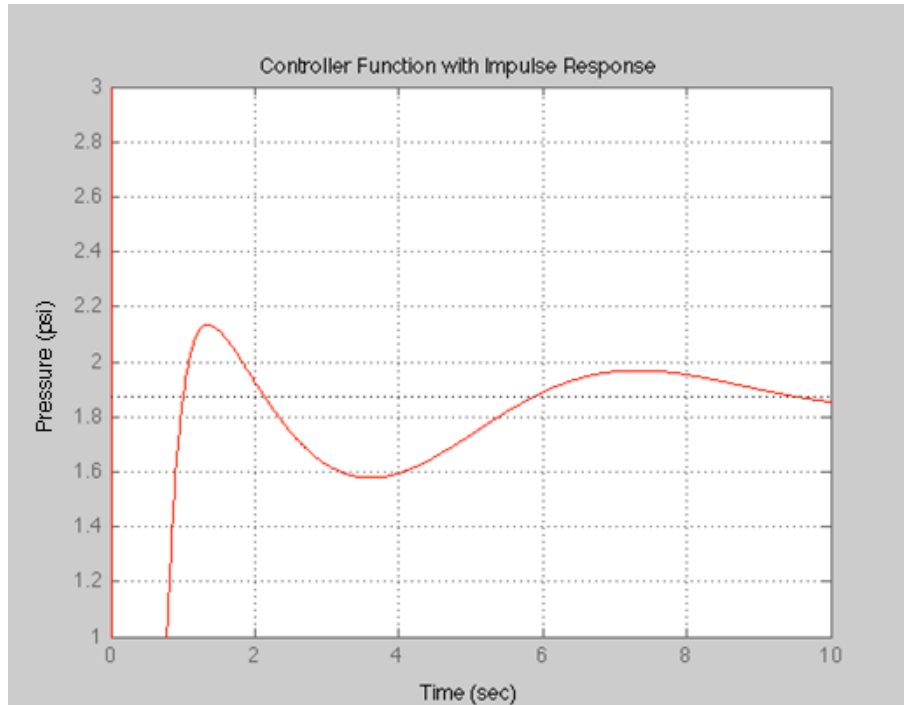
Figure 6.12. Controller function for modified model

The driving function modifies the input pressure over time in order to reach the desired value quickly. Figure 6.13 is a comparison of the controller driving function and the plant transient response. The maximum amplitude of the controller driving function occurs around 1 second. As expected, the transient response lags a little more than 1 second behind, reaching its maximum overshoot at 2.6 seconds. Note that the steady state value of the driving function is higher than the steady state value of the transient system response. Just as voltage drop across a resistor will result in lower voltage, so does the pressure drop across a pneumatic component result in lower pressure downstream. The control must compensate for this loss by supplying a higher pressure than the desired bladder pressure. A ratio of 1.87 is seen between the steady state value of the driving function and the transient response. (Note that this ratio is also seen in the final value of Figure 6.6, 7.75 psi, compared to 14.5 psi input.)

84
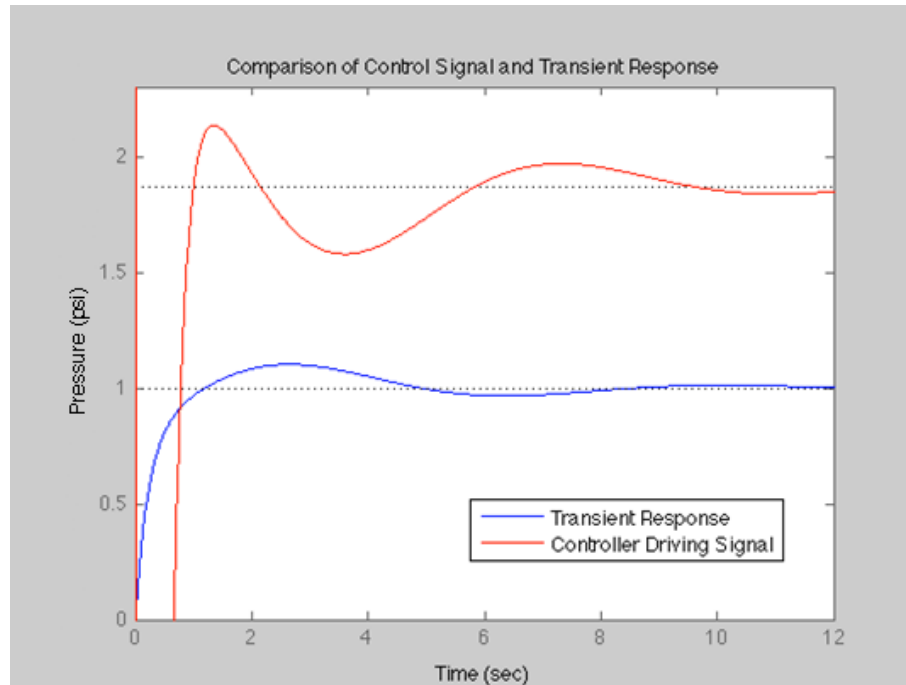
Figure 6.13. Comparison of control signal and transient response

As described above, the controller function changes the input pressure of the pump over time. However, the pump used in this research does not provide variable output. Instead, a duty cycle approach is used. Initially the pump is turned on for 8.2 seconds to allow the bladders to fill with air until the surface tension gives resistance. Then the pump is pulsed for $\frac{1}{8}$ second and turned off for 400 ms. In order to determine when the bladder has reached the desired pressure, the pressure sensor is monitored throughout the experiment. However, because the sensor is not located in the bladder but rather in a branch of the tubing connecting the bladder to the pump, the sensor will only give an accurate result at steady state, when the pump is off. Therefore this must happen during the low period of the duty cycle. The pressure sensor measurements are fairly noisy, so five samples are averaged in order to produce one measurement. This process of measuring the pressure requires 250 ms. Additionally, the solenoids

85

require 150 ms to complete a cycle bringing the required low time for each duty cycle to 400 ms.

This duty cycle approach results in the pump running for 23% of the full cycle. Assuming the system responds linearly to this input, the effective input to the plant would be about 3.22 psi. Figure 6.14 is the result of a test run with this duty cycle. It takes roughly 12.5 seconds for the bladders to reach 1 psi. The solenoid is opened and closed 23 times. The pressure in the bladder reaches .992 psi. This can be contrasted against the response of the system to the ideal controller (Figure 6.13). The transient response of that system shows the bladder reaches .992 psi in about 1.16 seconds but rises past this value. The pressure levels off between .992 psi and 1 psi as quickly as 8.14 seconds.
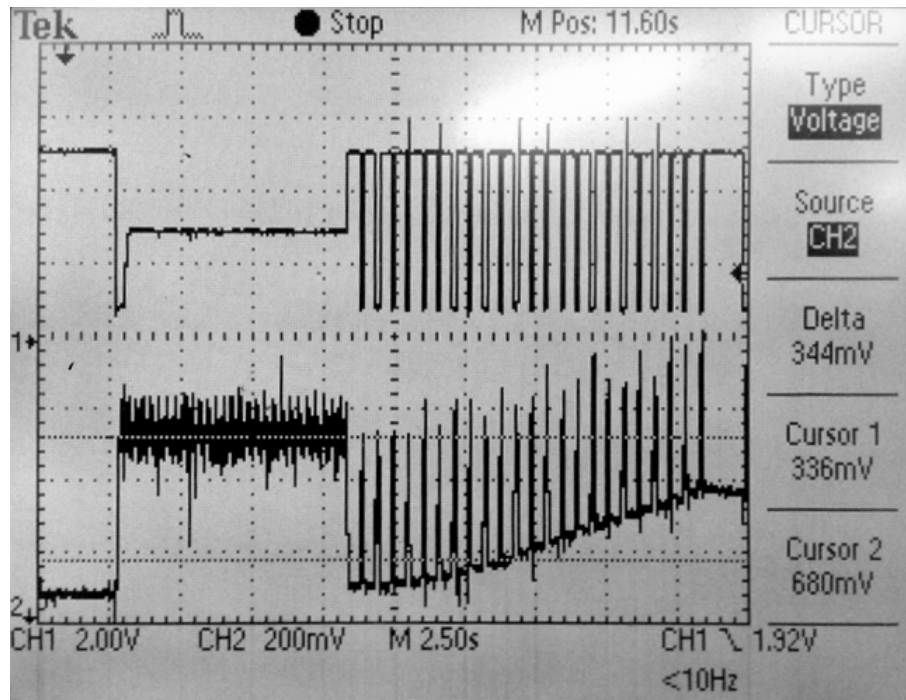
Figure 6.14. Duty cycle solenoids opened 23 times

There are many differences between these two approaches. The controller strictly modifies the input pressure to achieve 1 psi quickly with minimal overshoot. The

duty cycle approach is designed to produce a single effective pressure continually. The expected pressure output of the duty cycle is a higher value for a longer period of time than the mathematical controller. However, the duty cycle takes about 7 seconds longer to reach 1 psi than the mathematical controller. These results suggest that a typical duty cycle approach is not straight forward for a pneumatic pump. This may be a result of the relatively long rise time of the pump, observed to be approximately $\frac{1}{4}$ second, accounting for a significant portion of each pulse. Also, the compressibility and inertial effects of the air in the system must be overcome with each pulse, and the repetitive effects of these phenomena are not accounted for. Additionally, this indicates that varying the duty cycle to meet the demands of the driving function may not produce the expected result either. When the driving function must be varied by more than $\frac{1}{2}$ psi over 2 seconds, the $\frac{1}{4}$ second rise time will obviously limit the accuracy of the output.

Since the mathematical controller pumps air into a bladder continuously, the inertial effects only need to be overcome once. It appears from the comparison above that this approach greatly reduces the time it takes to get the bladder to the desired pressure. This approach, however, cannot be implemented since the bladder pressure can only be read when the pump is off and the pressure is at steady-state. Therefore, a modified duty cycle approach is taken. The controller driving function is used as a guideline in order to modify the duty cycle to reduce the number of times the pumped is cycled off and back on. The first pulse is equal to the time it takes the mathematical model to reach 90% of the settling value, .925 seconds. The next pulse is about half this value, .45 seconds, and the third and subsequent pulses are half again, .225 seconds.

The long pulse at the beginning of the process allows the pressure in the bladder to rise quickly, reducing settling time (similar to the ideal controller signal). The pulse

87

width must be short as the bladder pressure approaches the desired pressure. If the bladder pressure is very near the desired pressure but slightly under, the final pulse will overshoot the desired pressure by the amount of pressure increase contributed by the final pulse. Shorter pulse widths are used as the pressure approaches the desired value to ensure a smaller overshoot. This approach allows the system to reach the desired pressure of 1 psi quicker, with fewer solenoid cycles, and less overshoot. The results of this modified approach are shown in Figure 6.15. Excluding the initial 8.2 seconds, the bladders reach 1 psi in roughly 4.35 seconds. The solenoids are turned on and off six times. This final control sequence demonstrates that the concepts of the ideal controller can be used to improve the transient response when using a duty cycle approach.
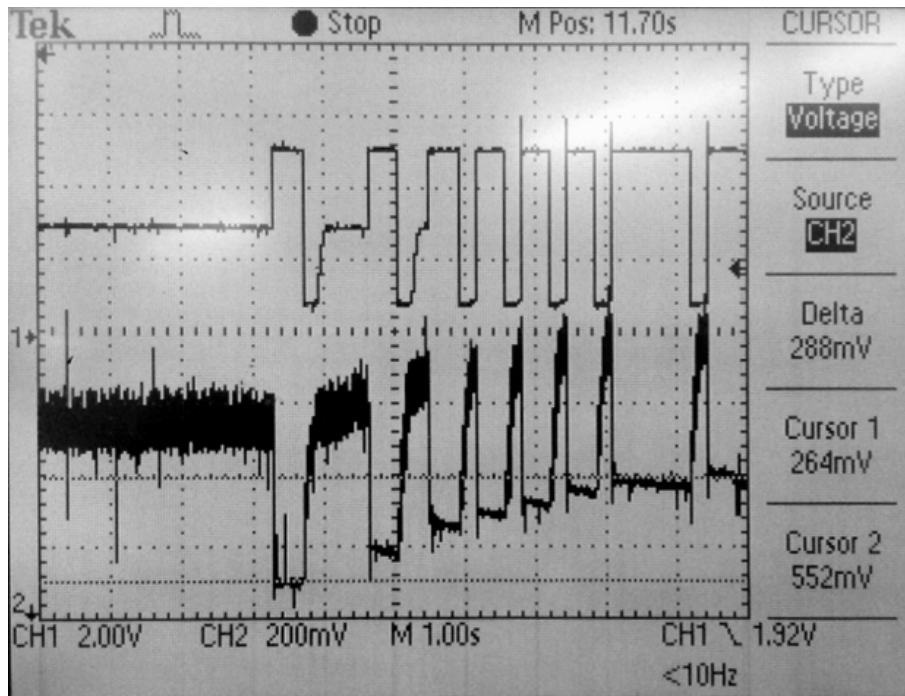
Figure 6.15. Modified duty cycle starting with 90% of final settling control value

88

Chapter 7

Conclusion and Future Work

7.1 Conclusion

The Active Cast is a device which is intended to off-load pressure from the sole of a patient's foot and distribute it to the calf in order to treat diabetic neuropathic ulcers. This is accomplished by a pneumatic system which maintains set pressure in multiple air bladders. In this research a model of the pneumatic system is created and compared to the physical system. Results show that the mathematical model accurately represents the system for the expected pressure range of 0 to 1 psi. Additionally, the model is used to evaluate three configuration options: series, parallel, and hybrid. Using a weighted decision matrix to analyze and compare the three configuration options in the areas of cost, complexity and performance, the parallel configuration is judged to be the most suitable. The performance rating of each system accounted for how well the configurations met the design requirements for settling time, rise time, and overshoot. Each of the configurations have zero steady-state error and less than 10% overshoot. There is, however, a large difference in settling times. The parallel configuration is the only one to meet the settling time of 10 seconds with a value of

7 seconds. In addition to this performance advantage, the bladders can be controlled independently and the controller designed for the parallel configuration is the least complicated to implement.

Physical limitations of the system prevent the ideal parallel controller from being implemented into the physical system. Some modifications are made to the model to more closely reflect the physical system, notably a reduction of gain to meet the output of a reasonably sized pump. Also, the amplitude of the controller driving function changes with time in order to produce the desired response. This presents a further limitation of the pump as it cannot vary the input to the system. Two different implementations are tested. First, a duty cycle with a constant 23% pulse width is applied to the system. This test reveals that a true duty cycle approach is problematic for a pneumatic system due to the pump rise time, the inertial effects of air, and compressibility. The next implementation is a modified duty cycle which uses the model driving function as guideline for the pulse lengths. The physical system responds much closer to the model response and the response meets the desired parameters.

In conclusion, the models developed in the research are good, but not perfect. The implementation is an approximation based on the controller driving function. More confidence can be obtained with implementation of the actual driving function, which requires a pump that can provide variable output.

7.2 Future Work

The results of this research are not exhaustive and many hardware changes are necessary before a production prototype is complete. This research began with an Aircast, but continuation should include a custom designed structure. The size and

locations of the air bladders must be determined based on medical research. One of the largest difficulties exposed by this research is the inadequacy of the pump. In order to implement the PID controllers designed here and reduce settling time to a minimum variable output from the pump is required. Additionally, two potential improvements include use of a mechanical pump or individual micro-pumps for each bladder. A mechanical pump could fill a reservoir using the mechanical motion from walking, providing power and potential space savings, though this would not provide the ability to adjust pressure. Use of solenoids which can throttle may provide an answer to this problem. Micro-pumps would reduce the spacial requirements significantly as half of the solenoids would not be needed in addition to the space saved by eliminating a large pump or reservoir. Future research should evaluate these options in order to move toward a production prototype of the Active Cast.

Bibliography

[1] A. A. Gordois, P. Scuffham, A. Shearer, A. Oglesby, and J. A. Tobian, "The health care costs of diabetic peripheral neuropathy in the U.S.," *Diabetes Care*, vol. 26, no. 6, pp. 1790–1795, 2003.

[2] E. S. Huang, A. Basu, M. O'Grady, and J. C. Capretta, "Projecting the future diabetes population size and related costs for the U.S.," *Diabetes Care*, vol. 32, pp. 2225–2229, Dec 2009.

[3] S. C. Wu, J. L. Jensen, A. K. Weber, D. E. Robinson, and D. G. Armstrong, "Use of pressure offloading devices in diabetic foot ulcers: do we practice what we preach?," *Diabetes Care*, vol. 31, pp. 2118–2119, Nov 2008.

[4] C. for Disease Control and Prevention, "National diabetes fact sheet: general information and national estimates on diabetes in the United States Atlanta, GA: U.S. Department of Health and Human Services, Centers for Disease Control and Prevention, 2008.," 2007.

[5] S. S. Wild, G. Roglic, A. Green, R. Sicree, and H. King, "Global prevalence of diabetes: Estimates for the year 2000 and projections for 2030," *Diabetes Care*, vol. 27, no. 5, pp. 1047–1053, 2004.

[6] J. J. Tuomilehto, J. Lindström, J. G. Eriksson, T. T. Valle, H. Hämäläinen, P. ILanne-Parikka, S. Keinänen-Kiukaanniemi, M. Laakso, A. Louheranta, M. Rastas, V. Salminen, and M. Uusitupa, "Prevention of type 2 diabetes mellitus by changes in lifestyle among subjects with impaired glucose tolerance," *The New England Journal of Medicine*, vol. 344, no. 18, pp. 1343–1350, 2001.

[7] M. Nirenberg, "Foot amputation worse than breast cancer." `http://www.test.org/doe/`, Jun 2009.

[8] A. Jernberger, "The neuropathic foot," *Prosthetics and Orthotics International*, vol. 17, pp. 189–195, Dec 1993.

[9] M. J. Mueller, D. Zou, and D. J. Lott, "Pressure gradient as an indicator of plantar skin injury," *Diabetes Care*, vol. 28, pp. 2908–2912, Dec 2005.

[10] A. Piaggesi, P. Viacava, L. Rizzo, G. Naccarato, F. Baccetti, M. Romanelli, V. Zampa, and S. D. Prato, "Semiquantitative analysis of the histopathological features of the neuropathic foot ulcer: effects of pressure relief," *Diabetes Care*, vol. 26, pp. 3123–3128, Nov 2003.

[11] M. H. Nabuurs-Franssen, R. Sleegers, M. S. Huijberts, W. Wijnen, A. P. Sanders, G. Walenkamp, and N. C. Schaper, "Total contact casting of the diabetic foot in daily practice: a prospective follow-up study," *Diabetes Care*, vol. 28, pp. 243–247, Feb 2005.

[12] J. G. Fleischli, L. A. Lavery, S. A. Vela, H. Ashry, and D. C. Lavery, "1997 William J. Stickel Bronze Award. Comparison of strategies for reducing pressure at the site of neuropathic ulcers," *Journal of the American Podiatric Medical Association*, vol. 87, pp. 466–472, Oct 1997.

[13] Z. Pataky, D. de Leon Rodriguez, L. Allet, A. Golay, M. Assal, J. P. Assal, and C. A. Hauert, "Biofeedback for foot offloading in diabetic patients with peripheral neuropathy," *Diabetic Medicine : A Journal of the British Diabetic Association*, vol. 27, pp. 61–64, Jan 2010.

[14] D. G. Armstrong, L. A. Lavery, and T. R. Bushman, "Peak foot pressures influence the healing time of diabetic foot ulcers treated with total contact casts," *Journal of Rehabilitation Research and Development*, vol. 35, pp. 1–5, Jan 1998.

[15] A. Piaggesi, S. Macchiarini, L. Rizzo, F. Palumbo, A. Tedeschi, L. A. Nobili, E. Leporati, V. Scire, I. Teobaldi, and S. D. Prato, "An off-the-shelf instant contact casting device for the management of diabetic foot ulcers: a randomized prospective trial versus traditional fiberglass cast," *Diabetes Care*, vol. 30, pp. 586–590, Mar 2007.

[16] D. G. Armstrong, L. A. Lavery, S. Wu, and A. J. Boulton, "Evaluation of removable and irremovable cast walkers in the healing of diabetic foot wounds: a randomized controlled trial," *Diabetes Care*, vol. 28, pp. 551–554, Mar 2005.

[17] D. G. Armstrong and L. A. Lavery, "Diabetic foot ulcers: prevention, diagnosis and classification," *American Family Physician*, vol. 57, pp. 1325–32, 1337–8, Mar 1998.

[18] J. Karam, Jr., "A new model for fluidics transmission lines," *Control Engineering*, Dec 1966.

[19] K. Ogata, *System Dynamics.* Upper Saddle River, NJ: Pearson Prentice Hall, 2004.

[20] R. V. Dukkipati and E. Corporation, *Solving Engineering System Dynamics Problems with MATLAB.* New Delhi: New Age International Pvt. Ltd., Publishers, 2007.

[21] R. C. Dorf and R. H. Bishop, *Modern Control Systems.* Addison Wesley Longman, Inc., 1998.

[22] D. Hristu-Varsakelis and W. S. Levine, *Handbook of networked and embedded control systems.* Boston, MA: BirkhŠuser, 2005.

[23] R. A. Bryant, *Acute and chronic wounds: nursing management.* Mosby, 1992.

[24] M. A. Johnson, M. H. Moradi, J. Crowe, and SpringerLink, *PID control.* New York: Springer, 2005.

[25] A. Visioli and SpringerLink, *Practical PID control.* London: Springer, 2006.

[26] A. G. O. Mutambara, *Design and analysis of control systems.* Boca Raton, Fla: CRC Press, 1999.

[27] C. L. Phillips and R. D. Harbor, *Feedback control systems.* Englewood Cliffs, N.J.: Prentice Hall, 1988. Charles L. Phillips, Royce D. Harbor.; :ill. ;25 cm; Includes bibliographical references and index.

[28] B. C. Kuo, *Automatic Control Systems.* Englewood Cliffs, New Jersey: Prentice-Hall, Inc., 1995.

[29] J. Hellerstein and I. ebrary, *Feedback control of computing systems.* New York: IEEE Press, 2004.

[30] K. J. Astrom, R. M. Murray, and E. Corporation, *Feedback Systems :An Introduction for Scientists and Engineers.* Princeton: Princeton University Press, 2009.

[31] K. Ogata, *Modern control engineering.* Englewood Cliffs, N.J.: Prentice-Hall, 1970.

[32] B. Kulakowski, J. F. Gardner, J. L. Shearer, and E. Corporation, *Dynamic Modeling and Control of Engineering Systems.* Leiden: Cambridge University Press, 2007.

[33] P. C. Chau, *Process control: a first course with MATLAB*. Cambridge Univ Pr, 2002.

[34] N. S. Nise, *Control Systems Engineering*. 1992.

[35] O. Fruchter, "Prevention of type 2 diabetes mellitus by changes in lifestyle," *The New England Journal of Medicine*, vol. 345, pp. 696; author reply 696–7, Aug 30 2001.

[36] S. O. Oyibo, E. B. Jude, I. Tarawneh, H. C. Nguyen, L. B. Harkless, and A. J. Boulton, "A comparison of two diabetic foot ulcer classification systems: the Wagner and the University of Texas wound classification systems," *Diabetes Care*, vol. 24, pp. 84–88, Jan 2001.

Appendix A

Datasheets

A.1 Pump

TYPICAL PRODUCT PARAMETERS

SOUND LEVEL:	58 dBA
OPERATING TEMPERATURE RANGE:	50°F - 104°F (10°C to 40°C); 10 to 95% RH
FOAM INTAKE FILTER:	Expanded Polyurethane
SAFETY SYSTEMS:	High temperature compressor shutdown.
REGULATORY LISTING:	In compliance with EN 60601-1
DIMENSIONS WITHOUT BATTERY: WITH BATTERY:	5.1 x 3.6 x 1.6 inches (13cm x 9cm x 4cm) 5.1 x 3.6 x 2.6 inches (13cm x 9cm x 7cm)
*WEIGHT WITHOUT BATTERY: WITH BATTERY:	1 lbs (450 g) 1.4 lbs (650 g)
POWER SUPPLY:	100-120 VAC 50-60 Hz, 12 VDC, 1.4 A
MAXIMUM PRESSURE:	29 psi (200 kPa)
MAXIMUM FLOW RATE:	10 L/min
STORAGE CONDITIONS:	-13°F to 158°F (-25° to 70°C); 10 to 95% RH
OPERATING FLOW RATE:	3.5 L/min @ 14.5 PSI operating pressure
MODE OF OPERATION:	Intermittent Use 30 min ON/30 min OFF

NOTE: *Weight is without nebulizer and tubing.

Part No 1150755   **9**   **Stratos™ Portable Plus**

A.2 Airflow Sensor

Airflow Sensors   AWM40000 Series

Microbridge Mass Airflow/Unamplified and Amplified

FEATURES
- Manifold mount/o-ring sealed
- Ceramic flow-tube (non-outgassing), 0-1000 sccm
- Plastic flow tube, 0-6 SLPM
- High common mode pressure (150 psi ceramic flow-tube only)
- Operating temperature up to 125°C (unamplified only)
- High stability at null and full-scale

The AWM40000 Series mass flow sensor family is based on proven microbridge technology and includes both amplified signal conditioned devices and unamplified sensor only devices.

When using the unamplified devices (AWM42150VH and AWM42300V), the heater control circuit in Figure 1 and the sensing bridge supply circuit in Figure 2 are both required for operation per specification. These two circuits are **NOT** on board the sensor and must be supplied in the application. The differential amplifier circuitry in Figure 3 may be useful in providing output gain and/or introducing voltage offsets to the sensor output (Ref. Equation 1).

The amplified devices (AWM43300V and AWM43600V) can be used to increase output gain and introduce voltage offsets. The differential instrumentation amplifier circuitry, heater control circuitry and sensing bridge supply circuitry are all provided onboard the amplified sensors.

Figure 1
Heater Control Circuit
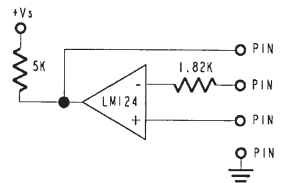
Figure 2
Sensing Bridge Supply Circuit
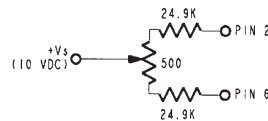
Figure 3
Differential Instrumentation Amplifier Circuit
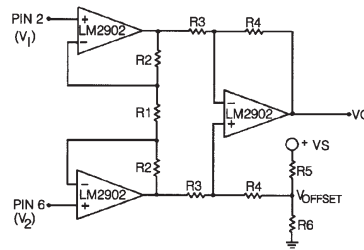
Equation 1:

$$V_o = \left(\frac{2R_2 + R_1}{R_1} \right) \left(\frac{R_4}{R_3} \right) \left(V_2 - V_1 \right) + V \text{ offset}$$

$$\text{where } V \text{ offset} = V_s \left(\frac{R_6}{R_5 + R_6} \right)$$

Airflow Sensors

Microbridge Mass Airflow/Unamplified and Amplified

AWM40000 SERIES ORDER GUIDE (Performance Characteristics @ 10.01 ±0.01 VDC, 25°C)

Catalog Listings	AWM42150VH	AWM42300V	AWM43300V	AWM43600V
Flow Range (Full Scale)	±25 sccm	±1000 sccm	+1000 sccm	+6 SLPM
Output Voltage @ Trim Point	8.5 mV ±1.5 mV @ 25 sccm	54.7 mV ±3.7 mV DC @ 1000 sccm	5 V ±0.15 VDC @ 1000 sccm	5 V ±0.15 VDC @ 6 SLPM
Null Voltage	0.0 ±1.0 mVDC	0.0 ±1.5 mVDC	1.0 ±0.05 VDC	1.0 ±0.05 VDC
Null Voltage Shift +25° to −25°C, +25° to +85°C	±0.20 mVDC	±0.20 mVDC	±0.025 VDC	±0.025 VDC
Output Voltage Shift +25° to −25°C +25° to +85°C	+2.5% Reading typ. −2.5% Reading typ.	+2.5% Reading max. −2.5% Reading max.	−5.0% Reading max. +6.0% Reading max.	−6.0% Reading max. +6.0% Reading max.
Power Consumption (mW)	60 (Max.)	60 (Max.)	60 (Max.)	75 (Max.)
Repeatability & Hysteresis	±0.35% Reading (3)	±0.50% Reading	±0.50% Reading	±1.00% Reading
Pressure Drop @ Full Scale (in H₂O)	0.008″ H₂O (Typ.)	1.02 (Typ.)	1.02 (Typ.)	8.00 (Typ.)

	Min.	Typ.	Max.	
Excitation VDC	8.0	10±0.01	15	
Response Time (msec)	—	1.0	3.0 (Note 1)	
Common Mode Pressure (psi) (max.)	—	—	150 psi (10 Bar)	25 psi (1.7 Bar)
Output Load		NPN (Sinking): 10 mA PNP (Sourcing): 20 mA		
Temperature Range	Operating: −40° to +125°C (−40° to +251°F) Storage: −40° to +125°C (−40° to +251°F)		Operating: −25° to +85°C (−13° to +185°F) Storage: −40° to +90°C (−40° to +194°F)	
Calibration Gas		Nitrogen		
Ratiometricity Error		±0.30% Reading		
Weight (grams)		14 g		11 g
Shock Rating		100 g peak (5 drops, 6 axes)		
Termination		2,54 mm (.100″) centers, 0,635 cm (0.025″) square		

Notes:
1. Response time is typically 1 msec from 10 to 90%.
2. Repeatability & Hysteresis tolerances reflect inherent inaccuracies of the measurement equipment.
3. Maximum allowable rate of flow change to prevent damage: 5.0 SLPM/1.0 sec.

MOUNTING DIMENSIONS (for reference only)

Amplified Sensors

Unamplified Sensors

Airflow
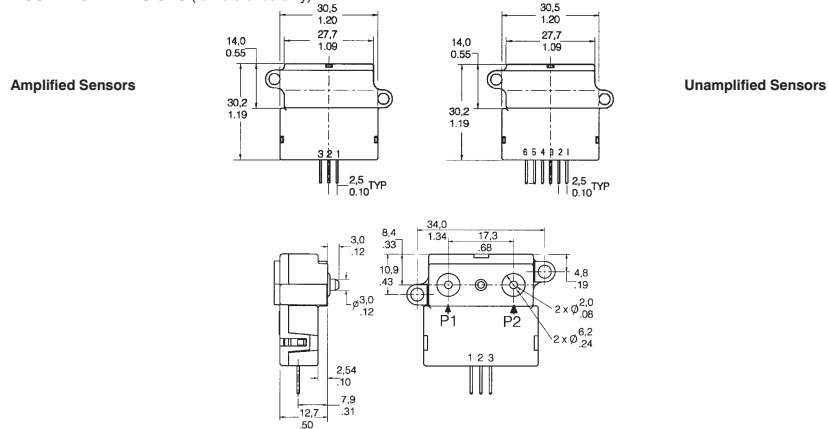
Note: Positive flow direction is defined as proceeding from Port 1 (P1) to Port 2 (P2), and results in positive output.

99

Microbridge Mass Airflow/Unamplified and Amplified

OUTPUT FLOW VS INTERCHANGEABILITY (Note 1) **Performance Characteristics @ 10.0 ± 0.01 VDC, 25°C**

AWM42150VH				AWM42300V				AWM43300V				AWM43600V			
Press µBar	Flow sccm	Nom. mV	Tol. ± mV	Press. mBar	Flow sccm	Nom. mV	Tol. ± mV	Press. mBar	Flow sccm	Nom. VDC	Tol. ± VDC	Press. mBar	Flow SLPM	Nom. VDC	Tol. ± VDC
20	**30**	9.9	1.5	2.23	**1000**	54.7	2.00	2.23	**1000**	5.00	0.15	20.0	**6**	5.00	0.15
17	**25**	8.5	1.5	1.52	**800**	53.0	2.0	1.87	**900**	4.97	0.16	14.7	**5**	4.89	0.20
14	**20**	6.8	1.5	0.94	**600**	49.3	2.5	1.52	**800**	4.89	0.17	9.07	**4**	4.70	0.25
10	**15**	5.2	1.0	0.49	**400**	42.5	3.5	1.16	**700**	4.78	0.18	6.40	**3**	4.40	0.35
7	**10**	3.5	1.0	0.19	**200**	29.8	4.0	0.94	**600**	4.63	0.19	3.35	**2**	3.80	0.30
3	**5**	1.7	1.0	0.00	**0**	0.0	1.5	0.71	**500**	4.43	0.20	1.17	**1**	3.10	0.30
0	**0**	0.0	1.0	-0.19	**-200**	-29.8	4.0	0.50	**400**	4.15	0.21	0.00	**0**	1.00	0.05
				-0.49	**-400**	-42.5	5.0	0.33	**300**	3.76	0.19				
				-0.94	**-600**	-49.3	6.0	0.19	**200**	3.23	0.17				
				-1.52	**-800**	-53.0	6.0	0.08	**100**	2.49	0.14				
				-2.23	**-1000**	-55.2	6.0	0.00	**0**	1.00	0.05				

Notes:
1. Numbers in **BOLD** type indicate calibration type, mass flow or differential pressure.
   Tolerance values apply to calibration type only.

AWM42150VH
Output Voltage vs Flow

AWM42300V
Output Voltage vs Flow

AWM43300V
Output Voltage vs Flow

AWM43600V
Output Voltage vs Flow

100

A.3 Solenoid

Innovation in Miniature

LEE
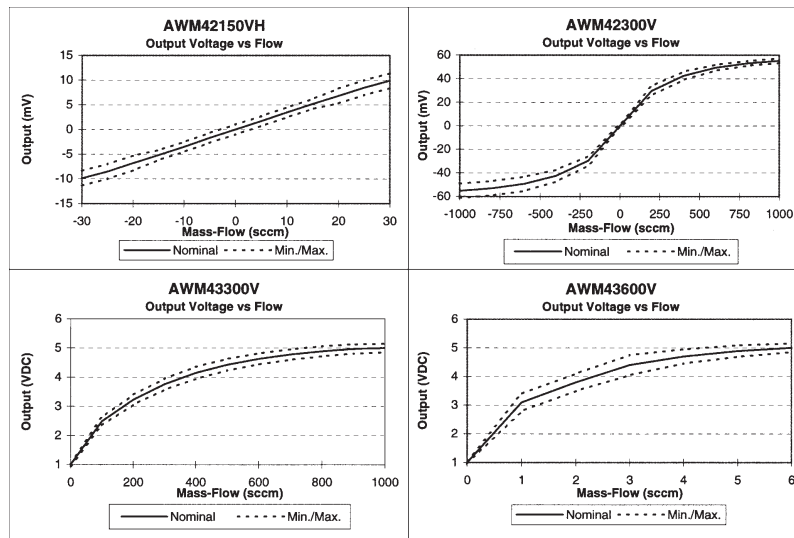
SEMI INERT SOLENOID VALVE

The Lee Company's new perfluorinated semi-inert solenoid valve is specifically designed to handle moderately aggressive gases and liquids in a wide range of fluid handling applications. The valve is ideal for use in anesthesia delivery, inkjet printing, gas detection systems, reagent delivery and other OEM flow switching applications requiring chemical resistance.

Available in face mount and soft tube ported configurations, the valve's wetted materials include:

- PFE/FFKM elastomer seal
- PPS plunger head
- PBT housing
- 316 CRES spring
- Epoxy
- Chrome Core 18® Alloy armature and plunger stop for superior corrosion resistance

The Lee Company offers an array of standard manifolds for testing as well as customer-designed manifold configurations for production. Performance parameters can be optimized for a specific application.

Contact your Lee Sales Engineer for additional technical assistance and application information.

See reverse side for mounting surface detail.

- Light weight: less than 4.5 grams
- Compact size
- Superior perfluoro elastomer (PFE/FFKM) inertness
- Low internal volume: 75 µL

FACE MOUNT STYLE

1.35 [34.2]
2X .28 [7]
.30 [7.5]
.29 [7.5]
NORMALLY CLOSED PORT
NORMALLY OPEN PORT
COMMON PORT
GASKET
MOUNTING SURFACE

SOFT TUBE PORTED STYLE

NORMALLY CLOSED PORT
COMMON PORT
NORMALLY OPEN PORT
.29 [7.5]
.51 [12.9]
2X .28 [7]
1.35 [34.2]

STYLE	LEE PART NUMBER	DESCRIPTION
Face Mount	LHDA0521515H	5 VDC
	LHDA1221515H	12 VDC
	LHDA2421515H	24 VDC
Soft Tube Ported	LHDA0531515H	5 VDC
	LHDA1231515H	12 VDC
	LHDA2431515H	24 VDC
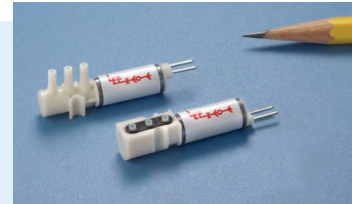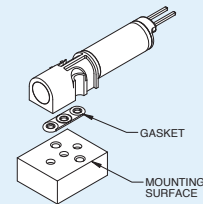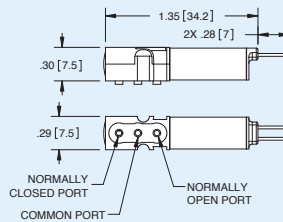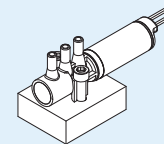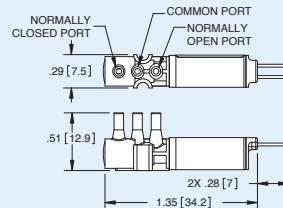
PERFORMANCE CHARACTERISTICS
Response time: 2 ms
Flow capacity (air) – 3-Way: 1500 Lohms; Cv = .013 (4.4 SLPM @ 10 psig)
Leakage: less than 25µL / minute @ 5 psig (air)
Operating pressure: vac – 45 psig (0-15 psid)
Power consumption: 850 mW
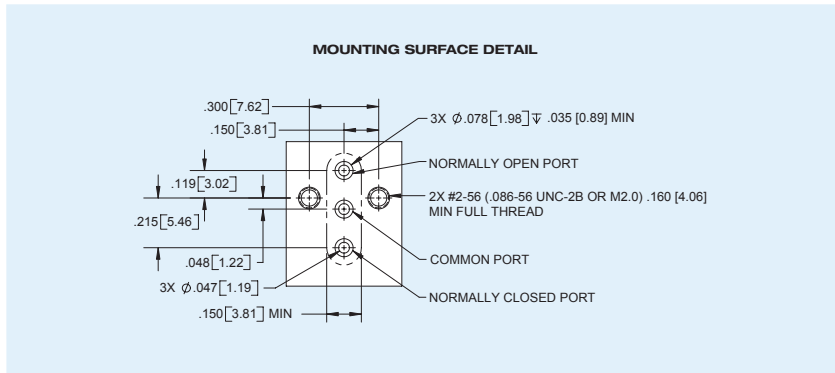
® Chrome Core 18 is a registered trademark of CRS Holdings, Inc., a subsidiary of Carpenter Technology Corporation.

SEMI INERT SOLENOID VALVE

MOUNTING SURFACE DETAIL

.300 [7.62]

.150 [3.81]

3X Ø.078 [1.98] ↧ .035 [0.89] MIN

NORMALLY OPEN PORT

.119 [3.02]

2X #2-56 (.086-56 UNC-2B OR M2.0) .160 [4.06]
MIN FULL THREAD

.215 [5.46]

.048 [1.22]

COMMON PORT

3X Ø.047 [1.19]

NORMALLY CLOSED PORT

.150 [3.81] MIN

A.4 Pressure Sensor

Integrated Silicon Pressure Sensor On-Chip Signal Conditioned, Temperature Compensated, and Calibrated

The MPX5100 series piezoresistive transducer is a state-of-the-art monolithic silicon pressure sensor designed for a wide range of applications, but particularly those employing a microcontroller or microprocessor with A/D inputs. This patented, single element transducer combines advanced micromachining techniques, thin-film metallization, and bipolar processing to provide an accurate, high level analog output signal that is proportional to the applied pressure.

Features

- 2.5% Maximum Error over 0° to 85°C
- Ideally suited for Microprocessor or Microcontroller-Based Systems
- Patented Silicon Shear Stress Strain Gauge
- Available in Absolute, Differential and Gauge Configurations
- Durable Epoxy Unibody Element
- Easy-to-Use Chip Carrier Option

Typical Applications

- Patient Monitoring
- Process Control
- Pump/Motor Control
- Pressure Switching

MPX5100/MPXV5100 SERIES

INTEGRATED PRESSURE SENSOR
0 to 100 kpa (0 to 14.5 psi)
15 to 115 kPa
(2.2 to 16.7 psi)
0.2 to 4.7 V Output

SMALL OUTLINE PACKAGES

MPXV5100GC6U
CASE 482A-01

MPXV5100GC7U
CASE 482C-03

MPXV5100DP
CASE 1351-01
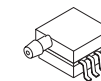
MPXV5100GP
CASE 1369-01

PIN NUMBER[1]			
1	N/C	5	N/C
2	V_S	6	N/C
3	GND	7	N/C
4	V_{OUT}	8	N/C

1. Pins 1, 5, 6, 7, and 8 are internal device connections. Do not connect to external circuitry or ground. Pin1 is noted by the notch in the lead.

PIN NUMBER[1]			
1	V_{OUT}	4	N/C
2	GND	5	N/C
3	V_S	6	N/C

1. Pins 4, 5, and 6 are internal device connections. Do not connect to external circuitry or ground. Pin 1 is noted by the notch in the lead.

ORDERING INFORMATION

Device Type	Options	Case No.	MPX Series Order Number	Device Marking
UNIBODY PACKAGE (MPX5100 SERIES)				
Basic Elements	Absolute	867	MPX5100A	MPX5100A
	Differential	867	MPX5100D	MPX5100D
Ported Elements	Differential Dual Ports	867C	MPX5100DP	MPX5100DP
	Absolute, Single Port	867B	MPX5100AP	MPX5100AP
	Gauge, Single Port	867B	MPX5100GP	MPX5100GP
	Gauge, Axial PC Mount	867F	MPX5100GSX	MPX5100D
	Gauge, Axial Port, SMT	482A	MPXV5100GC6U	MPXV5100G
	Gauge, Axial Port, DIP	482C	MPX5V100GC7U	MPXV5100G
	Gauge, Dual Port, SMT	1351	MPXV5100DP	MPXV5100
	Gauge, Side Port, SMT	1369	MPXV5100GP	MPXV5100G

UNIBODY PACKAGES

MPX5100A/D
CASE 867-08

MPX5100AP/GP
CASE 867B-04

MPX5100DP
CASE 867C-05

MPX5100GSX
CASE 867F-03
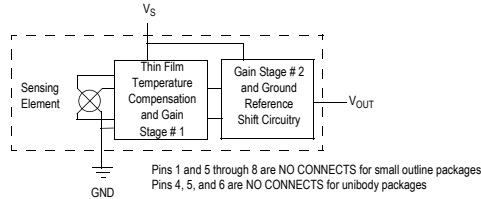
Figure 1. Fully Integrated Pressure Sensor Schematic

Pins 1 and 5 through 8 are NO CONNECTS for small outline packages
Pins 4, 5, and 6 are NO CONNECTS for unibody packages

TABLE 1. Maximum Ratings[1]

Rating	Symbol	Value	Unit
Maximum Pressure (P1 > P2)	P_{MAX}	400	kPa
Storage Temperature	T_{STG}	-40° to +125°C	°C
Operating Temperature	T_A	-40° to +125°C	°C

1. Exposure beyond the specified limits may cause permanent damage or degradation to the device.

TABLE 2. Operating Characteristics (V_S = 5.0 V_{DC}, T_A = 25°C unless otherwise noted, P1 > P2. Decoupling circuit shown in Figure 4 required to meet electrical specifications.)

Characteristic	Symbol	Min	Typ	Max	Unit

Pressure Range[1]
   Gauge, Differential: MPX5100D/MPX5100G/MPXV5100G
   Absolute: MPX5100A
	P_{OP}	
		0
		15
			
			—
			—
				
				100
				115
					kPa

Supply Voltage[2]	V_S	4.75	5.0	5.25	V_{DC}
Supply Current	I_O	—	7.0	10	mAdc
Minimum Pressure Offset[3] (0 to 85°C) @ V_S = 5.0 V	V_{OFF}	0.088	0.20	0.313	V_{DC}
Full Scale Output[4] Differential and Absolute (0 to 85°C) @ V_S = 5.0 V	V_{FSO}	4.587	4.700	4.813	V_{DC}
Full Scale Span[5] Differential and Absolute (0 to 85°C) @ V_S = 5.0 V	V_{FSS}	—	4.500	—	V_{DC}
Accuracy[6]	—	—	—	±2.5	%V_{FSS}
Sensitivity	V/P	—	45	—	mV/kPa
Response Time[7]	t_R	—	1.0	—	ms
Output Source Current at Full Scale Output	I_{O+}	—	0.1	—	mAdc
Warm-Up Time[8]	—	—	20	—	ms
Offset Stability[9]	—	—	±0.5	—	%V_{FSS}

1. 1 kPa (kiloPascal) equals 0.145 psi.
2. Device is ratiometric within this specified excitation range.
3. Offset (V_{OFF}) is defined as the output voltage at the minimum rated pressure.
4. Full Scale Output (V_{FSO}) is defined as the output voltage at the maximum or full rated pressure.
5. Full Scale Span (V_{FSS}) is defined as the algebraic difference between the output voltage at full rated pressure and the output voltage at the minimum rated pressure.
6. Accuracy (error budget) consists of the following:
   - Linearity: Output deviation from a straight line relationship with pressure over the specified pressure range.
   - Temperature Hysteresis: Output deviation at any temperature within the operating temperature range, after the temperature is cycled to and from the minimum or maximum operating temperature points, with zero differential pressure applied.
   - Pressure Hysteresis: Output deviation at any pressure within the specified range, when this pressure is cycled to and from minimum or maximum rated pressure at 25°C.
   - TcSpan: Output deviation over the temperature range of 0° to 85°C, relative to 25°C.
   - TcOffset: Output deviation with minimum pressure applied over the temperature range of 0° to 85°C, relative to 25°C.
   - Variation from Nominal: The variation from nominal values, for Offset or Full Scale Span, as a percent of V_{FSS} at 25°C.

MPX5100

7. Response Time is defined as the time for the incremental changed in the output to go from 10% to 90% of its final value when subjected to a specified step change in pressure.
8. Warm-Up Time is defined as the time required for the product to meet the specified output voltage after the Pressure has been stabilized.
9. Offset Stability is the product's output deviation when subjected to 1000 hours of Pulsed Pressure, Temperature Cycling with Bias Test.

ON-CHIP TEMPERATURE COMPENSATION, CALIBRATION AND SIGNAL CONDITIONING

Figure 2 shows the sensor output signal relative to pressure input. Typical, minimum, and maximum output curves are shown for operation over a temperature range of 0× to 85×C using the decoupling circuit shown in Figure 4. The output will saturate outside of the specified pressure range.

Figure 3 illustrates both the Differential/Gauge and the Absolute Sensing Chip in the basic chip carrier (Case 867). A fluorosilicone gel isolates the die surface and wire bonds from the environment, while allowing the pressure signal to be transmitted to the sensor diaphragm.

The MPX5100 series pressure sensor operating characteristics, and internal reliability and qualification tests are based on use of dry air as the pressure media. Media, other than dry air, may have adverse effects on sensor performance and long-term reliability. Contact the factory for information regarding media compatibility in your application.

$V_{out} = V_S*(0.009*P+0.04)$
± (Pressure Error * Temperature Factor * 0.009 * V_S
V_S = 5.0 V ± 0.25 Vdc
PE = 2.5
TM = 1
TEMP = 0 to 85°C
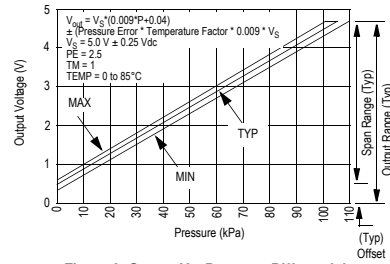
Figure 2. Output Vs. Pressure Differential
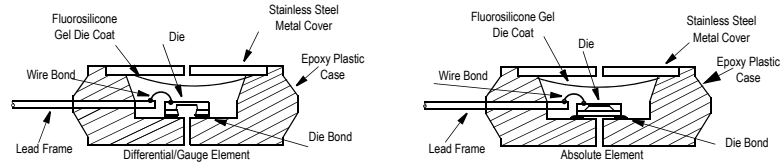
Figure 3. Cross Sectional Diagrams (Not to Scale)

Figure 4 shows the recommended decoupling circuit for interfacing the output of the integrated sensor to the A/D input of a microprocessor or microcontroller. Proper decoupling of the power supply is recommended.
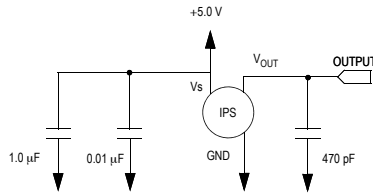
Figure 4. Recommended Power Supply Decoupling and Output Filtering
(For additional output filtering, please refer to Application Note AN1646.)

MPX5100

Sensors
Freescale Semiconductor

3

105

Transfer Function (MPX5100D, MPX5100G, MPXV5100G

Nominal Transfer Value: $V_{OUT} = V_S$ (P x 0.009 + 0.04)

$\pm$ (Pressure Error x Temp. Mult. x 0.009 x V_S)

$V_S = 5.0 \text{ V} \pm 5\%$ P kPa

Temperature Error Multiplier

MPX5100D/MPX5100G/MPXV5100G Series

Break Points

Temp	Multiplier
- 40	3
0 to 85°C	1
+125°	3
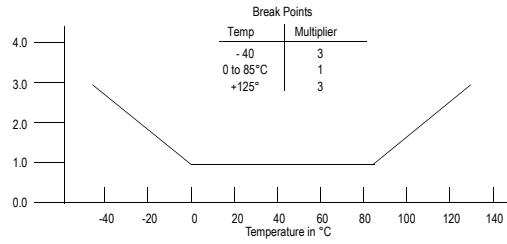
Temperature in °C

Note: The Temperature Multiplier is a linear response from 0° to -40°C and from 85° to 125°C.

Pressure Error Band

MPX5100D/MPX5100G/MPXV5100G Series
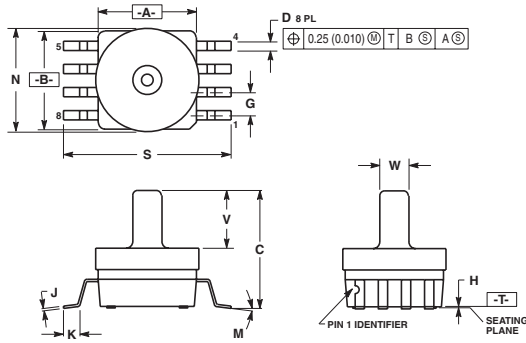
Error Limits for Pressure

Pressure in kPa

Pressure	Error (max)
0 to 100 kPa	$\pm$ 2.5 kPa

MPX5100

PACKAGE DIMENSIONS

NOTES:
1. DIMENSIONING AND TOLERANCING PER ANSI Y14.5M, 1982.
2. CONTROLLING DIMENSION: INCH.
3. DIMENSION A AND B DO NOT INCLUDE MOLD PROTRUSION.
4. MAXIMUM MOLD PROTRUSION 0.15 (0.006).
5. ALL VERTICAL SURFACES 5° TYPICAL DRAFT.

DIM	INCHES		MILLIMETERS	
	MIN	MAX	MIN	MAX
A	0.415	0.425	10.54	10.79
B	0.415	0.425	10.54	10.79
C	0.500	0.520	12.70	13.21
D	0.038	0.042	0.96	1.07
G	0.100 BSC		2.54 BSC	
H	0.002	0.010	0.05	0.25
J	0.009	0.011	0.23	0.28
K	0.061	0.071	1.55	1.80
M	0°	7°	0°	7°
N	0.444	0.448	11.28	11.38
S	0.709	0.725	18.01	18.41
V	0.245	0.255	6.22	6.48
W	0.115	0.125	2.92	3.17

CASE 482A-01
ISSUE A
SMALL OUTLINE PACKAGE
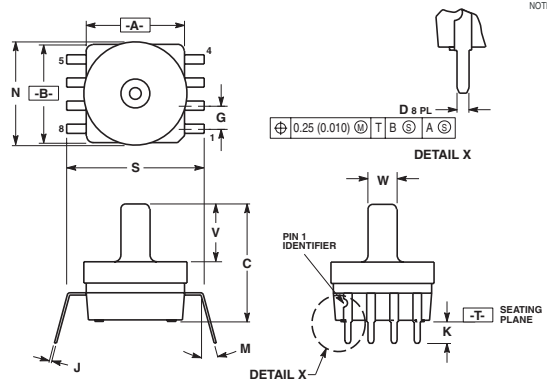
NOTES:
1. DIMENSIONING AND TOLERANCING PER ANSI Y14.5M, 1982.
2. CONTROLLING DIMENSION: INCH.
3. DIMENSION A AND B DO NOT INCLUDE MOLD PROTRUSION.
4. MAXIMUM MOLD PROTRUSION 0.15 (0.006).
5. ALL VERTICAL SURFACES 5° TYPICAL DRAFT.
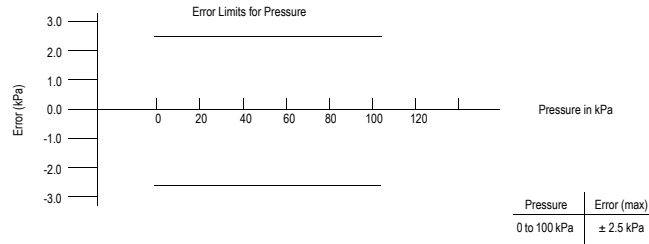6. DIMENSION S TO CENTER OF LEAD WHEN FORMED PARALLEL.

DIM	INCHES		MILLIMETERS	
	MIN	MAX	MIN	MAX
A	0.415	0.425	10.54	10.79
B	0.415	0.425	10.54	10.79
C	0.500	0.520	12.70	13.21
D	0.026	0.034	0.66	0.864
G	0.100 BSC		2.54 BSC	
J	0.009	0.011	0.23	0.28
K	0.100	0.120	2.54	3.05
M	0°	15°	0°	15°
N	0.444	0.448	11.28	11.38
S	0.540	0.560	13.72	14.22
V	0.245	0.255	6.22	6.48
W	0.115	0.125	2.92	3.17

CASE 482C-03
ISSUE B
SMALL OUTLINE PACKAGE

MPX5100

107

Appendix B

MATLAB Scripts

B.1 Proportional Integral Control

```
% SYSTEM PARAMETERS
clear all;
close all;
clc;
L2=4.3*10^-4;
R1=1.87;
L1=3.5;
R2=.339;
C=3.719;


OL_num=[1]; % removed s term to cancel zero at origin. Later add 1/s.
OL_den = [(C*L1*L2) (L2*R1+R2*L1+R2*L2)*C (C*R2*R1+L1+L2) R1];
P = tf(OL_num, OL_den);

% Ziegler-Nichols first method
L=.4175;
T=4.712-L;
Kp=150;
Ti = 2*L;
Td = 0.5*L;
s=tf('s');
```

```
K_init=Kp

sisotool(K_init*P);


% SISO tool shows need to increase loop gain by ~0.013341 to meet
% damping ratio of 0.707 design requirement
 K=0.013341*K_init;

% Verify this work for original plant
OL_num=[1 0];
P1 = tf(OL_num, OL_den);
K1=K/s;
PI=minreal(P1*K1)
t=0:.01:20;
step(PI,t)
% axis([0 20 0 1.3])
title('Step Response of Plant with PI Control')
% sisotool(PI)
```

B.2 Proportional-Integral-Integral Control

```
% SYSTEM PARAMETERS
clear all;
clc;
L2=4.3*10^-4;
R1=1.87;
L1=3.5;
R2=.339;
C=3.719;

OL_num=[1]; % removed s term to cancel zero at origin. Later add 1/s.
OL_den = [(C*L1*L2) (L2*R1+R2*L1+R2*L2)*C (C*R2*R1+L1+L2) R1];
P = tf(OL_num, OL_den);

% Based on ZN first method
L=.4175;
T=4.712-L;
Kp=1;
Ti = 2*L;

s=tf('s');
K_init=Kp*(1+(1/(Ti*s)));

sisotool(K_init*P);

% SISO tool shows need to increase loop gain by ~0.33087 to meet
% damping ratio of 0.707 design requirement
K=0.33087*K_init;%0.020183*K_init; %Kp when critically damped
OL_num=[1 0];
P1 = tf(OL_num, OL_den);
K1=K/s;
PI=minreal(P1*K1)
% step(PI)
```

B.3 Proportional-Integral-Derivative-Integral Control

```
% Final Transient Response of Plant with PIDI Control
clear all;
close all;
clc;

% SYSTEM PARAMETERS
L2=4.3*10^-4;
R1=1.87;
L1=3.5;
R2=.339;
C=3.719;

OL_num=[1]; % removed s term to cancel zero at origin. Later add 1/s.
OL_den = [(C*L1*L2) (L2*R1+R2*L1+R2*L2)*C (C*R2*R1+L1+L2) R1];
P = tf(OL_num, OL_den);

% ZN first method
Yhorz=[.535 .535];
Xhorz=[0 30];

% Vertical line to calculate T
xK=[4.712 4.712];
yK=[0 1];

% for Original plant with modified for ramp, but with small gain
y2= .215;
y1= .0856;
x2= 2.14;
x1= 1.1;

% calculating L and T for Ziegler-Nichols Tuning
L=.4175;
```

```matlab
T=4.712-L;
m=(y2-y1)/(x2-x1);
b=-m*x2+y2;
ytan=m*Xhorz+b;

% Plant with ramp input using step, removing "s" term in numerator
Ramp_num = [1];
OL_den_ramp =
[(C*L1*L2) (L2*R1+R2*L1+R2*L2)*C (C*R2*R1+L1+L2) R1];
Ramp_Plant = TF(Ramp_num, OL_den_ramp);%num = [1]
step(Ramp_Plant)
hold on
% Plots to determine L, T, and slope
plot(Xhorz,Yhorz,'r-')%horizontal line
plot(Xhorz,ytan, 'm') %tangent line
plot(xK,yK,'g') %verticalal line

Kp=150;
Ti = 2*L
Td = 0.5*L;
s=tf('s');
K_init=Kp*(1+(Td*s) +(1/(Ti*s)));

sisotool(K_init*P);

% SISO tool shows need to increase loop gain by ~1.0205 to meet
% damping ratio of 0.707 design requirement
K=1.0205*K_init;

% Verify this work for original plant
OL_num=[1 0];
P1 = tf(OL_num, OL_den);
K1=K/s;
PIDI=(feedback(minreal(P1*K1),1));
```

```
t=0:.01:5;
figure
step(PIDI,t)
% axis([0 4 0 1.21])
title('Final Transient Response of Plant with PIDI Control')
```

B.4   2, 3, and 5 Bladders in Series

```
% Series of 2, 3, and 5
clear all;
close all;
clc;
% SYSTEM PARAMETERS
L2=4.3*10^-4;
R1=1.87;
L1=3.5;
R2=.339;
C=3.719;


yatXinf=.0437;
Lz2=2.186
Lz3=4.291
Lz5=8.767;


OL_num=[1]; % removed s term to cancel zero at origin. Later add 1/s.
OL_den = [(C*L1*L2) (L2*R1+R2*L1+R2*L2)*C (C*R2*R1+L1+L2) R1];
P = tf(OL_num, OL_den);
series2 = (P*P);
series3 = (P*P*P);
series5 = (P*P*P*P*P);


Kp= 1;
Ti2 = (2*Lz2)/1.1
Td2 = (0.5*Lz2)/1.1;
Ti3 = (2*Lz3)/1.35
Td3 = (0.5*Lz3)/1.35;
Ti5 = (2*Lz5)/1.75
Td5 = (0.5*Lz5)/1.75;


s=tf('s');
```

```
K_init2=Kp*(1+(Td2*s)+(1/(Ti2*s)));
K_init3=Kp*(1+(Td3*s)+(1/(Ti3*s)));
K_init5=Kp*(1+(Td5*s)+(1/(Ti5*s)));

OL2=minreal(K_init2*series2);
OL3=minreal(K_init3*series3);
OL5=minreal(K_init5*series5);

K2=3.2098*K_init2;
K3=6*K_init3;
K5=17.141*K_init5;

OL_num=[1 0];
P1 = tf(OL_num, OL_den);
K12=K2/(s^2);
K13=K3/(s^3);
K15=K5/(s^5);
t=1:01:100;
serTwo=P1*P1
serThree=P1*P1*P1
serFive=P1*P1*P1*P1*P1
PIDII=(feedback(minreal(serTwo*K12),1));
PIDIII=(feedback(minreal(serThree*K13),1));
PIDIIIII=(feedback(minreal(serFive*K15),1));
hold on

step(PIDII,'r',PIDIII,'g',PIDIIIII,'b',t)
title('Transient Response of Two, Three, & Five Subsystems in Series')
legend('Series 2','Series 3','Series 5');
```

B.5 Parallel Configuration

```
% SYSTEM PARAMETERS
clear all;
close all;
clc;
L2=4.3*10^-4;
R1=1.87;
L1=3.5;
R2=.339;
C=3.719;


%VERTICAL LINE TO CALCULATE T
xK=[9.364 9.364];
yK=[0 1];


%for Original plant with modified for ramp, but with small gain
y2= .159;
y1= .0728;
x2= 6.15;
x1= 3.97;


L=.4175;
T=4.712-L;


num = [1];
den = [(C*L1*L2) (L2*R1+R2*L1+R2*L2)*C (C*R2*R1+L1+L2) R1];
P = TF(num, den);%num = [1 0]
five=(P+P+P+P+P)
% step(five)
hold on

OL_num=[1]; % removed s term to cancel zero at origin. Later add 1/s.
OL_den = [(C*L1*L2) (L2*R1+R2*L1+R2*L2)*C (C*R2*R1+L1+L2) R1];
```

```
P = tf(OL_num, OL_den);
% step(P)

Kp= 150;
Ti = 2*L%/1.1
Td = 0.5*L*2%/1.1;
s=tf('s');
K_init=Kp*(1+(Td*s)+(1/(Ti*s)));

OL=minreal(K_init*five);
CL=(feedback(minreal(OL),1));
step(CL)
sisotool(OL);

% SISO tool shows need to increase loop gain by ~1.0205 to meet
% damping ratio of 0.707 design requirement
K=1.0205*K_init;

hold on;
%% Verify this work for original plant
OL_num=[1 0];
P1 = tf(OL_num, OL_den);
K1=(K/s)/5;
fiveP1=(P1+P1+P1+P1+P1)
MRfiveP1=minreal(P1+P1+P1+P1+P1)
PIDI=(feedback(minreal(fiveP1*K1),1));
step(PIDI)
```

B.6   Hybrid Configuration

```
% SYSTEM PARAMETERS
clear all;
close all;
clc;
L2=4.3*10^-4;
R1=1.87;
L1=3.5;
R2=.339;
C=3.719;


L=2.4; % loosely based around ZN approach


OL_num=[1]; % removed s term to cancel zero at origin. Later add 1/s.
OL_den = [(C*L1*L2) (L2*R1+R2*L1+R2*L2)*C (C*R2*R1+L1+L2) R1];
P = tf(OL_num, OL_den);
series3 = (P*P*P);
series2=(P*P);
Hy=parallel(series3, series2);
step(Hy)
axis ([0 20 0 1]);


Kp= 1;
Ti = 2*L;
Td = 0.5*L/5;
s=tf('s');
K_init=Kp*(1+(Td*s)+(1/(Ti*s)));


OL=minreal(K_init*Hy);
sisotool(OL);


% SISO tool shows need to increase loop gain by ~1.8795 to meet
% damping ratio of 0.707 design requirement
```

```
 K=1.8795*K_init;

OL=minreal(K*Hy);
CL=(feedback(minreal(OL),1));
step(CL)

title('Step Response of Hybrid Configuration')
xlabel('t')
ylabel('Amplitude')
```

B.7 Sensitivity

```
% SYSTEM PARAMETERS
clear all;
close all;
clc;
L2=4.3*10^-4;

R11=1.87*1.5;
R12=1.87*1.25;
R1=1.87;
R13=1.87*.75;
R14=1.87*.25;

L11=3.5*1.5;
L12=3.5*1.25;
L1=3.5;
L13=3.5*.75;
L14=3.5*.5;

C11=3.719*1.5;
C12=3.719*1.25;
C=3.719;
C13=3.719*.75;
C14=3.719*.25;

R2=.339;

OL_num=[1]; % removed s term to cancel zero at origin. Later add 1/s.

% Vary coefficients to produce desired variance curve
OL_den50more =
[(C11*L11*L2) (L2*R11+R2*L11+R2*L2)*C11
```

```
(C11*R2*R11+L11+L2) R11];
OL_den25more =
[(C12*L12*L2) (L2*R12+R2*L12+R2*L2)*C12
(C12*R2*R12+L12+L2) R12];
OL_den =
[(C*L1*L2) (L2*R1+R2*L1+R2*L2)*C (C*R2*R1+L1+L2) R1];
OL_den25less =
[(C13*L13*L2) (L2*R13+R2*L13+R2*L2)*C13
(C13*R2*R13+L13+L2) R13];
OL_den50less =
[(C14*L14*L2) (L2*R14+R2*L14+R2*L2)*C14
(C14*R2*R14+L14+L2) R14];

L=.4175;
T=4.712-L;
Kp=150;
Ti = 2*L*1.6
Td = 0.5*L*2;
s=tf('s');
K_init=Kp*(1+(Td*s) +(1/(Ti*s)));

sisotool(K_init*P);

% SISO tool shows need to increase loop gain by ~1.0205 to meet
% damping ratio of 0.707 design requirement
K=1.0205*K_init;

hold on;
%% Verify this work for original plant
OL_num=[1 0];
P50more = tf(OL_num, OL_den50more);
P25more = tf(OL_num, OL_den25more);
P = tf(OL_num, OL_den);
P25less = tf(OL_num, OL_den25less);
```

```
P50less = tf(OL_num, OL_den50less);

K1=K/s;

PIDI50more=(feedback(minreal(P50more*K1),1));
PIDI25more=(feedback(minreal(P25more*K1),1));
PIDI=(feedback(minreal(P*K1),1));
PIDI25less=(feedback(minreal(P25less*K1),1));
PIDI50less=(feedback(minreal(P50less*K1),1));

step(PIDI50more,'b')
step(PIDI25more,'g')
step(PIDI,'r')
step(PIDI25less,'m')
step(PIDI50less,'k')

axis([0 2.5 0 1.3]);
legend('50% Increase', '25% Increase',
'Measured Value','25% Decrease','50% Decrease')
title('Sensitivity of System Response to Changes in R1, L1, and C')
```

B.8   Open Loop Model Matching Physical System

```
% Model of Test Setup
clear all;
close all;
clc;

% System Parameters
L2=4.3*10^-4;
R1=1.87;
L1=3.5;
R2=.339;
C=3.719;

OL_num=[1]; % removed s term to cancel zero at origin  Later add 1/s.
OL_den = [(C*L1*L2) (L2*R1+R2*L1+R2*L2)*C (C*R2*R1+L1+L2) R1];
P = tf(OL_num, OL_den);

Kp=14.5; % The pump is 14.5 times greater than the desired output
s=tf('s');
t=0:.01:12;
hold on
step(Kp*P,t)
grid minor
title('Model of Test Setup')
```

B.9 Adjusted Gain for Controller Driving Function and Transient Response

```
% Transient Response of Plant with PIDI control and gain of 14
% Control Error Signal of Plant with PIDI and gain of 14
clear all;
close all;
clc;
L2=4.3*10^-4;
R1=1.87;
L1=3.5;
R2=.339;
C=3.719;


OL_num=[1]; % removed s term to cancel zero at origin. Later add 1/s.
OL_den = [(C*L1*L2) (L2*R1+R2*L1+R2*L2)*C (C*R2*R1+L1+L2) R1];
P = tf(OL_num, OL_den);


L=.4175;
T=4.712-L;
Kp=150;
Ti = 2*L
Td = 0.5*L*6;
s=tf('s');
K_init=Kp*(1+(Td*s) +(1/(Ti*s)));


K=.09*K_init;
hold on;
%% Verify this work for original plant
OL_num=[1 0];
P1 = tf(OL_num, OL_den);
K1=K/s;
PIDI=(feedback(minreal(P1*K1),1));
t=0:.01:15;
```

```
figure
grid  minor
step(PIDI,t)
title('14 PSI input with PIDI')

s=tf('s');

cont_sig = K1/(1+K1*P1)

% 0.06599s^7+52.12s^6+110.7s^5+127s^4+83.64s^3+21.08s^2
% -------------------------------------------------------------------
% 0.003902 s^7 + 3.079 s^6 + 15.87 s^5 + 10.72 s^4 + 11.27 s^3

v=[0.06599 52.12 110.7 127 83.64 21.08 0 0];
u=[0.003902 3.079 15.87 10.72 11.27 0 0 0];

[q,r] = deconv(v,u)
q =16.9118
r =[0 0.0484 -157.6909 -54.2949 -106.9564 21.0800 0 0]

t=0:.01:10;
Duty_sys=tf(r, u);
hold on
% figure
impulse(Duty_sys,'r',t);
axis ([0 12 0 2.3]);
title('Comparison of Control Signal and Transient Response')
legend('Transient Response','Controller Driving Signal')
% grid minor
% [Y,T] = impulse(Duty_sys);
%  plot(T,Y+q,'b');
```

B.10 Effect of Kp on System Response

```
clear all;
close all;
clc;
L2=4.3*10^-4;
R1=1.87;
L1=3.5;
R2=.339;
C=3.719;

OL_num=[1]; % removed s term to cancel zero at origin. Later add 1/s.
OL_den =
[(C*L1*L2) (L2*R1+R2*L1+R2*L2)*C (C*R2*R1+L1+L2) R1];
P = tf(OL_num, OL_den);

L=.4175;
T=4.712-L;
Kp=153;
Ti = 2*L
Td = 0.5*L;
s=tf('s');

K7=(7/153)*Kp*(1+(Td*s)*(153/7)+(1/(Ti*s)))/s;
K14=(14/153)*Kp*(1+(Td*s)*(153/14)+(1/(Ti*s)))/s;
K28=(28/153)*Kp*(1+(Td*s)*(153/28)+(1/(Ti*s)))/s;
K56=(56/153)*Kp*(1+(Td*s)*(153/56)+(1/(Ti*s)))/s;
K112=(112/153)*Kp*(1+(Td*s)*(153/112)+(1/(Ti*s)))/s;
K153=(153/153)*Kp*(1+(Td*s)*(153/153)+(1/(Ti*s)))/s;

OL_num=[1 0];
P1 = tf(OL_num, OL_den);

PIDI7=(feedback(minreal(P1*K7),1));
```

```
PIDI14=(feedback(minreal(P1*K14),1));
PIDI28=(feedback(minreal(P1*K28),1));
PIDI56=(feedback(minreal(P1*K56),1));
PIDI112=(feedback(minreal(P1*K112),1));
PIDI153=(feedback(minreal(P1*K153),1));
t=0:.01:15;
figure
hold on

step(PIDI7,t)
step(PIDI14,t)
step(PIDI28,t)
step(PIDI56,t)
step(PIDI112,t)
step(PIDI153,t)

title('Effect of Varied Kp on Transient Response')
legend('Kp=7','Kp=14','Kp=28','Kp=56','Kp=112','Kp=153')
```